UiT The Arctic University of Norway

Faculty of Science and Technology

Department of Geosciences

## Arctic planktonic calcifiers in a changing ocean

A study on recent planktonic foraminifera and shelled pteropods in the Fram Strait-Barents Sea region

Siri Eline Ofstad

A dissertation for the degree of Philosophiae Doctor – October 2021

**Siri Eline Ofstad**


A dissertation for the degree of Philosophiae Doctor

Tromsø, October 2021


UiT – The Arctic University of Norway in Tromsø

Faculty of Sciences and Technology

Department of Geosciences

Supervisors:


Prof. Tine L. Rasmussen
CAGE – Centre for Arctic Gas Hydrate, Environment and Climate, Department of Geosciences,
UiT – the Arctic University of Norway, Tromsø, Norway

Dr. Katarzyna Zamelczyk
Department of Geosciences,
UiT – the Arctic University of Norway, Tromsø, Norway

Dr. Julie Meilland
MARUM – Center for Marine Environmental Sciences, University of Bremen, Germany

Front page image: R/V Helmer Hanssen in the Barents Sea during the AMGG CAGE 17-2 cruise, June 2017 (Photo: Siri Ofstad)

# Acknowledgments

This PhD project has allowed me to go places and see things that most people will never have the privilege to. However, making it to the other end would not have been possible without bountiful help, support, and encouragement along the way.

First of all, I would like to thank my main supervisor Tine L. Rasmussen and co-supervisor Kasia Zamelczyk. Thank you for giving me the opportunity to be a part of this project and giving me the freedom to explore and think independently along with continued support, especially in the final year. Thank you to Julie Meilland, my co-supervisor for the second half of my PhD and my first friend in Tromsø. You believed in me when I needed it the most, and your guidance and support has been invaluable and inspiring. I would also like to thank the always friendly and encouraging Melissa Chierici and Agenta Fransson for the nice collaboration over the years. A special thank you to Katsunori Kimoto, a.k.a. Kimopy, your generosity and openness elevated this project to a new level. I extend my gratitude to Naomi Harada and the rest of the JAMSTEC team, my time doing research in Japan is something I will cherish for the rest of my life.

This work would not have been possible without the captain and crew of RV Helmer Hanssen, and engineers especially Steinar Iversen and Bjørn Runar Olsen. My thanks also goes to the always helpful and friendly laboratory technicians Trine, Karina, Ingvild and Matteus. I already miss working in the lab!

I would like to thank my office mates and colleagues throughout the years for always providing social relief and a friendly work environment. A huge thanks goes to the past and present members of WP6. Naima for your infectious positivity, encouragement, and inspiring work ethic. Andrea S for guiding me through my teaching duties. The rest of the foraminifera gang: Kasia M, Haoyi and Griselda, I have thoroughly enjoyed learning and laughing with you. The beloved "B it up" gang, Arunima and Jared, Sandra, and Bérengère. Our poker nights, cabin trips and quiz shenanigans were always a much-needed distraction. A special thank you to Nikhil for your many words of wisdom and never doubting that I would get there in the end. You're a true homie.

# Table of Contents

# Preface

This doctoral thesis was carried out at the Department of Geosciences and UiT - The Arctic University of Norway, Tromsø, from January 2016 to October 2021. Funding was provided from the Research Council of Norway; funding scheme # 223259 for its Centre of Excellence CAGE – Centre for Arctic Gas Hydrate, Environment and Climate. The scientific content of this doctoral thesis has been supervised by main supervisor Professor Tine L. Rasmussen (Department of Geosciences, UiT - The Arctic University of Norway, Tromsø), and co-supervisors Dr. Katarzyna Zamelczyk (Department of Geosciences, UiT - The Arctic University of Norway, Tromsø) and Dr. Julie Meilland (MARUM, University of Bremen).

During my doctoral education, I participated in 14 cruises and spent over 100 days at sea. The cruises were mainly onboard RV Helmer Hanssen, but also RV Dana (collaboration with Aarhus University and GEUS, Denmark), MS Polarsyssel (through AGF-852 at UNIS), Garinko-go II (collaboration with the the Japanese Agency for Marine-Earth Science and Technology) and RV L'Atalante (collaboration with CNRS, Gif-sur-Yvette, Paris, France).

Findings and conclusions from this doctoral project have been presented in poster and oral presentations in national and international conferences and meetings within the field of geoscience, micropaleontology, marine ecology and Arctic biology: the PhD trainee school (forskerskole) in Arctic Marine Geology and Geophysics (AMGG)/Geoscience Research Academy of Tromsø (GReAT) Annual Meeting in 2016 and 2019 in Tromsø; CAGE winter meeting 2018 and 2019 in Tromsø; Arctic Change 2017 Conference in Quebec City (Canada); FORAMS2018 in Edinburgh (Scotland), Ecosystem Studies of Subarctic and Arctic Seas (ESSAS) in Tromsø; the 33rd International Symposium on Okhotsk Sea & Polar Oceans in Hokkaido (Japan). Additionally, part of the thesis was featured on the research spotlight of Eos – Science News by AGU.

In order to fulfill the educational requirements of the PhD program, I completed courses on Chemical oceanography in the Arctic (AGF-852 at UNIS), Arctic marine zooplankton (AB-820 at UNIS) and research ethics (SVT-8600 at UiT). I also took part in the Arctic Marine Geology and Geophysics (AMGG) educational scientific cruise and workshop in 2017 (GEO-8144 and GEO-8145 at UiT). Furthermore, the position at the department of Geosciences has included assigned duty work, where

I have been involved in teaching (GEO-3122 and GEO-3111), teaching and research cruises, seminars, and other activities within the department.

In 2018, I received a five-month travel grant from UiT, and I visited the Japanese Agency for Marine-Earth Science and Technology (JAMSTEC), in the Marine Ecosystem Dynamics Research Group, to learn and apply X-ray microcomputed tomography (XMCT) to foraminifera and the pteropod *Limacina helicina* for a shell density study. There was a short visit in January 2020 for additional analysis. This collaborating work with JAMSTEC lead to the production of a scientific paper presented hereafter in the thesis.

As a doctoral candidate at the Department of Geosciences UiT - The Arctic University of Norway, Tromsø, I have been a member of two research schools: The former AMGG, now GReAT – Geoscience Research Academy of Tromsø, and ARCTOS - The Arctic Marine Ecosystem Research Network, in Tromsø.

This thesis consists of an introduction to the following research articles:

<u>Article I:</u>
Ofstad, S., Meilland, J., Zamelczyk, K., Chierici, M., Fransson, A. and Rasmussen T. L. (2020).
**Development, Productivity, and Seasonality of Living Planktonic Foraminiferal Faunas and *Limacina helicina* in an Area of Intense Methane Seepage in the Barents Sea.**
Journal of Geophysical Research: Biogeosciences. <u>https://doi.org/10.1029/2019JG005387</u>

<u>Article II:</u>
Ofstad, S., Zamelczyk, K., Kimoto, K., Chierici, M., Fransson, A. and Rasmussen T. L**.** (2021).
**Shell density of planktonic foraminifera and pteropod species *Limacina helicina* in the Barents Sea: Relation to ontogeny and water chemistry.**
PLOS One. <u>https://doi.org/10.1371/journal.pone.0249178</u>

<u>Article III:</u>
Ofstad, S., Meilland, J., Rasmussen, T. L., Zamelczyk, K. and Seidenkrantz, M.S.
**Northeast Greenland planktonic foraminiferal fauna: present distribution patterns and paleo-perspectives.**
Under review in Frontiers in Marine Science (submitted: September 1$^{st}$ 2021).

# SECTION I - Synthesis

# 1   Introduction

## 1.1   Background and motivation

The Arctic is changing, and the effects of the present rapid climate warming are already apparent (IPCC, 2021). This part of the planet is characterized by highly dynamic and heterogeneous environments due to the highly variable influence of e.g., sea ice, glaciers, deep-water formation, polynyas and gas hydrates. These environments are being transformed due to the anthropogenically-induced climate change which have been intensified due to polar amplification, and led to processes in the ocean such as 'Atlantification' (due to increase in Atlantic water inflow and northward migration of southern organisms), sea-ice retreat (accelerated by atmospheric and surface ocean warming) and ocean acidification (due to increased uptake of $CO_2$ from the atmosphere) (e.g. Andrews et al., 2019; Serreze and Barry, 2011; Stroeve et al., 2012; Yamamoto-Kawai et al., 2009). The rate of the current climate change in terms of increase of atmospheric carbon dioxide ($CO_2$) is unprecedented for the last 66 million years (Zeebe et al., 2016).

The remote Arctic is characterized by strong seasonality, making it a logistically difficult area to access and sample on a regular basis. For this thesis, rare investigations of planktonic foraminifera and shelled pteropods in the Northeast Greenland Shelf and Northern Barents Sea were conducted to shed light on their distribution patterns, absolute and relative abundance, seasonality, diversity, ontogeny, and calcification. The planktonic foraminifera (Phylum Retaria) and thecosomatous (shelled) pteropods (Phylum Mollusca) are the major calcifiers among zooplankton (Fabry et al., 2008). Only very few studies on living planktonic foraminifera and pteropods have been performed in the Arctic realm and several unknowns exist pertaining to their ecology and life cycles, and hence how they have and will continue to respond to climate change. Gaining knowledge of the current state of these planktonic calcifiers is particularly important because plankton dynamics in the Arctic will likely continue to shift in the coming decades (Ardyna et al., 2013; Beaugrand et al., 2013). By studying living planktonic foraminifera and pteropods at this moment in time, we can get a snapshot of how they are coping with the ongoing climate and environmental changes. Furthermore, such studies are important because they provide baseline data for future monitoring and allow comparison to historical studies when the effects of climate change were less apparent, and to the sediment records, which goes beyond the onset of the industrial revolution. Comparing new studies

to historical plankton tow datasets give an insight of how communities have evolved in the last few decades.

The ocean is teaming with microscopic organisms referred to as plankton, which stems from the Greek word *planktos* meaning drifter. Plankton are invertebrates that are commonly divided into categories based on their trophic mode, the main ones being phytoplankton and zooplankton. Phytoplankton are mainly autotrophic, or primary producers, meaning that they obtain energy from sunlight through photosynthesis. Zooplankton are essentially heterotrophic, meaning they consume other organisms for energy. Together these small organisms form the base of all pelagic food webs. Furthermore, plankton are easily impacted by changes in the climate, and although mostly microscopic, due to their sheer numbers they can impact the climate on several different timescales (Arrigo et al., 1999; Charlson et al., 1987; Krüger and Graßl, 2011; Park et al., 2015). Zooplankton may either be uni- or multicellular, and some biomineralize to form hard shells (often called tests) or exoskeletons. This is a common phenomenon in the animal kingdom often thought to be a means to protect the soft body of the organism. The secreted materials range from silica (e.g., diatoms and radiolarians) to chitin (e.g., copepods) and calcium carbonate ($CaCO_3$; e.g., foraminifera and pteropods). Marine organisms that use dissolved calcium and carbonate ions from seawater to build a $CaCO_3$ (or derived form) shell are known as calcifiers. The most common macro-examples being corals, mollusks, crustaceans, and echinoderms.

Planktonic foraminifera are microscopic (generally <1.5 mm), unicellular and heterotrophic zooplankton that inhabit the upper few hundred meters of the surface ocean. They secrete shells of calcite (a polymorph of $CaCO_3$) in a series of chambers and are globally ubiquitous in the open ocean, as well as a key component in the global carbon cycle (Schiebel et al., 2002). Currently there are 50 morphospecies of planktonic foraminifera living in the modern ocean (Schiebel and Hemleben, 2017). Pteropods are also heterotrophic zooplankton, but they are multicellular and larger in size (up to 8 mm). Pteropods also have two wing-like extensions of their soft body that enable them to "fly" through the water column (Figure 1) while planktonic foraminifera are not motile. There are seven species of pteropods in the shell-bearing (thecosome) genus *Limacina* (Lalli and Gilmer, 1989). Species from the genus *Limacina* are characterized by unusually thin and delicate shells compared to other pelagic gastropods (Lalli and Gilmer, 1989). *Limacina helicina* is the dominant pteropod species in the Arctic, and at times, they can make up a significant part of the zooplankton community

(Blachowiak-Samolyk et al., 2008; Lischka and Hagen, 2016), and be found in large swarms (Lalli and Gilmer, 1989). They also differ from planktonic foraminifera because they precipitate a delicate shell of aragonite. Aragonite is a high-magnesium polymorph of $CaCO_3$ which is 50% more soluble than calcite (Fabry et al., 2009; Mucci, 1983). *Limacina helicina* are both significant scavengers and important prey in the polar food web, representing a major food component for Arctic seabirds, whales and commercial fish such as e.g., cod, herring and salmon, (Hunt et al., 2008; Larson and Harbison, 1989; Pakhomov et al., 2002; Weslawski et al., 2000; Willette and Cooney, 2001). Since *Limacina helicina* play such an important role within the polar food web, changes to their populations due to anthropogenic change could have a knock-out effect on the entire polar ecosystem and even fisheries due to their socio-economic value.

Both planktonic foraminifera and shelled pteropods contribute significantly to the biological carbon pump (Anglada-Ortiz et al., 2021; Bathmann et al., 1991; Manno et al., 2010; Meilland et al., 2016, 2018; Schiebel, 2002). The sinking of marine calcifying organisms to the seafloor represents a long-term sink of $CO_2$, and every year approximately 3 billion tons of $CaCO_3$ is transferred and permanently buried in the seafloor (Milliman, 1993). However, the importance of planktonic foraminifera also goes beyond their role in exporting carbon from the surface to deep ocean: they have a sediment record extending back to the mid-Jurassic (170 Ma) (Caron and Homewood, 1983). In fact, they are a major component of deep-sea sediments (Berger and Parker, 1970), and occasionally especially carbonate-rich sediments, referred to as oozes, will be deposited below areas of high productivity (Sliter et al., 1975). Furthermore, because they are so ubiquitous, they are one of the most important tools used by micropaleontologists to reconstruct past climate and oceanography (Kučera, 2007). In contrast, the pteropod *Limacina helicina* is used to assess biological impacts of the current climate change. Considering the increasing awareness of ocean acidification, *L. helicina* has been a commonly used test-subject due to their thin and delicate aragonite shell and are occasionally referred to as the 'canary in the coal-mine' of ocean acidification (**Paper II**).

Figure 1 *Limacina helicina*, a thecosome pteropod found in high latitudes (Photo: Katsunori Kimoto).

Although pteropods are thought to have evolved in the early Cretaceous (139 Ma), making them contemporaries of foraminifera, *L. helicina* are rarely preserved in the sediment record due to aragonite-depleted deep water and degradation of their organic material (Oakes et al., 2019; Peijnenburg et al., 2020). *Limacina helicina* and other species of shelled pteropod are therefore mostly used as sentinels of modern change. This contrasts with planktonic foraminifera, which have a long sedimentary record and are used for reconstructing environmental change in the past and are less sensitive to changes in carbonate chemistry in the ocean. The contrasting properties of planktonic foraminifera and pteropods are thus complementary and the fact that they fulfill each other's shortcomings make them especially powerful when used together in investigations of environmental changes and carbonate chemistry conditions in the ocean. Moreover, their response including mitigation and adaptation strategies to offset the impacts of these changes provides a baseline for understanding how the progressing changes affect not only these organisms but also, by extension, the marine ecosystem as a whole (Bednaršek et al., 2017b; Rastrick et al., 2018).

The motivation for this thesis is to answer, in the Fram Strait-Barents Sea region, how planktonic foraminifera and *L. helicina* respond to methane seepage (**Paper I**), explore the relationship between shell size, habitat depth and calcification (**Paper II**) and sample a completely new area that is predicted to undergo drastic changes in the coming decades (**Paper III**).

## 1.2 Ontogeny and Calcification

The Polar and Arctic Regions where the shelled pteropods and planktonic foraminifera in this thesis are sampled from are highly seasonal. They live in strong seasonal contrasts of sea-ice cover, steep

4

gradients in the carbonate system and CaCO$_3$ saturation with short growth seasons of open water, low light and highly variable productivity from year to year. In order to survive within this setting, they must be able to take advantage of short pulses of food availability and endure prolonged periods of low resources (Atkinson et al., 1996; Brandner et al., 2017). Because planktonic foraminifera and shelled pteropods feed on phytoplankton and zooplankton, a drastic reduction in population occurs when phytoplankton biomass is suppressed (Seibel and Dierssen, 2003). Although juveniles of *L. helicina* can develop adaptive strategies and feed on degraded organic matter (marine snow) (Boissonnot et al., 2019; Gannefors et al., 2005). Typically, peak productivity of planktonic foraminifera appear from spring to summer (May-June) following the spring phytoplankton bloom and an increase in sea surface temperature (**Paper I**; Chernihovsky et al., 2020; Jonkers et al., 2010; Simstich et al., 2003), while *L. helicina* in the Arctic have their highest standing stock later in the summer (August) (Gannefors et al., 2005). Occasionally peak standing stocks of *L. helicina* and planktonic foraminifera can occur in autumn (September-November) (Boissonnot et al., 2021; Jonkers et al., 2010; Lischka and Hagen, 2016). In **Paper I** we show that pteropods and planktonic foraminifera from the Northern Barents Sea follow the same seasonal size and abundance trend from spring to summer.

Both planktonic foraminifera and *Limacina helicina* continuously calcify throughout their lives, as they grow larger. In **Paper II** we present a full inventory of planktonic foraminifera and pteropod shell density and diameter in various ontogenetic stages in the northern Barents Sea. It has long been thought that planktonic foraminifera have a life span of several weeks to several months (Nigam et al., 2003), that could be linked to the lunar cycle, i.e. one life span is approximately one lunar cycle, as long as they do not miss a cycle as a result of unfavorable conditions (Bijma et al., 1990; Jonkers et al., 2015; Spindler et al., 1984). Yet, *N. pachyderma* can survive in culture for up to 200 days (Kimoto, 2015), challenging the belief that planktonic foraminifera life spans are restricted by the lunar cycle. In **Paper I** the results of our seasonal sampling briefly explores the concept of lunar cyclicity. Foraminifera terminate their life after reproduction, i.e., gamete release if they reproduce sexually (Bé et al., 1977). Some specimens undergo a partial wall thickening of their test before gamete release, this is referred to as gametogenic calcification and may alter the morphology and/or surface texture (Schiebel et al., 1997; Schiebel and Hemleben, 2017). Why some specimens within a species undergo this additional wall thickening and others do not is unknown, as is why gametogenic calcification does not occur at all in some species, like *Globigerinoides ruber* (Hamilton et al., 2008).

It is thought that the degree of thickening of the test wall could be related to the amount of excess calcium stored in the cytoplasm at the time of gametogenesis (Erez, 2003). Furthermore, the percentage of the population that undergo synchronized gametogenesis is also not fully understood, may vary between clades and likely concerns less of the population than what had thus far been expected (Meilland et al., 2021). Specimens synchronizing their reproduction would do so on a lunar, semilunar or even annual cycle, and this in turn is linked to the topic of life span (Jonkers et al., 2015; Lončarić et al., 2005; Schiebel and Hemleben, 2017). However, synchronous gamete release may not be a necessity, as asexual reproduction has been observed in the polar *N. pachyderma* and subpolar *G. uvula* belonging to two different lineages (Davis et al., 2020; Takagi et al., 2020). In conclusion, to this day there are still several aspects concerning planktonic foraminiferal reproduction strategies and ontogeny that needs to be clarified. In **Paper II,** we use shell density cross-sections to explore potential gametogenic calcification in the lower water column and surface sediments.

For planktonic foraminifera, the number of chambers reflects growth changes from juvenile to adult stages of an individual life cycle (Brummer and Kroon, 1988). Typically, adult specimens consist of 10–20 chambers (Schiebel and Hemleben, 2005). Shell diameter is an unreliable measurement of ontogenetic stage, i.e., just because a specimen is "large" (> 150-200 µm) does not mean it is an adult, and thus capable of reproduction. Planktonic foraminifera have been shown to grow larger in diameter under optimum conditions (Schmidt et al., 2003), therefore their growth can be characterized as non-linear. In **Paper I** we use shell diameter to distinguish different cohorts, meaning we used shell diameter as a proxy for ontogenetic stages. In this case, we considered shell size as an acceptable measure of ontogeny because they were sampled from the same location (Bjørnøyrenna craters in the northern Barents Sea) and were therefore exposed to the same environmental conditions. In order to build their test, calcite is deposited on either side of a primary organic membrane or Inner Organic Lining (IOL), which results in a bilamellar wall. Only the genus *Hastigerina* produces a monolamellar wall. Planktonic foraminifera can be divided into four groups according to test architecture: spinose, non-spinose, microperforate and Hastigerinidae. The two dominant species discussed in this thesis are *Neogloboquadrina pachyderma* and *Turborotalita quinqueloba,* which are non-spinose and spinose, respectively.

The life span of *L. helicina* is also not fully known, but is most commonly reported to be between one and two years for the morphotype found in the Arctic (Wang et al., 2017). The *Limacina helicina* shell

has a crossed lamellar arrangement of aragonite fibers, in between two thinner fibrous layers (Ramos-Silva et al., 2021). This is the most common microstructure found in modern pteropods, and has a wide distribution among mollusks (Ramos-Silva et al., 2021). Growth rate, hence calcification in Limacinidae is thought to be linear throughout their life cycle (Lalli and Gilmer, 1989; Lalli and Wells, 1978). This means that shell diameter is used as a proxy for maturity, the size classes for veligers, juveniles and adults being < 0.3 mm, 0.3–4 mm and > 4 mm, respectively (Lalli and Gilmer, 1989). *Limacina helicina* are protandrous hermaphrodites (starting life as males and developing female gonads as they age), meaning that shell diameter is also a proxy for gender, with females being > 4 mm. In reality, growth rate is likely influenced by environmental factors such as food availability and timing of spawning (Dadon and Cidre, 1992; Hunt et al., 2008), as is the case with planktonic foraminifera (Schmidt et al., 2003). In contrast to planktonic foraminifera, the genus *Limacina* do not terminate their life after reproduction, and can spawn multiple times (Dadon and Cidre, 1992). Spawning is ongoing from spring to summer, but also during winter (Kobayashi, 1974). *Limacina helicina* also do not undergo ontogenetic secondary calcification after they spawn. Pteropod ontogeny and calcification was also explored in **Paper I** and **Paper II** in terms of how shell thickness and density changed with increasing shell size (i.e. ontogeny), and how abundance of different size classes changed from spring to summer.

## 1.3 Vertical and horizontal distribution

Planktonic foraminiferal assemblages are distributed in five major biogeographical provinces: polar, subpolar, temperate, subtropical and tropical (Bé et al., 1977). For both shelled pteropods and planktonic foraminifera, the species diversity is greatest in warm waters (Lalli and Gilmer, 1989; Schiebel and Hemleben, 2017), and peak abundances, including in the Arctic, are often found in the upper few hundred meters of the surface ocean (Anglada-Ortiz et al., 2021; Gardner, 2019; Schiebel and Hemleben, 2017; **Paper I**; **Paper III**). The spatial distribution of both shelled pteropods and planktonic foraminifera is influenced mainly by abiotic factors such as temperature, salinity, oxygen, light, turbidity, and degree of sea-ice cover, which in turn partly determine biotic factors such as productivity (food availability), symbiosis, predation (shelled pteropods), and competition (Greco et al., 2019). Both of these groups are characterized by a patchy distribution superimposed on larger scale spatial patterns (Boissonnot et al., 2021; Meilland et al., 2019; Siccha et al., 2012; **Paper I**). Furthermore, different species of planktonic foraminifera are characteristic of different water depths, habitats, and latitudes (Kučera, 2007), and some species have photosynthetic symbionts,

which will restrict their depth habitat to the photic zone (Takagi et al., 2019). In **Paper II**, we show that on average, the shell density peak of *N. pachyderma* is deeper than *T. quinqueloba*, suggesting that they have different depth habitat preferences.

Planktonic foraminifera do not perform diurnal vertical migration, meaning they do not ascend to the sea surface during the night and migrate to deeper water during the day (Meilland et al., 2019). There is however some evidence pointing towards ontogenetic vertical migration, meaning that a part of the population (<50 %) (Meilland et al., 2021), sink progressively deeper in the water column with age (Erez et al., 1991). Ontogenetic vertical migration is a central concept in **Paper II**. When noticeable, it has been shown that ontogenetic vertical migration reaches to different depths depending on the species (Meilland et al., 2021), supporting our findings in **Paper II**. Targeting a specific depth interval is thought to be a mechanism for concentrating gametes at the same depth to maximize chances of fusion, and a way for adults to avoid predators (Erez et al., 1991; Weinkauf et al., 2020). Similarly, the vertical size distribution has been observed to evolve with the lunar cycle, with significantly more small specimens in the upper water column around the full moon (Meilland et al., 2021). Differences in the vertical size distribution in spring and summer were explored in **Paper I**. A large range of test sizes were found in all the water depth intervals, but the smallest tests in spring were found in the 0–50 m water depth interval, while in summer they were in the 200–300 m depth interval. The plankton tow samples were not taken close enough to the full moon to formulate any conclusion about its influence.

In contrast to planktonic foraminifera, it is a common assumption that *Limacina helicina* perform diurnal vertical migration in the Arctic (Falk-Petersen et al., 2008). Mature individuals diurnally migrate in the upper 200 m of the water column in order to avoid predators during the day, while veligers and juveniles migrate in the top 50 m, likely to stay in the food rich layer (Falk-Petersen et al., 2008). This means that in a given moment there may be a large bias towards smaller (juvenile) shells in the upper water column (0–50 m), which has been shown in other studies in the Arctic (Anglada-Ortiz et al., 2021; Kobayashi, 1974; **Paper I**), as well as the Southern Ocean (Gardner, 2019). However, this size distribution with depth may be a summer phenomenon due to spawning in spring (Wang et al., 2017). Data from June in **Paper I** shows that smaller shells are indeed concentrated in the 0–50 m water depth interval, and that the range of shell diameters is much smaller compared to the underlying sampling intervals. Like planktonic foraminifera, the abundance tends to peak in the

0–100 m water depth interval (Anglada-Ortiz et al., 2021; Gardner, 2019; Jensen, 1998; Kohfeld et al., 1996; Meilland et al., 2020; **Paper I**, **Paper III**), where higher concentration of plankton to feed on is located. If the towing speed of the plankton net is not low enough to accommodate the mesh size of the net, adult specimens of *Limacina helicina* may be able to avoid being captured using their parapodia (wings), meaning they are potentially underrepresented in in-situ studies (Lischka and Hagen, 2016).

## 1.4   Marine calcifiers in a changing world

Due to their sensitivity to environmental conditions, it does not come as a surprise that there has been a documented shift in planktonic foraminiferal assemblages in terms of species composition since the industrial revolution (Jonkers et al., 2019). Until now, the two dominant planktonic foraminiferal species reported in the Fram Strait-Barents Sea region have been *Neogloboquadrina pachyderma* and *Turborotalita quinqueloba* (Carstens et al., 1997; Jensen, 1998; Kohfeld et al., 1996; Pados and Spielhagen, 2014; Volkmann, 2000; **Paper I**). But recent studies reveal increasing abundances of *Globigerinita uvula* and *Neogloboquadrina incompta*, two subpolar species from temperate waters (Husum and Hald, 2012; Meilland et al., 2020). In fact, a dominance of *G. uvula* has been found in some locations of the western Barents Sea (Meilland et al., 2020). This northward migration is likely linked to increasing water temperature and increased food availability due to production of thinner ice and a general decreasing ice cover (Arrigo and van Dijken, 2015; Smedsrud et al., 2013). This shift in species assemblages changes the species richness scene in the Arctic but also has consequences in the role planktonic foraminifera play to the biological carbon pump. The inorganic carbon fluxes they generate are species-specific; a change in the assemblages will ultimately lead to a reduction or an increase of their impact in the marine carbon cycle (Anglada-Ortiz et al., 2021; Meilland et al., 2018). As a result of their sensitivity to water column properties, planktonic foraminifera (and other microfossil groups) can be thought of as a "biological time machine", and have been used to reconstruct past climate variations on centennial, millennial, and million-year timescales (Yasuhara et al., 2020). Note that calcitic (planktonic foraminifera) tests are generally well preserved in the sediments (**Paper I**; **Paper II** and **Paper III**), whereas aragonitic (*Limacina helicina*) tests are consumed by predators and/or easily lost due to dissolution below the carbonate compensation depth, or on or below the seafloor.

Different planktonic foraminiferal species have different environmental preference and occupy a specific ecological niche, therefore shifts in abundances and proportions of species in the assemblages have been studied to document climate change (Imbrie and Kipp, 1971; Waterson et al., 2017). Furthermore, the chemical composition of their calcitic shells (stable isotopes and trace elements) act as proxies to the chemical and physical state of the ambient seawater and can help reconstruct, most notably temperature, but also salinity, pH, and biological productivity of the ancient marine environment (Duplessy et al., 1991; Foster and Rae, 2016; El Frihmat et al., 2015; Katz et al., 2010; Kucera et al., 2005). Past climatic events are well described thanks to paleoreconstructions using planktonic foraminiferal fossils found in high latitudes and which include e.g.,: Heinrich events (cold events of iceberg rafting), Dansgaard-Oeschger events (abrupt warmings on millennial time scales), the Younger Dryas cold spell (12,8–11,7 ka), and the Last Glacial Maximum (24–19 ka) (e.g., Cayre et al., 1999; Duplessy et al., 1996; Eynaud et al., 2009; Rasmussen et al., 1997, 2016).

Because they are made of aragonite, shells of pteropods do not preserve well in the sediment record and our ability to study them on a geological timescale is considerably more limited compared to foraminifera. However, we do know that pteropods survived major carbon cycle and climate perturbations such as the Cretaceous-Paleogene extinction event (~66 Ma) and the Paleocene-Eocene Thermal Maximum (~56 Ma) (Peijnenburg et al., 2020). Both events are analogous to the present day rise in $CO_2$, yet the current rate of increase in $CO_2$ is higher (Zeebe et al., 2016). Nevertheless, their survival demonstrates a resilience that was perhaps unexpected. Although sedimentary records of the Limacinidae family are rare (Wall-Palmer et al., 2012), historical samples dating back to the early and mid-20th century have provided a source of baseline information and a chance to investigate decadal scale variability (Beaugrand et al., 2013; Gardner, 2019; Head and Pepin, 2010; Howes et al., 2015, 2017). In likeness to planktonic foraminifera, long-term shifts in abundance and distribution in the north Atlantic and north Pacific have been related to changes in temperature (Beaugrand et al., 2013; MacKas and Galbraith, 2012).

## 1.4.1   Marine calcifiers as biological proxies for ocean acidification

Ocean acidification may lead to adverse effects on the ability of marine calcifiers to produce calcareous shells and skeletons. The crystal structure of calcite (planktonic foraminifera) is more

stable than aragonite (shelled pteropods), and the tendency for the crystal structure to dissolve is linked to the so-called "saturation state" or "$\Omega$" in the surrounding environment of the particular mineral phase. The crystal structures of aragonite and calcite are thermodynamically stable when $\Omega_{calcite}$ and $\Omega_{aragonite}$ > 1. Both planktonic foraminifera and *L. helicina* are sensitive to the carbonate chemistry in their environment and the extent of their calcification is commonly used as an indicator for ocean acidification (Beer et al., 2010; Fox et al., 2020; Howes et al., 2017; Iwasaki et al., 2019b; Marshall et al., 2013; de Moel et al., 2009; Oakes and Sessa, 2019; Osborne et al., 2016). In **Paper II** we use a novel approach for measuring shell density of marine calcifiers, which has a potential to be a common analytical method in the field.

Laboratory cultures and sediment cores showing reduced calcification of various planktonic foraminiferal species during conditions of lower marine carbonate ion concentrations ($[CO_3^{2-}]$) have been extensively documented (e.g., Barker and Elderfield, 2002; Gonzalez-Mora et al., 2008; Lombard et al., 2010; Manno et al., 2012), but quantifications and observations in the field are sparse (Aldridge et al., 2012; Beer et al., 2010). Dissolution of modern planktonic foraminiferal shells (*Globigerina bulloides*) resulting in a reduced shell weight by 30–35% compared to pre-industrial foraminifera has been found in the Southern Ocean (Moy et al., 2009). Similar observations of shell thinning (*Globigerinoides ruber*) in the Western Arabian Sea may potentially have been caused by ocean acidification (de Moel et al., 2009). Strong anti-correlation trends between shell weight and atmospheric $CO_2$ (Moy et al., 2009; Zamelczyk et al., 2012) showcases the relationship between atmospheric $CO_2$, marine carbonate chemistry and foraminiferal calcification.

Thus far, there are only a few studies that have been able to demonstrate any impacts of ocean acidification on *L. helicina* and planktonic foraminifera in situ (Bednaršek et al., 2012; Bednaršek and Ohman, 2015; Feely et al., 2016; Iwasaki et al., 2019b). The majority of the studies showing a link between decreased calcification and shell thinning at low saturation states as a result of increased $CO_2$ have been done in culture (Bednarsek et al., 2014; Comeau et al. 2010; Lischka et al., 2011; Lischka and Riebesell, 2012). The connection between low $\Omega_{Ar}$ and shell degradation in *L. helicina* has been confirmed by observations from marine environments with large natural gradients in the carbonate chemistry (Bednaršek and Ohman, 2015). However, recent studies on the periostracum of *L. helicina* suggests that they may not be as sensitive to ocean acidification as previously claimed (Peck et al., 2016, 2018). Furthermore, it is known that in order to calcify, foraminifera increase the

pH at the site of calcification relative to the surrounding sea water through proton pumping (Toyofuku et al., 2017). This means that foraminifera can manipulate pH and in theory could use this as a defense mechanism against ocean acidification. It is currently believed that shelled pteropods, and mollusks in general, exert little control over the pH of their calcifying fluid (Crenshaw, 1972), which serves as another contrasting characteristic to foraminifera and boosting their ability to act as climate change sentinels. In turn, it can be speculated that ocean acidification has a more significant impact on dead foraminiferal specimens. Therefore, the effects of ocean acidification in the sediment record may be more pronounced than what we can expect to document in the modern ocean.

To complicate matters further, an increased food supply for non-symbiont bearing planktonic foraminiferal species may reduce or even negate the effects of living in low-$\Omega$ waters (Weinkauf et al., 2016), but this relationship has not been shown for shelled pteropods (Bednaršek et al., 2017a; León et al., 2020). An abundant food supply would compensate for the increased energy expenditure for biomineralization under stressful conditions (Palmer, 1992). This positive relationship between ocean acidification and food supply has been shown for several marine calcifying groups of organisms (Brown et al., 2018; Hettinger et al., 2013; Ramajo et al., 2016; Thomsen et al., 2013; Towle et al., 2015).

In order to explore potential effects of ocean acidification on $CaCO_3$ shell conditions, a range of different methods have been used, many of which are subjective, and may not be able to resolve changes on the sub-micron level (Johnstone et al., 2010; Marshall et al., 2013; Osborne et al., 2016). There is a lack of established methodology to study biological effects of ocean acidification. Currently, it is common to use indirect methods to measure shell density (e.g. ,area-normalized weight), making it challenging to compare results across studies. The XMCT is an objective method, which provides a CT number as a representation of the average shell density of a calcifying organism (**Paper II**). It is important to have a quantitative and reproducible method to measure the effect of ocean acidification on marine calcifiers, and which constitutes a common tool among scientists within the field.

## 1.5   Objectives

The overarching aim of this thesis is to enhance the knowledge of modern planktonic foraminifera and shelled pteropods in the Fram Strait-Barents Sea region. Specific objectives are listed below and illustrated in Figure 2.

1)  Investigate effects of methane seepage on shell condition and abundance of planktonic foraminifera and shelled pteropod faunas (**Paper I**)

2)  Better assess seasonality patterns of planktonic foraminifera and shelled pteropods (**Paper I**)

3)  Explore how shell density varies with ontogeny, water depth and in relation to environmental conditions in the water column (**Paper II**)

4)  Characterize the effects of ocean acidification on *Limacina helicina* and climate change impact on calcifying plankton in the Barents Sea (**Paper II**) and on the Northeast Greenland shelf (**Paper III**)

5)  Provide an inventory of planktonic foraminiferal species and their distribution and abundance at a glaciated margin both in the water column and surface sediment on the Northeast Greenland shelf (**Paper III**)
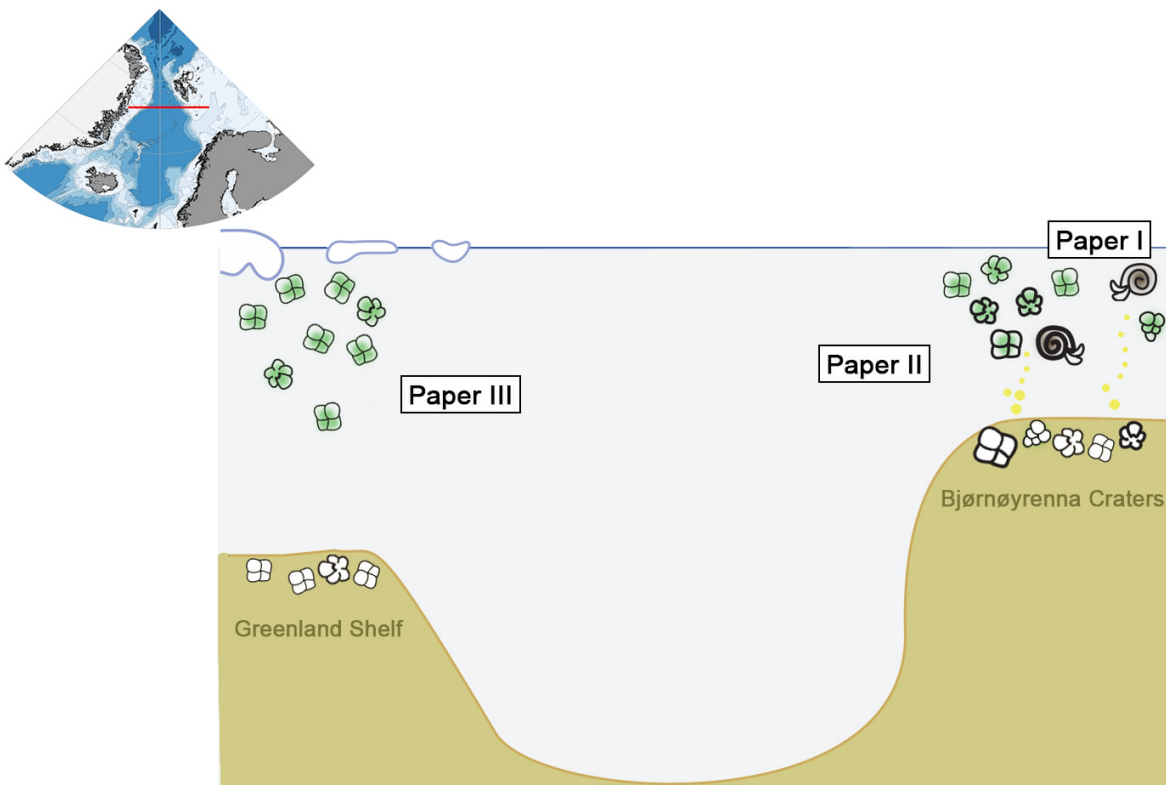


Figure 2  Schematic overview of the research objectives of this doctoral thesis.

# 2   Study Areas

The areas of focus for this thesis have been the Bjørnøyrenna Craters in the northern Barents Sea (**Paper I** and **Paper II**) and Northeast Greenland Shelf (**Paper III**) (Figure 3). Due to their high latitude location both study areas are particularly vulnerable to ongoing climate change in terms of water column properties (e.g. temperature, stratification, acidification, meltwater injections) and consequently, their plankton communities as well. Some effects on the marine ecosystem in the study areas have already been documented, like the increasing appearance of temperate and tropical species (Andrews et al., 2019; Bjørklund et al., 2012; Fossheim et al., 2015; Neukermans et al., 2018; Schiebel et al., 2017), increased primary productivity (Arrigo and van Dijken, 2015; Cherkasheva et al., 2014), and earlier onset of phytoplankton blooms (Kahru et al., 2011; Oziel et al., 2017). In addition, both study areas are highly dynamic, due to either intense methane seepage (Bjørnøyrenna Craters; **Papers I and II**), or sea-ice dynamics and the interplay between Polar and Atlantic Water (Northeast Greenland Shelf; **Paper III**).
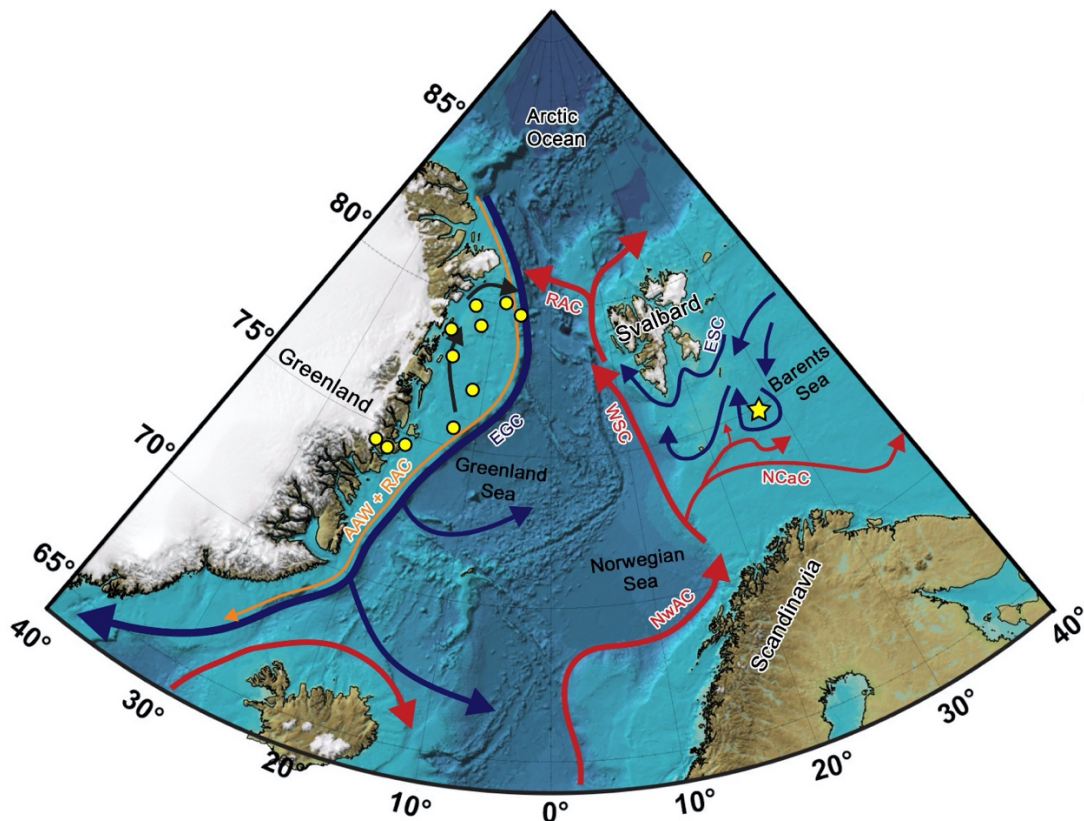


Figure 3 Map of the Nordic Seas and Barents Sea showing the major currents, seas, landmasses, and location of study areas. Yellow star marks eight sampling stations at Bjørnøyrenna Craters, and yellow dots are individual sampling stations on Northeast Greenland Shelft. Blue lines are Arctic Water outflows, red lines are Atlantic Water inflows, orange lines are cooled subsurface water masses of Atlantic origin (AAW and RAC), and black lines are coastal currents, subsurface Atlantic Water and surface Polar Water. Abbreviations: *EGC* East Greenland current, *ESC* East Spitsbergen Current, *AAW* Arctic Atlantic Water, *RAC* Return Atlantic Current, *WSC* West Spitsbergen Current, *NCaC* North Cape Current, *NwAC* Norwegian Atlantic Current, Basemap from IBCAO 3.0 (Jakobsson et al., 2012).

## 2.1 Northern Barents Sea (Bjørnøyrenna Craters)

The Bjørnøyrenna Crater area is located in the 850 km long cross-shelf trough Bjørnøyrenna (The Bear Island Trough) in the northern Barents Sea (74.91°N, 27.7°E), just east of the Polar Front. The sampling area is relatively shallow (~ 340 m) and is influenced by north-easterly flowing Atlantic water from the North Cape Current, a branch of the Norwegian Atlantic Current. The Bjørnøyrenna Craters are characterized by intense methane seepage from gas hydrates, from more than a hundred giant crater-mound systems, hence the name (Andreassen et al., 2017). The craters are hypothesized to be the result of abrupt release of methane during the deglaciation of the Barents Sea Ice Sheet (Andreassen et al., 2017 and references therein).

Gas hydrates are ice-like compounds in sediments formed by water and gas, most commonly methane ($CH_4$), that exist at relatively low temperatures and relatively high pressure (Sloan and Koh, 2007). Perturbing the conditions in which hydrates are stable can cause dissociation and the release of gas to the water column. Modelling of the gas hydrate stability zone showed that hydrate stability is much more sensitive to changes in temperature than sea-level (pressure), especially in shallower depths (Mienert et al., 2005). Warm bottom waters therefore have the potential to trigger the dissociation of gas hydrates (e.g. Biastoch et al., 2011; Kretschmer et al., 2015; Ruppel and Kessler, 2017; Westbrook et al., 2009). Once the $CH_4$ gas bubbles escape from the hydrate they are either anaerobically oxidized in the sediment, producing hydrogen sulphide ($H_2S$), or aerobically oxidized in the water column, utilizing oxygen and producing $CO_2$ as a byproduct. Methane flares up to 200 m tall, or roughly 140 m below the sea surface, have been documented by Andreassen et al. (2017).

## 2.2 Northeast Greenland Shelf

The Northeast Greenland Shelf (NEGS) is located in the Fram Strait, which constitutes one of the deep connections between the North Atlantic and Arctic Ocean. It is a shallow shelf (~ 300 m) with a complex bathymetry, more than 40 % of the NEGS is comprised of banks and troughs (Arndt et al., 2015). The NEGS is particularly sensitive to changes in sea ice and freshwater discharge from the Arctic Ocean (Jennings and Weiner, 1996). This is because the southward flowing East Greenland current (EGC) carries relatively fresh Polar water and underlying Arctic Atlantic Water (AAW) along the East Greenland margin. Atlantic Water is also injected onto the shelf by the Return Atlantic Current (RAC). The EGC is one of the main sea ice and freshwater export pathways from the Arctic

Ocean, and is partly recirculated over the deep basin of the Greenland Sea (Blindheim and Østerhus, 2005).

The sea-ice extent on the shelf has been decreasing rapidly over the past decades (IPCC, 2021), allowing for the collection of more in situ sampling (Pados-Dibattista et al., 2021; Syring et al., 2020). The sea-ice dynamics give rise to several annual polynyas along the coast (areas of open water surrounded by ice) (Pedersen et al., 2010; Schneider and Budeus, 1995), which allow for hot-spots of biological productivity (Pesant et al., 1996; Smith Jr., 1995). In addition, the temperature and influence of Atlantic water is increasing in the Fram Strait (Beszczynska-Møller et al., 2012; Karcher et al., 2003; Polyakov et al., 2017), which will, in theory, lead to an increase the proportion of Atlantic species on the NEGS.

# 3   Methodology

The materials collected for this thesis comprise water, plankton and surface sediment samples. Additional water column properties were measured with a conductivity, temperature, depth profiler (CTD). Below is a summary of all sampling and analytical methods, further details are presented in **Papers I–III**.

## 3.1   Water column sampling

Marine calcifiers (planktonic foraminifera and shelled pteropod species *Limacina helicina*) from the water column in the Bjørnøyrenna Crater area (**Paper I** and **Paper II**) and the Northeast Greenland Shelf (**Paper III**) were sampled with a stratified plankton tow from HydroBios (MultiNet, 63-µm mesh, net opening 0.5 m$^2$; Figure 1A). The MultiNet opens and closes at predetermined depths. Five depth intervals were sampled in the Bjørnøyrenna Craters: 300–200, 200–150, 150–100, 100–50, and 50–0 m. In total, 80 plankton net samples were collected, 40 in April and 40 in June 2016, across eight stations in the Bjørnøyrenna Craters (Figure 4A). However, only four depth intervals were sampled on the NEGS (**Paper III**), due to a defect net. The four water depth intervals sampled on the Northeast Greenland Shelf were: 400/300–200/150, 200/150–100, 100–50, and 50–0 m. Three depth intervals were sampled at ST16 due to the shallow bottom depth (164 m), which were 125–100, 100–50, and 50–0 m. In total, 39 plankton net samples across 10 stations were collected from the Northeast Greenland Shelf in September 2017. A flowmeter was attached to the opening of the plankton tow in order to measure the volume of water filtered through the nets in each depth interval. When sampling on the Northeast Greenland Shelf, the flowmeter was defective; therefore, the volume of water filtered through each net was calculated using the area of the net opening and length of sampling interval (net opening (m$^2$) x depth interval (m)).

Once onboard the plankton samples were transferred to a 63-µm sieve using a spray bottle with filtered sea water (Figure 4B). The residual material was then transferred to plastic bottles (250 ml; Figure 4C). To preserve the marine calcifiers and prevent dissolution, the bottles were filled with ethanol (98 %) and approximately a quarter of a teaspoon of buffering agent (hexamethylenetetramine (≥ 99 %) and stored at 2 °C (Figure 1C). The amount hexamethylenetetramine was adjusted to the amount of organic matter in the sample. A quarter of a teaspoon hexamethylenetetramine was the default amount added to the plankton samples, unless

the organic material exceeded approximately 25 ml. The samples were analyzed and planktonic foraminifera and pteropod shells were picked at a later date in the laboratory at the Department of Geoscience at UiT—The Arctic University of Norway, Tromsø, Norway, under a Leica MZ12.5 light microscope (Figure 5).
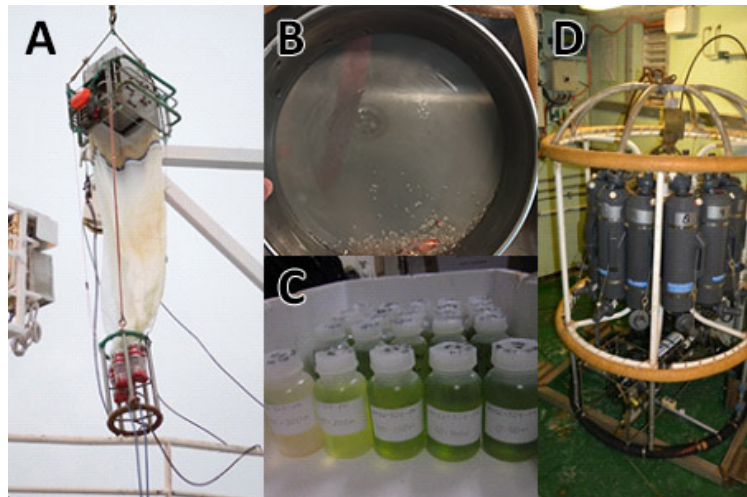


**Figure 4** A) MultiNet ready for deployment, B) sieved plankton tow sample after collection, C) plankton tow samples during a phytoplankton bloom, D) CTD rosette with Niskin bottles. (Photos: Siri Ofstad).

Water samples were taken at discrete depths at the same stations as the plankton tows prior to its deployment. The water samples were collected with 12x5 L Teflon-lined Niskin bottles for analysis of methane oxidation rate (**Paper I**), carbonate chemistry (**Paper I** and **Paper II**) and nutrients (**Paper III**) (Figure 4D). There were eight CTD stations in the Bjørnøyrenna Craters and 11 on the Northeast Greenland Shelf. There is one more CTD station than plankton net station on the Northeast Greenland Shelf, because the weather conditions prevented the deployment of plankton tows at ST22. On the Northeast Greenland Shelf, the water samples were collected from 1, 5, 10, 20, 30, 50 m, the depth of the chlorophyll maximum, 100 m and just above the seafloor. In the Bjørnøyrenna Craters, the water samples were collected from 1, 5, 10, 20, 30, 50 m, at the depth of the chlorophyll maximum, 100 m and just above the seafloor. In total, 140 water samples were collected in the Bjørnøyrenna Craters, 70 in April and 70 in June 2016, and 99 on the Northeast Greenland Shelf in September 2017. At both study areas, a CTD (Sea-Bird SBE 19+ or Sea-Bird 911) provided salinity, temperature and depth profiles, in addition to oxygen and fluorescence (Figure 1D).

## 3.2 Sediment sampling

Recently settled planktonic foraminifera were collected from the surface sediments. Surface sediments must be undisturbed so the top centimeters can be sub-sampled for analysis. There are several different instruments designed to sample surface sediments. In this thesis a box-corer (50 × 50 × 50 cm; **Paper I**; **Paper II** and **Paper III**) and a haps-corer (**Paper III**) were used. For this thesis, three surface sediment samples from the Bjørnøyrenna Craters and 10 from the Northeast Greenland Shelf were collected.

Immediately after recovering the sediment core, the top layer (1 cm) was scraped off by a spoon, and either preserved in ethanol (96%) with rose bengal (**Paper I** and **Paper II**), and stored at 2 °C, or frozen at -20 °C without any additives and freeze dried once on land (**Paper III**). Surface sediment samples from the Bjørnøyrenna Craters were preserved in rose bengal for the possibility to study living benthic fauna. At the laboratory, the sediment samples were wet-sieved through a 63-μm sieve and dried for at least 24 hours at 40 °C. Once dried, planktonic foraminifera were picked under a light microscope, with a fine brush, and identified to species level.

## 3.3 Morphometrical parameters

Physical measurements of planktonic foraminifera and *L. helicina* were done in order to assess seasonal growth (**Paper I**) and calcification rate (**Paper II**). For the determination of area density planktonic foraminiferal shells (*T. quinqueloba* n = 54, *N. pachyderma* n = 57) and *L. helicina* (n = 10) were weighed individually using a Sartorius microbalance (model M2P, 0.1 μg sensitivity). The given weight measurements were systematically based on three repeated measurements of a single specimen. Area density is given by shell weight divided by surface area. The shell diameter of planktonic foraminifera from the water column (*N. pachyderma* n = 1044, *T. quinqueloba* n = 518) and from the surface sediments (*N. pachyderma* n = 42, *T. quinqueloba* n = 14), and *L. helicina* (n = 331) was measured for **Paper I** by taking pictures of the shells with a Leica Z16 APO microscope and integrated Leica DFC450 camera with LAS version 4.12.0 software. The images were then imported to Adobe Photoshop CS6 where the ruler tool was used for measuring the diameter. For **Paper II** shell diameter in addition to the shell apex of *L. helicina* (n = 25) was measured with the Molcer Plus software (Version 1.35).
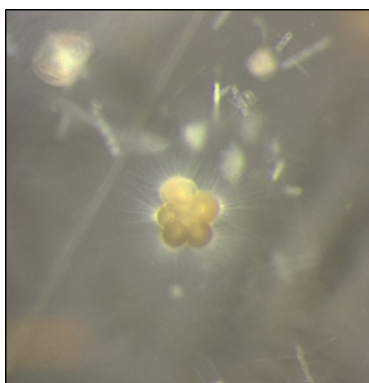
**Figure 5** A *T. quinqueloba* with green cytoplasm and a large spine network under the microscope. (Photo: Siri Ofstad).

## 3.4 Stable Isotopes

Stable isotopes of carbon ($\delta^{13}$C) and oxygen ($\delta^{18}$O) from planktonic foraminiferal shells collected in summer (June 2016) at the Bjørnøyrenna Craters were analyzed at The Stable Isotope Laboratory at CAGE—Centre for Arctic Gas Hydrate, Environment and Climate located at UiT—The Arctic University of Norway, Tromsø, Norway (**Paper I**). In total, 20 specimens of *Neogloboquadrina pachyderma* and 20 specimens of *Turborotalita quinqueloba* in the size class 150–200 μm were picked across all five sampling depth intervals (0–50 m, 50–100 m, 100–150 m, 150–200 m, and 200–300 m) and placed in 4.5 ml vials. A bulk analysis was done on *N. pachyderma* from the same depth interval, as with *T. quinqueloba.* A total of 20 samples were analyzed, 10 samples for each species (two from each plankton net sampling interval). Each sample weighed between 20 and 50 mg in order to achieve a sufficient signal strength. Due to the low planktonic foraminiferal standing stock and dominance of small specimen in April, isotopic analysis was not done on the April samples. Methane seepage could potentially influence the isotopic signature of the planktonic foraminifera shells by altering the DIC content in the environment. However, the methane seepage must be shallow enough and not fully consumed during anaerobic oxidation of methane in the sediment (Iversen and Jorgensen, 1985; Reeburgh, 1980) or by methanotrophic bacteria in the water column (Reeburgh, 2007). Stable isotopes in planktonic foraminifera, in theory, reflect the ambient conditions at the time of calcification (Cooke and Rohling, 1999). Foraminifera found in sediments that emit methane or have emitted methane in the past, tend to have a negative $\delta^{13}$C signal (e.g., Consolaro et al., 2015; Schneider et al., 2017; Sztybor and Rasmussen, 2017 and references therein).

## 3.5 Shell density analysis

Shell density of planktonic foraminifera and *Limacina helicina* from the Bjørnøyrenna Craters (June 2016) were measured at the the Japan Agency for Marine-Earth Science and Technology (JAMSTEC), Yokosuka, Japan, with an X-ray microcomputed tomography (XMCT; ScanXmate-DF160TSS105, Comscantecno Co. Ltd., Kanagawa, Japan; Figure 6) (**Paper II**). Well-preserved specimens were selected at random size, but with the intention of having a representative size range. Shell diameters of planktonic foraminifera and *L. helicina* sampled from the Bjørnøyrenna Craters in June 2016 had been measured and plotted in a histogram for **Paper I**. A total of 226 planktonic foraminiferal shells from the water column (*N. pachyderma* n = 120, *T. quinqueloba* n = 115), 30 recently settled planktonic foraminifera shells (*N. pachyderma* n = 12, *T. quinqueloba* n = 18), and 25 *L. helicina* shells from all five depth intervals (0–50 m, 50–100 m, 100–150 m, 150–200 m, and 200–300 m) were scanned with the XMCT (Figure 6). All scanned pteropod shells were either veligers, i.e. *Limacina* spp. (< 300 µm, n = 7), or juvenile *Limacina helicina* (300–4000 µm, n = 18). All of the scanned specimens came from Stations 1102, 1108 and 1110.

One to three specimens (depending on the shell size and apparent thickness) were placed on a stage made of a quartz glass bar. Tests were mounted on the sample stage with tragacanth gum. A calcite crystal ball was used to standardize the computed tomography (CT) number of each test sample and enabled us to distinguish the density distributions in the foraminiferal and pteropod tests with high resolution. In this study (**Paper II**), a limestone particle (diameter of approximately 130 µm; 1000 in mean CT number; NIST RM8544 (NBS19)) was placed next to the shells on the sample stage, and all of the shells were scanned with the same calcite standard. A high-resolution setting (X-ray focus spot diameter of 0.8 µm, X-ray tube voltage of 80 kV, detector array size of 1024x1024 for the pteropods and 992x992 for the foraminifera, spatial resolution of 0.833 µm for the pteropods and 0.964 µm for the foraminifera, 1200 projections/360˚, 4 s/projection) was used for 3-D quantitative densitometry of the planktonic foraminiferal and pteropod tests.
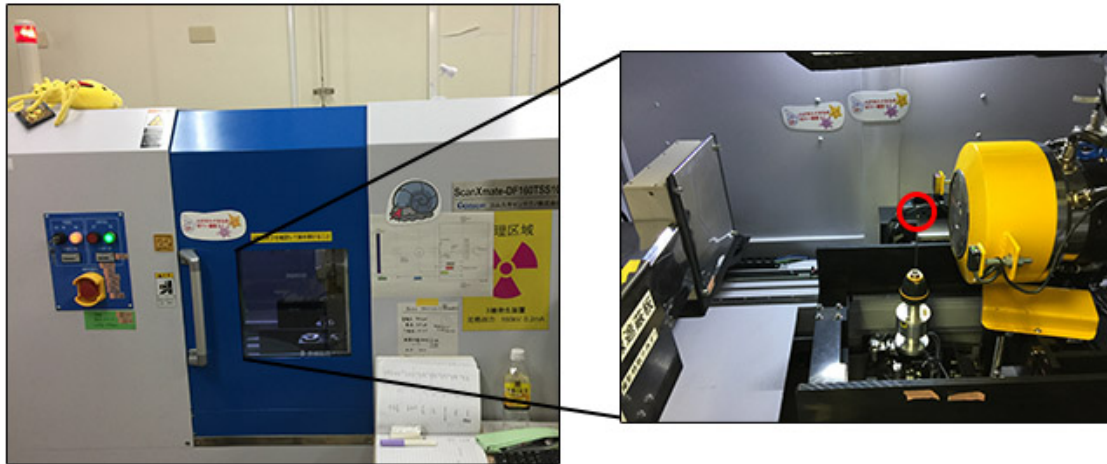
**Figure 6** The XMCT scanner at JAMSTEC exterior (left) and interior (right). Specimen were placed on quartz rod (red circle). (Photos: Siri Ofstad).

The XMCT provides a density metric in the form of a CT number, which in addition to being non-destructive, provides high precision three-dimensional morphometrics including calculated mean shell thickness and $CaCO_3$ volume measurements. XMCT scans also allow observations of the internal skeletal structures of the microorganisms and their density variations. The CT number generated by the XMCT has proven to be a useful quantitative tool to measure both post- and pre-depositional $CaCO_3$ dissolution in the planktonic foraminiferal species *Globigerina bulloides*, and the impact of changes in seawater carbonate chemistry on calcification rates of *G. bulloides*, both in the North Pacific (Iwasaki et al., 2015, 2019b).

# 4  Summary of papers

## 4.1  Paper I

Development, Productivity, and Seasonality of Living Planktonic Foraminiferal Faunas and *Limacina helicina* in an Area of Intense Methane Seepage in the Barents Sea.
*Ofstad, S., Meilland, J., Zamelczyk, K., Chierici, M., Fransson, A. and Rasmussen T. L.*
Journal of Geophysical Research: Biogeosciences.
doi: 10.1029/2019JG005387

In this study, we investigated planktonic foraminiferal faunas and pteropod species *Limacina helicina* living among methane plumes rising from the seafloor towards the surface in the Bjørnøyrenna Crater area in the northern Barents Sea. A study on marine calcifyers living above methane seepage had not been done before. Plankton tow and water chemistry data were collected during Spring and Summer 2016. The aim of the study was to examine whether planktonic foraminifera and shelled pteropods were more abundant or less abundant, or unaffected, above the active methane seepage. Special attention was paid to the shell conditions and stable isotopes in the foraminifera shells were measured. In terms of water chemistry, we aimed at assessing if the methane seepage had any impact on the surrounding carbonate system. Specifically, if the methane seepage has the potential to create hotspots of decreased pH (i.e., acidification potential).

Our results showed no evidence that the marine calcifyers would aggregate above large methane flares, and the $\delta^{13}C$ and $\delta^{18}O$ of *Neogloboquadrina pachyderma* and *Turborotalita quinqueloba* were comparable to previous observations in the Arctic (Simstich et al., 2003) suggesting no effect of the methane flares on the specimens geochemistry. The seasonal data also allowed us to assess the difference in abundance, size and species compositions between spring and summer in the northern Barents Sea. In spring, both populations were dominated by juveniles and young adults. In summer, we registered the subtropical species *Orcadia riedeli* and *Globigerinoides conglobatus*, which constitutes their first observation in the Barents Sea. From spring to summer the abundance of planktonic foraminifera in the water column increased 53-fold, while the abundance of *L. helicina* increased ten-fold. In terms of size the mean diameter of the planktonic foraminifera increased by 82.6 % (from 103.3 μm to 188.6 μm), while diameters of *L. helicina* increased by 90.5 % (from 175.6 μm to 334.6 μm). The assemblages in the surface sediments consisted of *Turborotalita quinqueloba*

(80 %), *Neogloboquadrina pachyderma* (16%) and *Globigerinita uvula* (4 %) showing a close similarity to the overlying water column.

In spring, a plume of elevated dissolved inorganic carbon, low pH, and calcium carbonate saturation states was found directly above one of the methane plumes in our transect, suggesting that the methane is rapidly oxidized in the water column. Methane may impact the carbonate system and regionally contribute to ocean acidification. This finding is particularly significant because gas hydrates are predicted to dissociate with warming of bottom water temperatures (Kretschmer et al., 2015).

Highlights:
- Planktonic foraminifera and shelled pteropods distribution are not affected by methane flares.
- Planktonic foraminifera and shelled pteropods display seasonality in the area with an increased productivity (no. individuals m$^{-3}$) and size from spring to summer.
- Sub-tropical species of planktonic foraminifera were present in the Northern Barents Sea during the summer.
- Methane may impact the carbonate system.

## 4.2   Paper II

Shell density of planktonic foraminifera and pteropod species *Limacina helicina* in the Barents Sea: Relation to ontogeny and water chemistry
*Ofstad, S., Zamelczyk, K., Kimoto, K., Chierici, M., Fransson, A.* and *Rasmussen T. L.*
PLOS One. doi: 10.1371/journal.pone.0249178

The goal of this study was to elucidate the natural variation in shell density of the pteropod *Limacina helicina* and the two most abundant planktonic foraminiferal species in the polar region (*Neogloboquadrina pachyderma* and *Turborotalita quinqueloba*) (**Paper I**). Planktonic foraminifera from surface sediments were also studied in terms of how well they are preserved and dissolution patterns of the faunas after settling on the sea floor. This was achieved by scanning shells in an x-ray microcomputed tomography (XMCT) scanner (Iwasaki et al., 2015, 2019a, 2019b).

We found that the pteropods and foraminifera living deeper in the water column, tended to have denser shells. We speculate that this is likely due to their life cycle, meaning that as pteropods and foraminifera get older they also tend to migrate deeper. Pteropods and foraminifera continuously calcify throughout their lives, with planktonic foraminifera adding additional layers of calcium carbonate ("ontogenetic secondary calcification"), therefore it is logical that the older specimens found in deeper waters are also denser. Planktonic foraminifera from surface sediments that had gametogenic calcite were more likely to remain intact in the sediments, i.e. not dissolve. We also found clear inter-species differences in shell density between *N. pachyderma* and *T. quinqueloba*. *N. pachyderma* tended to be both thicker and denser than *T. quinqueloba*, meaning that their preservation potential is greater, making it possible for the sediment record to be biased towards *N. pachyderma.* Some specimens of *T. quinqueloba* that were found in the 200–300 m depth interval had undergone internal dissolution. We hypothesize that the internal dissolution of *T. quinqueloba* is due to gamete formation and release.

Thickening of the shell apex with increasing number of whorls was found in *L. helicina*. This suggests that *L. helicina* are more resilient to ocean acidification as they grow larger and migrate to deeper water depths.

Highlights:
- The discovery of the natural variation in shell density is significant because planktonic foraminifera and shelled pteropods, specifically the density of their shells, are commonly used as biological indicators to identify declining habitat suitability owing to ocean acidification.
- Sampling depth and ontogenetic stage must be taken into consideration when using their shells as indicators for ocean acidification effects.
- Comparison between CT number and shell thickness can be used as a tool to identify planktonic foraminiferal shells, which have undergone either post-depositional dissolution or calcified in low $\Omega_{calcite}$ waters.

## 4.3 Paper III

Northeast Greenland planktonic foraminiferal fauna: present distribution patterns and paleo-perspectives
*Ofstad, S., Meilland, J., Rasmussen, T. L., Zamelczyk, K. and Seidenkrantz, M.S.*
(Under review in Frontiers in Marine Science)

For this manuscript we aimed at presenting an inventory of the planktonic foraminiferal faunas living over the Northeast Greenland shelf ((NEGS), 74° N–80°). Plankton tows were taken in September 2017 during the annual sea-ice minimum. A study this extensive has never been done before in this rapidly changing environment. Surface sediment samples were also taken at each station and compared to the overlying water column. Environmental parameters were sampled and recorded at each station, to shed light on what dictates spatial distribution of planktonic foraminifera on the NEGS.

Our data revealed high spatial heterogeneity and moderate to low abundances both in the water column (0–313 ind./m$^3$) and surface sediments (0–5500 ind./g (dry weight sediment)). Maximum abundance of planktonic foraminifera was found in the relatively fresh Polar surface Water (28.3–32.3) at 0–100 m in the water column. Five species were identified both in the water column and in the surface sediments: *Neogloboquadrina pachyderma*, *Turborotalita quinqueloba*, *Neogloboquadrina incompta*, *Globigerinita glutinata* and *Globigerina bulloides*. Unsurprisingly, *N. pachyderma* made up 86.2 % of the planktonic foraminifera fauna in the water column and 93.2 % of the recently settled. The second-most abundant species on the NEGS is *T. quinqueloba*, which made up 11.5 % of the planktonic foraminiferal faunas in the water column and 4.2 % of the recently settled. The larger percentage of *T. quinqueloba* in the water column is speculated to be due to the time of year of sampling. Previous studies have shown that the more Atlantic Water present in the Fram Strait the higher the percentage of *T. quinqueloba* (Jensen, 1998; Pados and Spielhagen, 2014; Volkmann, 2000).

Compared to previous studies, there is a lower percentage of *N. pachyderma* in the surface sediments. This may be a sign of Atlantification of the NEGS due to the higher temperature and increased presence of Atlantic water in the Fram Strait (Beszczynska-Møller et al., 2012; Karcher et al., 2003; Polyakov et al., 2017).

Highlights:

- The planktonic foraminiferal community on the Northeast Greenland shelf is characterized as highly heterogeneous in terms of standing stock.

- *N. pachyderma* proved to live in low salinity waters (28.3–32.3).

- Comparisons between surface sediment and plankton samples suggest no drastic changes in the assemblages over the last decades, yet there is a slightly lower percentage of the polar species *N. pachyderma* (93.2%) in the surface sediments compared to datasets from 1985-1987 (99%).

# 5   Significance of the study, concluding remarks and outlook

Knowledge of the distribution patterns and abundance of living planktonic foraminifera and pteropods in the Arctic and of the controlling environmental factors on the faunas is still limited. However, the conclusions of this thesis have greatly improved the current state of knowledge. All studies included in this thesis are entirely new and unprecedented studies/study areas, and plankton tows and sediments were collected from unexplored and highly dynamic regions and environments (**Paper I** and **Paper III**), which provide baseline datasets for future studies. Furthermore, new technology was used to shed light on the elusive calcification processes and preservation patterns in the sediment (**Paper II**). The results of this thesis have benefitted society by improving our ability to:

1. Predict how marine calcifiers will respond to future climate change.
2. Monitor the impacts of ocean acidification on the ecology of key marine calcifiers.
3. Make high precision paleo-reconstructions, which in turn increases our understanding and foresight of the ongoing climate change.

Due to the pioneering character of the investigations performed in this thesis it must be emphasized here that some conclusions may be only tentative and to some extent speculative. However, the results will constitute an important fundament for future studies as presented below.

Besides the papers written as part of this thesis, there are only a few recent studies of living planktonic foraminifera and shelled pteropod faunas in the high Arctic (e.g., Anglada-Ortiz et al., 2021; Kacprzak et al., 2017; Meilland et al., 2020; Pados and Spielhagen, 2014). Due to the sparseness of data from this region, our interpretations of environmental and faunal changes and development will require more studies in the future in order to be fully validated. This thesis has shown that the Fram Strait-Barents Sea region is characterized by low species diversity of the planktonic foraminiferal faunas, where *Neogloboquadrina pachyderma* dominates in Polar Water (**Paper III**) and *Turborotalita quinqueloba* dominates in Atlantic Water (**Paper I**). There may be a decrease in the relative abundance of *N. pachyderma* on the Northeast Greenland shelf compared to studies from the 1990s (**Paper III**), and sub-tropical species can be found in the Barents Sea (**Paper I**). Planktonic foraminifera and pteropods have a distinct vertical shell density gradient (**Paper II**) and are not affected by intense methane seepage even in the relatively shallow Barents Sea (**Paper I**). Planktonic

foraminifera and shelled pteropods from our study areas have a low standing stock in spring and a medium to high standing stock in summer (**Paper I** and **Paper III**). Furthermore, this thesis has helped in filling gaps in research into the impacts of ocean acidification in the Arctic, especially pertaining to methane release from dissociation of methane hydrates (**Paper I** and **Paper II**). There has been no previous research focusing on how methane seepage affects ocean carbonate chemistry and planktonic calcifiers in terms of decreased pH (i.e., acidification potential), which will only play an increasingly larger role in ocean acidification as the temperatures in the Arctic Ocean continue to rise and cause further destabilization of gas hydrates. Lastly, we have been able to show that planktonic foraminifera and pteropods in the same size class captured from the same location and depth interval have a wide range of shell densities (**Paper II**). The same is also true for planktonic foraminifera found in surface sediments (**Paper II**). These two points may complicate geochemical or ocean acidification studies.

## 5.1 Future work

### 5.1.1 Time series and interdisciplinary studies

The results from this thesis are comprised mainly of snapshots, with the exception of **Paper I**, which shows a transect sampled on a seasonal basis. Therefore, interpretations can only be tentative. Many of the unknowns about extant planktonic foraminifera are surrounding topics, which can only be properly resolved by time series data. Pteropods are usually included in arctic zooplankton studies/time series (Berge et al., 2014; Daase and Eiane, 2007; Kosobokova et al., 2011), likely due to their larger size (mesoplankton). Examples of these unknowns are ecological interactions concerning planktonic foraminifera are their trophic behaviors (Greco et al., 2020), life cycle and reproduction (Caron et al., 1990; Hamilton et al., 2008; Meilland et al., 2021; Takagi et al., 2020), and seasonality (Chernihovsky et al., 2020). Planktonic foraminifera tend to be studied in isolation, and not in conjunction with other zooplankton groups, this issue is discussed in depth by Jonkers et al. (2021). In polar regions, zooplankton studies are mainly focused on Calanoid copepods, that due to their high lipid content are very important constituents of the food chain (Falk-Petersen et al., 2009). More zooplankton studies should include planktonic foraminifera in order to get a holistic view of the marine ecosystem. Interdisciplinary studies, specifically collaboration between micropaleontologists (specialists in foraminifera) and marine biologists/ecologists, should also increase. By getting a more complete picture of the marine ecosystem, we will strengthen our ability to predict future changes.

Ideally, the study of extant planktonic foraminifera will become a more mainstream topic for marine biologists, which would bridge the gap between modern time series and paleo-studies.

## 5.1.2   Sampling in dynamic areas

This thesis has shown that there are already changes in the planktonic foraminiferal community in the Barents Sea (**Paper I**) and the Northeast Greenland shelf (**Paper III**). These changes in assemblages could be a sign of 'Atlantification', which occurs when there is an increase in both volume and temperature of inflowing Atlantic Water to a region, introducing more Atlantic species and increasing the likelihood that they will survive in that area. Regular plankton net sampling and CTD casts in these sensitive and dynamic areas would provide a better understanding of the ongoing shifts in the planktonic foraminiferal community, and how the pteropod *Limacina helicina* will respond in terms of their ecology and calcification. Increased sampling in regions exposed to Atlantification would also improve ecosystem models focused on predicting how zooplankton will respond to future climate change. UiT - The Arctic University of Norway in Tromsø has an exceptional location that is often referred to as the "Arctic Gateway", in addition to multiple seagoing vessels, making it one of the only institutes capable of achieving regular sampling in the high Arctic. These sampling efforts by UiT and other research institutions in Tromsø (The Institute of Marine Research and The Norwegian Polar Institute) should continue into the future and will provide valuable data for the marine calcifiers community and researchers focusing on Arctic zooplankton and marine ecosystems, and biological responses to ocean acidification.

## 5.1.3   Plankton net mesh size

Planktonic foraminifera and shelled pteropods are always present in the ocean. As ecological conditions change, small (juvenile, dormant, or resting) stages of some species may profit and start growing to become large enough to be sampled by plankton nets of a certain mesh size (e.g., 63 μm). Future studies should continue using a 63-μm mesh to capture the entirety of the community which can be identified. Many older studies used a mesh size as large as 180 μm, making it difficult to assess changes in absolute abundances and species composition through time. By using a larger mesh-size than 63 μm one could miss smaller species and juvenile and intermediate (neanic) stages.

### 5.1.4 Quantifying the effects of ocean acidification

In terms of resolving the effects of current climate change on shelled pteropods and planktonic foraminifera, it is important to have more long-term in situ studies of different $CaCO_3$ saturation states in relation to physical parameters of aragonite and calcite shells. By doing so, one could link their biological response (calcification and growth) to changes in ocean chemistry, i.e., ocean acidification. Longer studies would provide an even greater insight into the natural variability in shell density. This knowledge is important in order to use planktonic foraminifera and *Limacina helicina* as biological indicators for ocean acidification and to predict future developments in Arctic zooplankton dynamics, and when using planktonic foraminifera as paleo-proxies. Furthermore, it would be extremely valuable if any future living planktonic foraminifera and *Limacina helicina* samples used the XMCT method to assess shell density (**Paper II**). A common analytical method would allow a direct comparison between sites and water masses. The shell density data (**Paper II**) will hopefully contribute to decadal scale studies assessing the sensitivity of foraminifera and shelled pteropods to ocean acidification and contributing to ocean acidification models. The inter-species differences in shell density provokes the question of how species are affected by post-depositional dissolution and alteration (**Paper II**). Also, a significant range in shell density was found in the surface sediments (**Paper II**). There should be further research into the preservation potentials of different species. It is possible that *N. pachyderma* are very overrepresented in the Arctic sedimentary records due to their more robust shell. Furthermore, not much is known about how the internal chambers are affected by gametogenesis, and why some reproduce sexually (leading to gamete release and at times, secondary calcification) and others asexually. It is likely that gametogenic calcification increases preservation potential in the sedimentary record.

Studies that attempt to document changes in shell thickness over time using historical plankton tow samples and comparing them to present day, must also take sampling depth into consideration (Fox et al., 2020). This is because ontogenetic vertical migration may be present (**Paper II**, Meilland et al., 2021), meaning thicker and denser shells could be more concentrated at deeper water depth intervals, and vice versa. If this is not considered, studies could show an increase or decrease in shell thickness/density over time that does not exist. Lastly, and in the same reign, future studies which use planktonic foraminifera from surface sediment as a source of pre-industrial specimens to quantify

effects of anthropogenic climate change (de Moel et al., 2009; Moy et al., 2009), should be aware that there could be a bias towards thicker shells in the surface sediments (**Paper II**).

# 6  References

Aldridge, D., Beer, C. J. and Purdie, D. A.: Calcification in the planktonic foraminifera Globigerina bulloides linked to phosphate concentrations in surface waters of the North Atlantic Ocean, Biogeosciences, 9(5), 1725–1739, doi:10.5194/bg-9-1725-2012, 2012.

Andreassen, K., Hubbard, A., Winsborrow, M. C. M., Patton, H., Vadakkepuliyambatta, S., Plaza-Faverola, A., Gudlaugsson, E., Serov, P., Deryabin, A., Mattingsdal, R., Mienert, J. and Bünz, S.: Massive blow-out craters formed by hydrate-controlled methane expulsion from the Arctic seafloor, Science (80-. )., 356(6341), 948–953, doi:10.1126/science.aal4500, 2017.

Andrews, A. J., Christiansen, J. S., Bhat, S., Lynghammar, A., Westgaard, J. I., Pampoulie, C. and Præbel, K.: Boreal marine fauna from the Barents Sea disperse to Arctic Northeast Greenland, Sci. Rep., 9(1), 1–9, doi:10.1038/s41598-019-42097-x, 2019.

Anglada-Ortiz, G., Zamelczyk, K., Meilland, J., Ziveri, P., Chierici, M., Fransson, A. and Rasmussen, T. L.: Planktic Foraminiferal and Pteropod Contributions to Carbon Dynamics in the Arctic Ocean (North Svalbard Margin), Front. Mar. Sci., 8(June), doi:10.3389/fmars.2021.661158, 2021.

Ardyna, M., Babin, M., Gosselin, M., Devred, E., Bélanger, S., Matsuoka, A. and Tremblay, J. E.: Parameterization of vertical chlorophyll a in the Arctic Ocean: Impact of the subsurface chlorophyll maximum on regional, seasonal, and annual primary production estimates, Biogeosciences, 10(6), 4383–4404, doi:10.5194/bg-10-4383-2013, 2013.

Arndt, J. E., Jokat, W., Dorschel, B., Myklebust, R., Dowdeswell, J. A. and Evans, J.: A new bathymetry of the Northeast Greenland continental shelf: Constraints on glacial and other processes, Geochemistry Geophys. Geosystems, 16(10), 3733–3753, doi:10.1002/2015GC005931, 2015.

Arrigo, K. R. and van Dijken, G. L.: Continued increases in Arctic Ocean primary production, Prog. Oceanogr., 136, 60–70, doi:10.1016/j.pocean.2015.05.002, 2015.

Arrigo, K. R., Robinson, D. H., Worthen, D. L., Dunbar, R. B., DiTullio, G. R., VanWoert, M. and Lizotte, M. P.: Phytoplankton Community Structure and the Drawdown of Nutrients and CO&lt;sub&gt;2&lt;/sub&gt; in the Southern Ocean, Science (80-. )., 283(5400), 365 LP – 367, doi:10.1126/science.283.5400.365, 1999.

Atkinson, A., Shreeve, R. S., Pakhomov, E. A., Priddle, J., Blight, S. P. and Ward, P.: Zooplankton response to a phytoplankton bloom near South Georgia, Antarctica, Mar. Ecol. Prog. Ser., 144(1–3), 195–210, doi:10.3354/meps144195, 1996.

Barker, S. and Elderfield, H.: Foraminiferal Calcification Response to Glacial-Interglacial Changes in Atmospheric CO2, Science (80-. )., 297(5582), 833–836, doi:10.1126/science.1072815, 2002.

Bathmann, U. V., Noji, T. T. and von Bodungen, B.: Sedimentation of pteropods in the Norwegian Sea in autumn, Deep. Res., 38(10), 1341–1360, doi:10.1016/0198-0149(91)90031-A, 1991.

Bé, A. W. H., Hutson, W. H. and Be, A. W. H.: Ecology of Planktonic Foraminifera and Biogeographic Patterns of Life and Fossil Assemblages in the Indian Ocean, Micropaleontology, 23(4), 369, doi:10.2307/1485406, 1977.

Beaugrand, G., Mcquatters-Gollop, A., Edwards, M. and Goberville, E.: Long-term responses of North Atlantic calcifying plankton to climate change, Nat. Clim. Chang., 3(3), 263–267, doi:10.1038/nclimate1753, 2013.

Bednaršek, N. and Ohman, M. D.: Changes in pteropod distributions and shell dissolution across a frontal system in the California Current System, Mar. Ecol. Prog. Ser., 523, 93–103, doi:10.3354/meps11199, 2015.

Bednaršek, N., Tarling, G. A., Bakker, D. C. E., Fielding, S., Jones, E. M., Venables, H. J., Ward, P., Kuzirian, A., Lézé, B., Feely, R. A. and Murphy, E. J.: Extensive dissolution of live pteropods in the Southern Ocean, Nat. Geosci., 5(12), 881–885, doi:10.1038/ngeo1635, 2012.

Bednaršek, N., Tarling, G. A., Bakker, D. C. E., Fielding, S. and Feely, R. A.: Dissolution dominating calcification process in polar pteropods close to the point of aragonite undersaturation, PLoS One, 9(10), doi:10.1371/journal.pone.0109183, 2014.

Bednaršek, N., Feely, R. A., Tolimieri, N., Hermann, A. J., Siedlecki, S. A., Waldbusser, G. G., McElhany, P., Alin, S. R., Klinger, T., Moore-Maley, B. and Pörtner, H. O.: Exposure history determines pteropod vulnerability to ocean acidification along the US West Coast article, Sci. Rep., 7(1), 1–12, doi:10.1038/s41598-017-03934-z, 2017a.

Bednaršek, N., Klinger, T., Harvey, C. J., Weisberg, S., McCabe, R. M., Feely, R. A., Newton, J. and Tolimieri, N.: New ocean, new needs: Application of pteropod shell dissolution as a biological indicator for marine resource management, Ecol. Indic., 76, 240–244, doi:10.1016/j.ecolind.2017.01.025, 2017b.

Beer, C. J., Schiebel, R. and Wilson, P. A.: Testing planktic foraminiferal shell weight as a surface water [CO2-3] proxy using plankton net samples, Geology, 38(2), 103–106, doi:10.1130/G30150.1, 2010.

Berge, J., Cottier, F., Varpe, Ø., Renaud, P. E., Falk-Petersen, S., Kwasniewski, S., Griffiths, C., Søreide, J. E., Johnsen, G., Aubert, A., Bjærke, O., Hovinen, J., Jung-Madsen, S., Tveit, M. and Majaneva, S.: Arctic complexity: A case study on diel vertical migration of zooplankton, J. Plankton Res., 36(5), 1279–1297, doi:10.1093/plankt/fbu059, 2014.

Berger, W. H. and Parker, F. L.: Diversity of Planktonic Foraminifera in Deep-Sea Sediments, Science (80-. )., 168(3937), 1345 LP – 1347, doi:10.1126/science.168.3937.1345, 1970.

Beszczynska-Møller, A., Fahrbach, E., Schauer, U. and Hansen, E.: Variability in Atlantic water temperature and transport at the entrance to the Arctic Ocean, 1997–2010, ICES, 69(5), 852–863, doi:10.1093/icesjms/fss056, 2012.

Biastoch, A., Treude, T., Rüpke, L. H., Riebesell, U., Roth, C., Burwicz, E. B., Park, W., Latif, M., Böning, C. W., Madec, G. and Wallmann, K.: Rising Arctic Ocean temperatures cause gas hydrate destabilization and ocean acidification, Geophys. Res. Lett., 38(8), doi:10.1029/2011GL047222, 2011.

Bijma, J., Erez, J. and Hemleben, C.: Lunar and semi-lunar reproductive cycles in some spinose planktonic foraminifers, J. Foraminifer. Res., 20(2), 117–127, doi:10.2113/gsjfr.20.2.117, 1990.

Bjørklund, K. R., Kruglikova, S. B. and Anderson, O. R.: Modern incursions of tropical Radiolaria into the Arctic Ocean, J. Micropalaeontology, 31(2), 139–158, doi:10.1144/0262-821X11-030, 2012.

Blachowiak-Samolyk, K., Søreide, J. E., Kwasniewski, S., Sundfjord, A., Hop, H., Falk-Petersen, S. and Nøst Hegseth, E.: Hydrodynamic control of mesozooplankton abundance and biomass in northern Svalbard waters (79-81°N), Deep. Res. Part II Top. Stud. Oceanogr., 55(20–21), 2210–2224, doi:10.1016/j.dsr2.2008.05.018, 2008.

Blindheim, J. and Østerhus, S.: The Nordic Seas, Main Oceanographic Features, Nord. Seas An

Integr. Perspect., 11–37, doi:doi:10.1029/158GM03, 2005.

Boissonnot, L., Niehoff, B., Ehrenfels, B., Søreide, J. E., Hagen, W. and Graeve, M.: Lipid and fatty acid turnover of the pteropods Limacina helicina, L. Retroversa and Clione limacina from Svalbard waters, Mar. Ecol. Prog. Ser., 609(June 2019), 133–149, doi:10.3354/meps12837, 2019.

Boissonnot, L., Kohnert, P., Ehrenfels, B., Søreide, J. E., Graeve, M., Stübner, E., Schrödl, M. and Niehoff, B.: Year-round population dynamics of Limacina spp. early stages in a high-Arctic fjord (Adventfjorden, Svalbard), Polar Biol., doi:10.1007/s00300-021-02904-6, 2021.

Brandner, M. M., Stübner, E., Reed, A. J., Gabrielsen, T. M. and Thatje, S.: Seasonality of bivalve larvae within a high Arctic fjord, Polar Biol., 40(2), 263–276, doi:10.1007/s00300-016-1950-x, 2017.

Brown, N. E. M., Bernhardt, J. R., Anderson, K. M. and Harley, C. D. G.: Increased food supply mitigates ocean acidification effects on calcification but exacerbates effects on growth, Sci. Rep., 8(9800), doi:10.1038/s41598-018-28012-w, 2018.

Brummer, G. J. A. and Kroon, D.: Planktonic foraminifers as tracers of ocean-climate history, Free University Press, Amsterdam., 1988.

Caron, D. A., Anderson, O. R., Lindsey, J. L., Faber, W. W. and Lin, E. E.: Effects of Gametogenesis on Test Structure and Dissolution of Some Spinose Planktonic Foraminifera and Implications for Test Preservation, Mar. Micropaleontol., 16(1–2), 93–116, doi:10.1016/0377-8398(90)90031-G, 1990.

Caron, M. and Homewood, P.: Evolution of early planktic foraminifers, Mar. Micropaleontol., 7(6), 453–462, doi:10.1016/0377-8398(83)90010-5, 1983.

Carstens, J., Hebbeln, D. and Wefer, G.: Distribution of planktic foraminifera at the ice margin in the Arctic (Fram Strait), Mar. Micropaleontol., 29(3–4), 257–269, doi:10.1016/S0377-8398(96)00014-X, 1997.

Cayre, O., Lancelot, Y., Vincent, E. and Hall, M. A.: Paleoceanographic reconstructions from planktonic foraminifera off the Iberian Margin: Temperature, salinity, and Heinrich events, Paleoceanography, 14(3), 384–396, doi:10.1029/1998PA900027, 1999.

Charlson, R. J., Lovelock, J. E., Andreae, M. O. and Warren, S. G.: Oceanic phytoplankton, atmospheric sulphur, cloud albedo and climate, Nature, 326(6114), 655–661, doi:10.1038/326655a0, 1987.

Cherkasheva, A., Bracher, A., Melsheimer, C., Köberle, C., Gerdes, R., Nöthig, E. M., Bauerfeind, E. and Boetius, A.: Influence of the physical environment on polar phytoplankton blooms: A case study in the Fram Strait, J. Mar. Syst., 132, 196–207, doi:10.1016/j.jmarsys.2013.11.008, 2014.

Chernihovsky, N., Almogi-Labin, A., Kienast, S. S. and Torfstein, A.: The daily resolved temperature dependence and structure of planktonic foraminifera blooms, Sci. Rep., 10(1), 1–13, doi:10.1038/s41598-020-74342-z, 2020.

Comeau, S., Jeffree, R., Teyssie, J. L. and Gattuso, J. P.: Response of the arctic pteropod Limacina helicina to projected future environmental conditions, PLoS One, 5(6), 1–7, doi:10.1371/journal.pone.0011362, 2010.

Consolaro, C., Rasmussen, T. L., Panieri, G., Mienert, J., Bünz, S. and Sztybor, K.: Carbon isotope (d13C) excursions suggest times of major methane release during the last 14 kyr in Fram Strait, the deep-water gateway to the Arctic, Clim. Past, 11(4), 669–685, doi:10.5194/cp-11-669-2015, 2015.

Cooke, S. and Rohling, E. J.: Stable isotopes in foraminiferal carbonate, in Modern Foraminifera, pp.

239–258, Springer, Dordrecht., 1999.

Crenshaw, M. A.: The inorganic composition of molluscan extrapallial fluid, Biol. Bull., 143(3), 506–512, doi:10.2307/1540180, 1972.

Daase, M. and Eiane, K.: Mesozooplankton distribution in northern Svalbard waters in relation to hydrography, Polar Biol., 30(8), 969–981, doi:10.1007/s00300-007-0255-5, 2007.

Dadon, J. R. and Cidre, L. L. De: The reproductive cycle of the Thecosomatous pteropod Limacina retroversa in the western South Atlantic, Mar. Biol., 442(114), 439–442, doi:10.1007/BF00350035, 1992.

Davis, C. V., Livsey, C. M., Palmer, H. M., Hull, P. M., Thomas, E., Hill, T. M. and Benitez-Nelson, C. R.: Extensive morphological variability in asexually produced planktic foraminifera, Sci. Adv., 6(28), 1–8, doi:10.1126/sciadv.abb8930, 2020.

Duplessy, J. C., Labeyrie, L., Juillet-Leclerc, A., Maitre, F., Duprat, J. and Sarnthein, M.: Surface salinity reconstruction of the North Atlantic Ocean during the Last Glacial maximum, Oceanol. Acta, 14(4), 311–324, 1991.

Duplessy, J. C., Labeyrie, L. D. and Paterne, M.: North Atlantic sea surface conditions during the Younger Dryas cold event, Geol. Soc. Spec. Publ., 111(January 1996), 167–175, doi:10.1144/GSL.SP.1996.111.01.11, 1996.

Erez, J.: The Source of Ions for Biomineralization in Foraminifera and Their Implications for Paleoceanographic Proxies, Rev. Mineral. Geochemistry, 54(1), 115–149, doi:10.2113/0540115, 2003.

Erez, J., Almogi-Labin, A. and Avraham, S.: On the Life History of Planktonic Foraminifera: Lunar Reproduction Cycle in Globigerinoides Sacculifer (Brady), Paleoceanography, 6(3), 295–306, doi:10.1029/90PA02731, 1991.

Eynaud, F., De Abreu, L., Voelker, A., Schönfeld, J., Salgueiro, E., Turon, J. L., Penaud, A., Toucanne, S., Naughton, F., Sánchez Goñi, M. F., Malaizé, B. and Cacho, I.: Position of the Polar Front along the western Iberian margin during key cold episodes of the last 45 ka, Geochemistry, Geophys. Geosystems, 10(7), doi:10.1029/2009GC002398, 2009.

Fabry, V., McClintock, J., Mathis, J. and Grebmeier, J.: Ocean Acidification at High Latitudes: The Bellwether, Oceanography, 22(4), 160–171, doi:10.5670/oceanog.2009.105, 2009.

Fabry, V. J., Seibel, B. A., Feely, R. A. and Orr, J. C.: Impacts of ocean acidification on marine fauna and ecosystem processes, ICES J. Mar. Sci., 65(3), 414–432, doi:10.1093/icesjms/fsn048, 2008.

Falk-Petersen, S., Leu, E., Berge, J., Kwasniewski, S., Nygård, H., Røstad, A., Keskinen, E., Thormar, J., von Quillfeldt, C., Wold, A. and Gulliksen, B.: Vertical migration in high Arctic waters during autumn 2004, Deep. Res. Part II Top. Stud. Oceanogr., 55(20–21), 2275–2284, doi:10.1016/j.dsr2.2008.05.010, 2008.

Falk-Petersen, S., Mayzaud, P., Kattner, G. and Sargent, J. R.: Lipids and life strategy of Arctic *Calanus*, Mar. Biol. Res., 5(1), 18–39, doi:10.1080/17451000802512267, 2009.

Feely, R. A., Alin, S. R., Carter, B., Bednaršek, N., Hales, B., Chan, F., Hill, T. M., Gaylord, B., Sanford, E., Byrne, R. H., Sabine, C. L., Greeley, D. and Juranek, L.: Chemical and biological impacts of ocean acidification along the west coast of North America, Estuar. Coast. Shelf Sci., 183, 260–270, doi:10.1016/j.ecss.2016.08.043, 2016.

Fossheim, M., Primicerio, R., Johannesen, E., Ingvaldsen, R. B., Aschan, M. M. and Dolgov, A. V.: Recent warming leads to a rapid borealization of fish communities in the Arctic, Nat. Clim. Chang., 5(7), 673–677, doi:10.1038/nclimate2647, 2015.

Foster, G. L. and Rae, J. W. B.: Reconstructing Ocean pH with Boron Isotopes in Foraminifera, Annu. Rev. Earth Planet. Sci., 44, 207–237, doi:10.1146/annurev-earth-060115-012226, 2016.

Fox, L., Stukins, S., Hill, T. and Miller, C. G.: Quantifying the Effect of Anthropogenic Climate Change on Calcifying Plankton, Sci. Rep., 10(1620), 1–9, doi:10.1038/s41598-020-58501-w, 2020.

El Frihmat, Y., Hebbeln, D., Jaaidi, E. B. and Mhammdi, N.: Reconstruction of productivity signal and deep-water conditions in Moroccan Atlantic margin (~35°N) from the last glacial to the Holocene, Springerplus, 4(1), doi:10.1186/s40064-015-0853-6, 2015.

Gannefors, C., Böer, M., Kattner, G., Graeve, M., Eiane, K., Gulliksen, B., Hop, H. and Falk-Petersen, S.: The Arctic sea butterfly Limacina helicina: Lipids and life strategy, Mar. Biol., 147(1), 169–177, doi:10.1007/s00227-004-1544-y, 2005.

Gardner, J.: Winners and losers in a changing ocean: Impact on the physiology and life history of pteropods in the Scotia Sea; Southern Ocean, Univeristy of East Anglia. [online] Available from: https://ueaeprints.uea.ac.uk/id/eprint/71886/, 2019.

Gonzalez-Mora, B., Sierro, F. J. and Flores, J. A.: Controls of shell calcification in planktonic foraminifers, Quat. Sci. Rev., 27, 956–961, doi:10.1016/j.quascirev.2008.01.008, 2008.

Greco, M., Jonkers, L., Kretschmer, K., Bijma, J. and Kucera, M.: Variable habitat depth of the planktonic foraminifera Neogloboquadrina pachyderma in the northern high latitudes explained by sea-ice and chlorophyll concentration, Biogeosciences, 16(17), 3425–3437, doi:10.5194/bg-16-3425-2019, 2019.

Greco, M., Morard, R. and Kucera, M.: Single-cell metabarcoding reveals biotic interactions of the Arctic calcifier Neogloboquadrina pachyderma with the eukaryotic pelagic community, bioRxiv, (March), doi:10.1101/2020.10.20.347930, 2020.

Hamilton, C. P., Spero, H. J., Bijma, J. and Lea, D. W.: Geochemical investigation of gametogenic calcite addition in the planktonic foraminifera Orbulina universa, Mar. Micropaleontol., 68(3–4), 256–267, doi:10.1016/j.marmicro.2008.04.003, 2008.

Head, E. J. H. and Pepin, P.: Spatial and inter-decadal variability in plankton abundance and composition in the Northwest Atlantic (1958-2006), J. Plankton Res., 32(12), 1633–1648, doi:10.1093/plankt/fbq090, 2010.

Hettinger, A., Sanford, E., Hill, T. M., Hosfelt, J. D., Russell, A. D. and Gaylord, B.: The influence of food supply on the response of Olympia oyster larvae to ocean acidification, Biogeosciences, 10(10), 6629–6638, doi:10.5194/bg-10-6629-2013, 2013.

Howes, E. L., Stemmann, L., Assailly, C., Irisson, J. O., Dima, M., Bijma, J. and Gattuso, J. P.: Pteropod time series from the North Western Mediterranean (1967-2003): Impacts of pH and climate variability, Mar. Ecol. Prog. Ser., 531, 193–206, doi:10.3354/meps11322, 2015.

Howes, E. L., Eagle, R. A., Gattuso, J. P. and Bijma, J.: Comparison of Mediterranean pteropod shell biometrics and ultrastructure from historical (1910 and 1921) and present day (2012) samples provides baseline for monitoring effects of global change, PLoS One, 12(1), 1–23, doi:10.1371/journal.pone.0167891, 2017.

Hunt, B. P. V., Pakhomov, E. A., Hosie, G. W., Siegel, V., Ward, P. and Bernard, K.: Pteropods in Southern Ocean ecosystems, Prog. Oceanogr., 78(3), 193–221, doi:10.1016/j.pocean.2008.06.001, 2008.

Husum, K. and Hald, M.: Arctic planktic foraminiferal assemblages: Implications for subsurface temperature reconstructions, Mar. Micropaleontol., 96–97(December), 38–47, doi:10.1016/j.marmicro.2012.07.001, 2012.

Imbrie, J. and Kipp, N. G.: A new micropaleontological method for quantitative paleoclimatology: application to a Late Pleistocene Caribbean core, in The Late Cenozoic Glacial Ages, edited by K. K. Turekian, pp. 77–181, Yale University Press, New Haven., 1971.

IPCC: Ocean, cryosphere, and sea level change, in Climate Change 2021: The Physical Science Basis. Contribution of Working Group I to the Sixth Assessment Report of the Intergovernmental Panel on Climate Change, edited by V. Masson-Delmotte, P. Zhai, A. Pirani, S. L. Connors, C. Péan, S. Berger, N. Caud, Y. Chen, L. Goldfarb, M. I. Gomis, M. Huang, K. Leitzell, E. Lonnoy, J. B. R. Matthews, T. K. Maycock, T. Waterfield, O. Yelekçi, R. Yu, and B. Zhou, p. 271, Cambridge University Press, Cambridge. [online] Available from: https://www.ipcc.ch/report/ar6/wg1/downloads/report/IPCC_AR6_WGI_Chapter_09.pdf, 2021.

Iversen, N. and Jorgensen, B. B.: Anaerobic methane oxidation rates at the sulfate-methane transition in marine sediments from Kattegat and Skagerrak (Denmark), Limnol. Oceanogr., 30(5), 944–955, doi:10.4319/lo.1985.30.5.0944, 1985.

Iwasaki, S., Kimoto, K., Sasaki, O., Kano, H., Honda, M. C. and Okazaki, Y.: Observation of the dissolution process of Globigerina bulloides tests (planktic foraminifera) by X-ray microcomputed tomography, Paleoceanography, 30(4), 317–331, doi:10.1002/2014PA002639, 2015.

Iwasaki, S., Kimoto, K., Okazaki, Y. and Ikehara, M.: Micro - CT Scanning of Tests of Three Planktic Foraminiferal Species to Clarify Dissolution Process and Progress, J. Geophys. Res. Geochemistry, Geophys. Geosystems, 1–15, doi:10.1029/2019GC008456, 2019a.

Iwasaki, S., Kimoto, K., Sasaki, O., Kano, H. and Uchida, H.: Sensitivity of planktic foraminiferal test bulk density to ocean acidification, , (June), 1–9, doi:10.1038/s41598-019-46041-x, 2019b.

Jakobsson, M., Mayer, L., Coakley, B., Dowdeswell, J. A., Forbes, S., Fridman, B., Hodnesdal, H., Noormets, R., Pedersen, R., Rebesco, M., Schenke, H. W., Zarayskaya, Y., Accettella, D., Armstrong, A., Anderson, R. M., Bienhoff, P., Camerlenghi, A., Church, I., Edwards, M., Gardner, J. V, Hall, J. K., Hell, B., Hestvik, O., Kristoffersen, Y., Marcussen, C., Mohammad, R., Mosher, D., Nghiem, S. V, Pedrosa, M. T., Travaglini, P. G. and Weatherall, P.: The International Bathymetric Chart of the Arctic Ocean (IBCAO) Version 3.0, Geophys. Res. Lett., 39(12), doi:10.1029/2012GL052219, 2012.

Jennings, A. E. and Weiner, N. J.: Environmental change in eastern Greenland during the last 1300 years: Evidence from foraminifera and lithofacies in Nansen Fjord, 68°N, Holocene, 6(2), 179–191, doi:10.1177/095968369600600205, 1996.

Jensen, S.: Planktische Foraminiferen im Europäischen Nordmeer: Verbreitung und Vertikalfluß sowie ihre Entwicklung während der letzten 15000 Jahre, Berichte Sonderforschungsbereich 313, Univ. Kiel, 75(75), 1–105, 1998.

Johnstone, H. J. H., Schulz, M., Barker, S. and Elderfield, H.: Inside story: An X-ray computed tomography method for assessing dissolution in the tests of planktonic foraminifera, Mar. Micropaleontol., 77(1–2), 58–70, doi:10.1016/j.marmicro.2010.07.004, 2010.

Jonkers, L., Brummer, G. J. A., Peeters, F. J. C., Van Aken, H. M. and De Jong, M. F.: Seasonal stratification, shell flux, and oxygen isotope dynamics of leftcoiling N. pachyderma and T. quinqueloba in the western subpolar North Atlantic, Paleoceanography, 25(2), 1–13, doi:10.1029/2009PA001849, 2010.

Jonkers, L., Reynolds, C. E., Richey, J. and Hall, I. R.: Lunar periodicity in the shell flux of planktonic foraminifera in the Gulf of Mexico, Biogeosciences, 12(10), 3061–3070, doi:10.5194/bg-12-3061-2015, 2015.

Jonkers, L., Hillebrand, H. and Kučera, M.: Global change drives modern plankton communities away from the pre-industrial state, Nature, doi:10.1038/s41586-019-1230-3, 2019.

Jonkers, L., Meilland, J., Rillo, M. C., Kitchener, J. A. and Kucera, M.: Food for Thought: Linking zooplankton time series to the fossil record, ICES J. Mar. Sci., doi:10.1093/icesjms/fsab123, 2021.

Kacprzak, P., Panasiuk, A., Wawrzynek, J. and Weydmann, A.: Distribution and abundance of pteropods in the western Barents Sea, Oceanol. Hydrobiol. Stud., 46(4), 393–404, doi:10.1515/ohs-2017-0039, 2017.

Kahru, M., Brotas, V., Manzano-Sarabia, M. and Mitchell, B. G.: Are phytoplankton blooms occurring earlier in the Arctic?, Glob. Chang. Biol., 17(4), 1733–1739, doi:10.1111/j.1365-2486.2010.02312.x, 2011.

Karcher, M. J., Gerdes, R., Kauker, F. and Köberle, C.: Arctic warming: Evolution and spreading of the 1990s warm event in the Nordic seas and the Arctic Ocean, J. Geophys. Res. Ocean., 108(2), 1–16, doi:10.1029/2001jc001265, 2003.

Katz, M. E., Cramer, B. S., Franzese, A., Hönisch, B., Miller, K. G., Rosenthal, Y. and Wright, J. D.: Traditional and emerging geochemical proxies in foraminifera, J. Foraminifer. Res., 40(2), 165–192, doi:10.2113/gsjfr.40.2.165, 2010.

Kimoto, K.: Planktic Foraminifera, in Marine protists: diversity and dynamics, edited by S. Ohtsuka, T. Suzaki, T. Horiguchi, N. Suzuki, and F. Not, pp. 129–178, Springer Japan, Tokyo., 2015.

Kobayashi, H. A.: Growth Cycle and Related Vertical Distribution of the Thecosomatous Pteropod Spiratella (" Limacina ") helicina in the Central Arctic Ocean, Mar. Biol., 26, 295–301, doi:10.1007/BF00391513, 1974.

Kohfeld, K. E., Fairbanks, R. G., Smith, S. L. and Walsh, I. D.: Neogloboquadrina pachyderma (sinistral coiling) as paleoceanographic tracers in polar oceans: Evidence from Northeast Water Polynya plankton tows, sediment traps, and surface sediments, Paleoceanography, 11(6), 679–699, doi:10.1029/96PA02617, 1996.

Kosobokova, K. N., Hopcroft, R. R. and Hirche, H. J.: Patterns of zooplankton diversity through the depths of the Arctic's central basins, Mar. Biodivers., 41(1), 29–50, doi:10.1007/s12526-010-0057-9, 2011.

Kretschmer, K., Biastoch, A., Rüpke, L. and Burwicz, E.: Modeling the fate of methane hydrates under global warming, , 610–625, doi:10.1002/2014GB005011.Received, 2015.

Krüger, O. and Graßl, H.: Southern Ocean phytoplankton increases cloud albedo and reduces precipitation, Geophys. Res. Lett., 38(8), doi:https://doi.org/10.1029/2011GL047116, 2011.

Kucera, M., Weinelt, M., Kiefer, T., Pflaumann, U., Hayes, A., Weinelt, M., Chen, M. Te, Mix, A. C., Barrows, T. T., Cortijo, E., Duprat, J., Juggins, S. and Waelbroeck, C.: Reconstruction of sea-surface

temperatures from assemblages of planktonic foraminifera: Multi-technique approach based on geographically constrained calibration data sets and its application to glacial Atlantic and Pacific Oceans, Quat. Sci. Rev., 24(7-9 SPEC. ISS.), 951–998, doi:10.1016/j.quascirev.2004.07.014, 2005.

Kučera, M.: Chapter Six Planktonic Foraminifera as Tracers of Past Oceanic Environments, in Developments in Marine Geology, vol. 1, pp. 213–262., 2007.

Lalli, C. M. and Gilmer, R. W.: Pelagic Snails - The biology of holoplanktonic gastropod mollusks, Stanford University Press, Stanford, CA., 1989.

Lalli, C. M. and Wells, F. E.: Reproduction in the genus Limacina (Opisthobranchia Thecosomata), J. Zool., 186(1), 95–108, doi:10.1111/j.1469-7998.1978.tb03359.x, 1978.

Larson, R. J. and Harbison, G. R.: Source and Fate of Lipids in Polar Gelatinous Zooplankton, Arctic, 42(4), 339–346, doi:10.14430/arctic1675, 1989.

León, P., Bednaršek, N., Walsham, P., Cook, K., Hartman, S. E., Wall-Palmer, D., Hindson, J., MacKenzie, K., Webster, L. and Bresnan, E.: Relationship between shell integrity of pelagic gastropods and carbonate chemistry parameters at a Scottish Coastal Observatory monitoring site, ICES J. Mar. Sci., 77(1), 436–450, doi:10.1093/icesjms/fsz178, 2020.

Lischka, S. and Hagen, W.: Seasonal dynamics of mesozooplankton in the Arctic Kongsfjord (Svalbard) during year-round observations from August 1998 to July 1999, Polar Biol., 39(10), 1859–1878, doi:10.1007/s00300-016-2005-z, 2016.

Lischka, S. and Riebesell, U.: Synergistic effects of ocean acidification and warming on overwintering pteropods in the Arctic, Glob. Chang. Biol., 18(12), 3517–3528, doi:10.1111/gcb.12020, 2012.

Lischka, S., Büdenbender, J., Boxhammer, T. and Riebesell, U.: Impact of ocean acidification and elevated temperatures on early juveniles of the polar shelled pteropod Limacina helicina: Mortality, shell degradation, and shell growth, Biogeosciences, 8(4), 919–932, doi:10.5194/bg-8-919-2011, 2011.

Lombard, F., Da Rocha, R. E., Bijma, J. and Gattuso, J. P.: Effect of carbonate ion concentration and irradiance on calcification in planktonic foraminifera, Biogeosciences, 7(1), 247–255, doi:10.5194/bg-7-247-2010, 2010.

Lončarić, N., Brummer, G. J. A. and Kroon, D.: Lunar cycles and seasonal variations in deposition fluxes of planktic foraminiferal shell carbonate to the deep South Atlantic (central Walvis Ridge), Deep. Res. Part I Oceanogr. Res. Pap., 52(7), 1178–1188, doi:10.1016/j.dsr.2005.02.003, 2005.

MacKas, D. L. and Galbraith, M. D.: Pteropod time-series from the NE Pacific, ICES J. Mar. Sci., 69(3), 448–459, doi:10.1093/icesjms/fsr163, 2012.

Manno, C., Accornero, A. and Umani, S. F.: Importance of the contribution of Limacina helicina faecal pellets to the carbon pump in Terra Nova Bay (Antarctica), J. Plankton Res., 32(2), 145–152, doi:10.1093/plankt/fbp108, 2010.

Manno, C., Morata, N. and Bellerby, R.: Effect of ocean acidification and temperature increase on the planktonic foraminifer Neogloboquadrina pachyderma (sinistral), Polar Biol., 35(9), 1311–1319, doi:10.1007/s00300-012-1174-7, 2012.

Marshall, B. J., Thunell, R. C., Henehan, M. J., Astor, Y. and Wejnert, K. E.: Planktonic foraminiferal area density as a proxy for carbonate ion concentration: A calibration study using the Cariaco Basin ocean time series, Paleoceanography, 28(2), 363–376, doi:10.1002/palo.20034, 2013.

Meilland, J., Fabri-Ruiz, S., Koubbi, P., Monaco, C. Lo, Cotte, C., Hosie, G. W., Sanchez, S. and Howa, H.: Planktonic foraminiferal biogeography in the Indian sector of the Southern Ocean: Contribution from CPR data, Deep. Res. Part I Oceanogr. Res. Pap., 110, 75–89, doi:10.1016/j.dsr.2015.12.014, 2016.

Meilland, J., Schiebel, R., Lo Monaco, C., Sanchez, S. and Howa, H.: Abundances and test weights of living planktic foraminifers across the Southwest Indian Ocean: Implications for carbon fluxes, Deep. Res. Part I Oceanogr. Res. Pap., 131(March 2017), 27–40, doi:10.1016/j.dsr.2017.11.004, 2018.

Meilland, J., Siccha, M., Weinkauf, M. F. G., Jonkers, L. and Morard, R.: Highly replicated sampling reveals no species-specific vertical habitats in diurnal vertical migration but stable planktonic foraminifera, J. Plankton Res., 41(2), 127–141, doi:10.1093/zoolinnean/zly093, 2019.

Meilland, J., Howa, H., Hulot, V., Demangel, I., Salaün, J. and Garlan, T.: Population dynamics of modern planktonic foraminifera in the western Barents Sea, Biogeosciences, 17(6), 1437–1450, 2020.

Meilland, J., Siccha, M., Kaffenberger, M. and Bijma, J.: Population dynamics and reproduction strategies of planktonic foraminifera in the open ocean Population dynamics and reproduction strategies of planktonic foraminifera in the open ocean, , (August), doi:10.5194/bg-2021-141, 2021.

Mienert, J., Vanneste, M., Bünz, S., Andreassen, K., Haflidason, H. and Sejrup, H. P.: Ocean warming and gas hydrate stability on the mid-Norwegian margin at the Storegga Slide, edited by A. SOLHEIM, P. BRYN, K. BERG, H. P. SEJRUP, and J. B. T.-O. L. I. S. for S. F. D. in the S. S. A. MIENERT, pp. 233–244, Elsevier, Oxford., 2005.

Milliman, J. D.: Production and accumulation of calcium carbonate in the ocean: Budget of a nonsteady state, Global Biogeochem. Cycles, 7(4), 927–957, doi:https://doi.org/10.1029/93GB02524, 1993.

de Moel, H., Ganssen, G. M., Peeters, F. J. C., Jung, S. J. A., Kroon, D., Brummer, G. J. A. and Zeebe, R. E.: Planktic foraminiferal shell thinning in the Arabian Sea due to anthropogenic ocean acidification?, Biogeosciences, 6(9), 1917–1925, doi:10.5194/bg-6-1917-2009, 2009.

Moy, A. D., Howard, W. R., Bray, S. G. and Trull, T. W.: Reduced calcification in modern Southern Ocean planktonic foraminifera, Nat. Geosci., 2(4), 276–280, doi:10.1038/ngeo460, 2009.

Mucci, A.: The solubility of calcite and aragonite in seawater at various salinities, temperatures, and one atmosphere total pressure., Am. J. Sci., 283(7), 780–799, doi:10.2475/ajs.283.7.780, 1983.

Neukermans, G., Oziel, L. and Babin, M.: Increased intrusion of warming Atlantic water leads to rapid expansion of temperate phytoplankton in the Arctic, Glob. Chang. Biol., 24(6), 2545–2553, doi:10.1111/gcb.14075, 2018.

Nigam, R., Saraswat, R. and Mazumder, a: Life spans of planktonic foraminifers: New sight through sediment traps, J. Palaeontol. Soc. India, 48(April 2020), 129–133, 2003.

Oakes, R. L. and Sessa, J. A.: Assessing annual variability in the shell thickness of the pteropod Heliconoides inflatus in the Cariaco Basin using micro-CT scanning, , (October), 2019.

Oakes, R. L., Peck, V. L., Manno, C. and Bralower, T. J.: Degradation of Internal Organic Matter is the Main Control on Pteropod Shell Dissolution After Death, Global Biogeochem. Cycles, 33(6), 749–760, doi:10.1029/2019GB006223, 2019.

Osborne, E. B., Thunell, R. C., Marshall, B. J., Holm, J. A., Tapa, E. J., Benitez-Nelson, C., Cai, W.-J. and Chen, B.: Calcification of the planktonic foraminifera Globigerina bulloides and carbonate ion concentration: Results from the Santa Barbara Basin, Paleoceanography, 31(8), 1083–1102, doi:10.1002/2016PA002933, 2016.

Oziel, L., Neukermans, G., Ardyna, M., Sirven1, J., Ruiz-Pino, D., Gascard1, J.-C., Lancelot, C., Tison, J.-L. and Wassmann, P.: Role for Atlantic inflows and sea ice loss on shifting phytoplankton blooms in the Barents Sea, J. Geophys. Res. Ocean., 1–19, doi:10.1002/2016JC012582.Received, 2017.

Pados-Dibattista, T., Pearce, C., Detlef, H. and Brendtsen, J.: Holocene paleoceanography of the Northeast Greenland shelf, Clim. Past Discuss., 1–30, doi:10.5194/cp-2021-59, 2021.

Pados, T. and Spielhagen, R. F.: Species distribution and depth habitat of recent planktic foraminifera in Fram Strait, Arctic Ocean, Polar Res., 33(1), 22483, doi:10.3402/polar.v33.22483, 2014.

Pakhomov, E., Froneman, P., Wassmann, P., Ratkova, T. and Arashkevich, E.: Contribution of algal sinking and zooplankton grazing to downward flux in the Lazarev Sea (Southern Ocean) during the onset of phytoplankton bloom: a lagrangian study, Mar. Ecol. Prog. Ser., 233, 73–88, 2002.

Palmer, A. R.: Calcification in marine molluscs : How costly is it ?, Proc. Natl. Acad. Sci., 89(4), 1379–1382, doi:10.1073/pnas.89.4.1379, 1992.

Park, J.-Y., Kug, J.-S., Bader, J., Rolph, R. and Kwon, M.: Amplified Arctic warming by phytoplankton under greenhouse warming, Proc. Natl. Acad. Sci., 112(19), 5921 LP – 5926, doi:10.1073/pnas.1416884112, 2015.

Peck, V. L., Tarling, G. A., Manno, C., Harper, E. M. and Tynan, E.: Outer organic layer and internal repair mechanism protects pteropod Limacina helicina from ocean acidification, Deep. Res. Part II Top. Stud. Oceanogr., 127, 41–52, doi:10.1016/j.dsr2.2015.12.005, 2016.

Peck, V. L., Oakes, R. L., Harper, E. M., Manno, C. and Tarling, G. A.: Pteropods counter mechanical damage and dissolution through extensive shell repair, Nat. Commun., 9(1), 264, doi:10.1038/s41467-017-02692-w, 2018.

Pedersen, J. B. T., Kaufmann, L. H., Kroon, A. and Jakobsen, B. H.: The Northeast Greenland Sirius Water Polynya dynamics and variability inferred from satellite imagery, Geogr. Tidsskr., 110(2), 131–142, doi:10.1080/00167223.2010.10669503, 2010.

Peijnenburg, K. T. C. A., Janssen, A. W., Wall-Palmer, D., Goetze, E., Maas, A. E., Todd, J. A. and Marlétaz, F.: The origin and diversification of pteropods precede past perturbations in the Earth's carbon cycle, Proc. Natl. Acad. Sci. U. S. A., 117(41), 25609–25617, doi:10.1073/pnas.1920918117, 2020.

Pesant, S., Legendre, L., Gosselin, M., Smith, R. E. H., Ramseier, R. O., Pesant, S., Legendre, L., Gosselin, M., Smith, R. E. H., Kattner, G. and Ramseier, R. O.: Size-differential regimes of phytoplankton production in the Northeast Water Polynya ( 77°-81° N ), Mar. Ecol. Prog. Ser., 142(1/3), 75–86, 1996.

Polyakov, I. V., Pnyushkov, A. V., Alkire, M. B., Ashik, I. M., Baumann, T. M., Carmack, E. C., Goszczko, I., Guthrie, J., Ivanov, V. V., Kanzow, T., Krishfield, R., Kwok, R., Sundfjord, A., Morison, J., Rember, R. and Yulin, A.: Greater role for Atlantic inflows on sea-ice loss in the Eurasian Basin of the Arctic Ocean, Science (80-. )., 291(April), 285–291, doi:10.1126/science.aai8204, 2017.

Ramajo, L., Pérez-León, E., Hendriks, I. E., Marbà, N., Krause-Jensen, D., Sejr, M. K., Blicher, M. E.,

Lagos, N. A., Olsen, Y. S. and Duarte, C. M.: Food supply confers calcifiers resistance to ocean acidification, Sci. Rep., 6, 19374, doi:10.1038/srep19374, 2016.

Ramos-Silva, P., Wall-Palmer, D., Marlétaz, F., Marin, F. and Peijnenburg, K. T. C. A.: Evolution and biomineralization of pteropod shells, J. Struct. Biol., 107779, doi:10.1016/j.jsb.2021.107779, 2021.

Rasmussen, T. L., Van Weering, T. C. E. and Labeyrie, L.: Climatic instability, ice sheets and ocean dynamics at high northern latitudes during the last glacial period (58-10 KA BP), Quat. Sci. Rev., 16(1), 71–80, doi:10.1016/S0277-3791(96)00045-5, 1997.

Rasmussen, T. L., Thomsen, E. and Moros, M.: North Atlantic warming during Dansgaard-Oeschger events synchronous with Antarctic warming and out-of-phase with Greenland climate, Sci. Rep., 6(January), 1–12, doi:10.1038/srep20535, 2016.

Rastrick, S. S. P., Graham, H., Azetsu-Scott, K., Calosi, P., Chierici, M., Fransson, A., Hop, H., Hall-Spencer, J., Milazzo, M., Thor, P. and Kutti, T.: Using natural analogues to investigate the effects of climate change and ocean acidification on Northern ecosystems, ICES J. Mar. Sci., 75(7), 2299–2311, doi:10.1093/icesjms/fsy128, 2018.

Reeburgh, W. S.: Anaerobic methane oxidation: Rate depth distributions in Skan Bay sediments, Earth Planet. Sci. Lett., 47(3), 345–352, doi:10.1016/0012-821X(80)90021-7, 1980.

Reeburgh, W. S.: Oceanic methane biogeochemistry, Chem. Rev., 107, 486–513, doi:10.1016/B978-0-08-095975-7.00403-4, 2007.

Ruppel, C. D. and Kessler, J. D.: The interaction of climate change and methane hydrates, Rev. Geophys., 55(1), 126–168, doi:10.1002/2016RG000534, 2017.

Schiebel, R.: Planktic foraminiferal sedimentation and the marine calcite budget, Global Biogeochem. Cycles, 16(4), 1–21, doi:10.1029/2001GB001459, 2002.

Schiebel, R. and Hemleben, C.: Modern planktic foraminifera, Paläontologische Zeitschrift, 79(1), 135–148, doi:10.1007/BF03021758, 2005.

Schiebel, R. and Hemleben, C.: Planktic Foraminifers in the Modern Ocean, Springer-Verlag, Berlin Heidelberg., 2017.

Schiebel, R., Bijma, J. and Hemleben, C.: Population dynamics of the planktic foraminifer Globigerina bulloides from the eastern North Atlantic, Deep. Res. Part I Oceanogr. Res. Pap., 44(9–10), 1701–1713, doi:10.1016/S0967-0637(97)00036-8, 1997.

Schiebel, R., Spielhagen, R. F., Garnier, J., Hagemann, J., Howa, H., Jentzen, A., Martínez-Garcia, A., Meilland, J., Michel, E., Repschläger, J., Salter, I., Yamasaki, M. and Haug, G.: Modern planktic foraminifers in the high-latitude ocean, Mar. Micropaleontol., 136(August), 1–13, doi:10.1016/j.marmicro.2017.08.004, 2017.

Schmidt, D. N., Renaud, S. and Bollmann, J.: Response of planktic foraminiferal size to late Quaternary climate change, Paleoceanography, 18(2), doi:10.1029/2002PA000831, 2003.

Schneider, A., Crémière, A., Panieri, G., Lepland, A. and Knies, J.: Diagenetic alteration of benthic foraminifera from a methane seep site on Vestnesa Ridge (NW Svalbard), Deep. Res. Part I Oceanogr. Res. Pap., 123(March), 22–34, doi:10.1016/j.dsr.2017.03.001, 2017.

Schneider, W. and Budeus, G.: On the generation of the Northeast Water Polynya, J. Geophys. Res., 100(C3), 4269–4286, doi:10.1029/94JC02349, 1995.

Seibel, B. A. and Dierssen, H. M.: Cascading Trophic Impacts of Reduced Biomass in the Ross Sea,

Antarctica: Just the Tip of the Iceberg?, Biol. Bull., 205(2), 93–97, doi:10.2307/1543229, 2003.

Serreze, M. C. and Barry, R. G.: Processes and impacts of Arctic amplification: A research synthesis, Glob. Planet. Change, 77(1–2), 85–96, doi:10.1016/j.gloplacha.2011.03.004, 2011.

Siccha, M., Schiebel, R., Schmidt, S. and Howa, H.: Short-term and small-scale variability in planktic foraminifera test flux in the Bay of Biscay, Deep. Res. Part I Oceanogr. Res. Pap., 64, 146–156, doi:10.1016/j.dsr.2012.02.004, 2012.

Simstich, J., Sarnthein, M. and Erlenkeuser, H.: Paired $\delta 18O$ signals of Neogloboquadrina pachyderma (s) and Turborotalita quinqueloba show thermal stratification structure in Nordic Seas, Mar. Micropaleontol., 48(1–2), 107–125, doi:10.1016/S0377-8398(02)00165-2, 2003.

Sliter, W. V, BE, W. H. and Berger, H. (eds ).: Dissolution of deep-sea carbonates, Cushman Found. Foram. Res. Spec. Publ., 13(1998), 159 pp., doi:10.1029/2002PA000756.Rickaby, 1975.

Sloan, E. D. and Koh, C.: Clathrate Hydrates of Natural Gases, Third., CRC Press, Boca Raton., 2007.

Smedsrud, L. H., Esau, I., Ingvaldsen, R. B., Eldevik, T., Haugan, P. M., Li, C., Lien, V. S., Olsen, A., Omar, A. M., Otterå, O. H., Risebrobakken, B., Sandø, A. B., Semenov, V. A. and Sorokina, S. A.: The role of the Barents Sea in the Arctic climate system, , 5(2012), 415–449, doi:10.1002/rog.20017.1.INTRODUCTION, 2013.

Smith Jr., W. O.: Primary productivity and new production in the Northeast Water (Greenland) Polynya during summer 1992, J. Geophys. Res. Ocean., 100(C3), 4357–4370, doi:https://doi.org/10.1029/94JC02764, 1995.

Spindler, M., Hemleben, C., Salomons, J. B. and Smit, L. P.: Feeding behavior of some planktonic foraminifers in laboratory cultures., J. Foraminifer. Res., 14(4), 237–249, doi:10.2113/gsjfr.14.4.237, 1984.

Stroeve, J. C., Serreze, M. C., Holland, M. M., Kay, J. E., Malanik, J. and Barrett, A. P.: The Arctic's rapidly shrinking sea ice cover: A research synthesis, Clim. Change, 110(3–4), 1005–1027, doi:10.1007/s10584-011-0101-1, 2012.

Syring, N., Stein, R., Fahl, K., Vahlenkamp, M., Zehnich, M., Spielhagen, R. F. and Niessen, F.: Holocene changes in sea-ice cover and polynya formation along the eastern North Greenland shelf: New insights from biomarker records, Quat. Sci. Rev., 231(February), doi:10.1016/j.quascirev.2020.106173, 2020.

Sztybor, K. and Rasmussen, T. L.: Diagenetic disturbances of marine sedimentary records from methane-influenced environments in the Fram Strait as indications of variation in seep intensity during the last 35 000 years, Boreas, 46(2), 212–228, doi:https://doi.org/10.1111/bor.12202, 2017.

Takagi, H., Kimoto, K., Fujiki, T., Saito, H., Schmidt, C., Kucera, M. and Moriya, K.: Characterizing photosymbiosis in modern planktonic foraminifera, Biogeosciences Discuss., 1–32, doi:10.5194/bg-2019-145, 2019.

Takagi, H., Kurasawa, A. and Kimoto, K.: Observation of asexual reproduction with symbiont transmission in planktonic foraminifera, J. Plankton Res., 42(4), 403–410, doi:10.1093/plankt/fbaa033, 2020.

Thomsen, J., Casties, I., Pansch, C., Körtzinger, A. and Melzner, F.: Food availability outweighs ocean acidification effects in juvenile Mytilus edulis: Laboratory and field experiments, Glob. Chang. Biol., 19(4), 1017–1027, doi:10.1111/gcb.12109, 2013.

Towle, E. K., Enochs, I. C. and Langdon, C.: Threatened Caribbean coral is able to mitigate the adverse effects of ocean acidification on calcification by increasing feeding rate, PLoS One, 10(4), 1–17, doi:10.1371/journal.pone.0123394, 2015.

Toyofuku, T., Matsuo, M. Y., Nooijer, L. J. De, Nagai, Y., Kawada, S., Fujita, K., Reichart, G., Nomaki, H., Tsuchiya, M., Sakaguchi, H. and Kitazato, H.: Proton pumping accompanies calcification in foraminifera, Nat. Commun., 8, 1–6, doi:10.1038/ncomms14145, 2017.

Volkmann, R.: Planktic foraminifers in the outer Laptev Sea and the Fram Strait - Modern distribution and ecology, J. Foraminifer. Res., 30(3), 157–176, doi:10.2113/0300157, 2000.

Wall-Palmer, D., Hart, M. B., Smart, C. W., Sparks, R. S. J., Le Friant, A., Boudon, G., Deplus, C. and Komorowski, J. C.: Pteropods from the Caribbean Sea: Variations in calcification as an indicator of past ocean carbonate saturation, Biogeosciences, 9(1), 309–315, doi:10.5194/bg-9-309-2012, 2012.

Wang, K., Hunt, B. P. V., Liang, C., Pauly, D. and Pakhomov, E. A.: Reassessment of the life cycle of the pteropod Limacina helicina from a high resolution interannual time series in the temperate North Pacific, ICES J. Mar. Sci., 74(7), 1906–1920, doi:10.1093/icesjms/fsx014, 2017.

Waterson, A. M., Edgar, K. M., Schmidt, D. N. and Valdes, P. J.: Quantifying the stability of planktic foraminiferal physical niches between the Holocene and Last Glacial Maximum, Paleoceanography, 32(1), 74–89, doi:10.1002/2016PA002964, 2017.

Weinkauf, M. F. G., Waniek, J. J., Kunze, J. G., Waniek, J. J. and Kucera, M.: Seasonal Variation in Shell Calcification of Planktonic Foraminifera in the NE Atlantic Reveals Species-Specific Response to Temperature , Productivity , and Optimum Growth Conditions, PLoS One, 11(2), e0148363, doi:10.1594/PANGAEA.846744, 2016.

Weinkauf, M. F. G., Siccha, M. and Weiner, A. K. M.: Reproduction of a marine planktonic protist : Individual success versus population survival, , (November), doi:10.1101/2020.11.04.368100, 2020.

Weslawski, J. M., Hacquebord, L., Stempniewicz, L. and Malinga, M.: Greenland whales and walruses in the Svalbard food web before and after exploitation, Oceanologia, 42(1), 37–56, 2000.

Westbrook, G. K., Thatcher, K. E., Rohling, E. J., Piotrowski, A. M., Osborne, A. H., Nisbet, E. G., Minshull, T. A., James, R. H., Hu, V., Green, D., Fisher, R. E., Crocker, A. J., Chabert, A. and Bolton, C.: Escape of methane gas from the seabed along the West Spitsbergen continental margin, Geophys. Res. Lett., 36, 1–5, doi:10.1029/2009GL039191, 2009.

Willette, T. M. and Cooney, R. T.: Ecological processes influencing mortality of juvenile pink salmon (Oncorhynchus gorbuscha) in Prince William Sound, Alaska, Fish. Oceanogr., 10, 14–41, doi:10.1046/j.1054-6006.2001.00043.x, 2001.

Yamamoto-Kawai, M., McLaughlin, F. A., Carmack, E. C., Nishino, S. and Shimada, K.: Aragonite Undersaturation in the Arctic Ocean: Effects of Ocean Acidification and Sea Ice Melt, Science (80-. )., 326, 1098–1100, 2009.

Yasuhara, M., Huang, H. H. M., Hull, P., Rillo, M. C., Condamine, F. L., Tittensor, D. P., Kučera, M., Costello, M. J., Finnegan, S., O'dea, A., Hong, Y., Bonebrake, T. C., McKenzie, N. R., Doi, H., Wei, C. L., Kubota, Y. and Saupe, E. E.: Time machine biology cross-timescale integration of ecology, evolution, and oceanography, Oceanography, 33(2), 16–28, doi:10.5670/oceanog.2020.225, 2020.

Zamelczyk, K., Rasmussen, T. L., Husum, K., Haflidason, H., de Vernal, A., Ravna, E. K., Hald, M. and Hillaire-Marcel, C.: Paleoceanographic changes and calcium carbonate dissolution in the central Fram Strait during the last 20ka, Quat. Res. (United States), 78(3), 405–416,

doi:10.1016/j.yqres.2012.07.006, 2012.

Zeebe, R. E., Ridgwell, A. and Zachos, J. C.: Anthropogenic carbon release rate unprecedented during the past 66 million years, Nat. Geosci., 9(4), 325–329, doi:10.1038/ngeo2681, 2016.

# SECTION II - Papers

Paper I

# Development, Productivity, and Seasonality of Living Planktonic Foraminiferal Faunas and *Limacina helicina* in an Area of Intense Methane Seepage in the Barents Sea

Siri Ofstad[1], Julie Meilland[2], Katarzyna Zamelczyk[1,3], Melissa Chierici[4], Agneta Fransson[3], Friederike Gründger[5], and Tine L. Rasmussen[1]

[1]CAGE—Centre for Arctic Gas Hydrate, Environment and Climate, Department of Geosciences, UiT, The Arctic University of Norway, Tromsø, Norway, [2]MARUM—Center for Marine Environmental Sciences, University of Bremen, Bremen, Germany, [3]Norwegian Polar Institute, Fram Centre, Tromsø, Norway, [4]Institute of Marine Research, Tromsø, Norway, [5]Arctic Research Centre, Department of Bioscience, Aarhus University, Aarhus, Denmark

**Abstract** Although the plankton communities in the Barents Sea have been intensely studied for decades, little is known about the living planktonic foraminiferal (LPF) and pteropod faunas, especially those found at methane seep sites. Along a repeated transect in the "crater area" (northern Barents Sea, 74.9° N, 27.7°E) in spring and summer 2016 the flux of LPF and of the pteropod species *Limacina helicina* showed a high degree of variability. The LPF had low concentration (0–6 individuals m$^{-3}$) and small tests ($\bar{x} = 103.3$ μm) in spring and a 53-fold increase (43–436 individuals m$^{-3}$) and larger tests ($\bar{x} = 188.6$ μm) in summer. Similarly, the concentration of *L. helicina* showed a tenfold increase between spring and summer. The LPF species composition remained stable with the exception of the appearance of subtropical species in summer. No relationship was observed between the spatial distribution of LPF, *L. helicina*, and methane concentrations in the area. The methane plumes in April coincided with elevated dissolved inorganic carbon, low pH, and calcium carbonate saturation states, and the methane concentration seemed to be controlled by lateral advection. The $\delta^{13}$C and $\delta^{18}$O of *Neogloboquadrina pachyderma* and *Turborotalita quinqueloba* are comparable to previous observations in the Arctic and do not show any influence of methane in the isotopic signals of the shells. Although no evidence of direct impact of high methane concentrations on the LPF (size and concentration) were found, we speculate that methane could indirectly enhance primary productivity, and thus biomass, through several potential pathways.

**Plain Language Summary** Planktonic foraminifera and the thecosome pteropod species *Limacina helicina* are microscopic organisms who live in the water column and build their shells out of calcium carbonate. Little is known about the planktonic foraminiferal faunas in the Barents Sea, and their seasonality in general. This study is the first on planktonic foraminifera and *Limacina helicina* in an area of intense methane seepage from the seafloor. Sampling at sea took place during spring and summer 2016. We found a significant increase in shell size and concentration (individuals m$^{-3}$) in both planktonic foraminifera and *Limacina helicina* between spring and summer. In spring, carbon dioxide was being added from the methane plumes, altering the sea-water chemistry at the site of methane release. The addition of carbon dioxide could stimulate primary production in the overlying water column. However, we did not find that the spatial distribution of planktonic foraminifera coincided with where the methane concentration was the highest, or that methane concentration coincided with the elevation of primary production indicators. This study sheds light on the planktonic foraminifera community and their seasonal development in the Barents Sea for the first time with stratified net samples.

## 1. Introduction

Humankind's industrial and agricultural activities since the mid-18th century have caused an increase in atmospheric carbon dioxide ($CO_2$) from ~280 parts per million (ppm) to the present level, which exceeds 400 ppm (Dlugokencky & Tans, 2019; IPCC: Climate change, 2013). The consensus is that this anthropogenic increase in atmospheric $CO_2$ has had significant effects on Earth's climate, in particular at high latitudes (IPCC: Climate change, 2013). The polar oceans are very sensitive to the increased temperature and

atmospheric $CO_2$ (Orr et al., 2005; Stouffer et al., 1989). Consequently, the Arctic Ocean has transformed over the past decades, experiencing, among other processes, loss of sea ice (e.g., Stroeve et al., 2012), freshening (Haine et al., 2015; Rabe et al., 2011), ocean acidification (e.g., AMAP: AMAP assessment, 2013, AMAP: AMAP Assessment, 2018), an increase in primary production (Arrigo & van Dijken, 2011, 2015), and introduction of tropical and subtropical species at high latitudes (e.g., Bjørklund et al., 2012; Fossheim et al., 2015). All of these processes may have far-reaching effects on the entirety of the Arctic food chain, and hence will have socioeconomic repercussions (AMAP: AMAP Assessment, 2018).

If the current trend in global emissions of $CO_2$ continues, the pH of the oceans is predicted to decrease 0.3–0.5 units by the end of the century (Caldeira & Wickett, 2005). The Arctic Ocean will see the most dramatic effects, due to it being an especially strong $CO_2$ sink as a result of cold surface water, high biological productivity, seasonal freshwater inputs, and decreasing sea-ice cover (Bates & Mathis, 2009; Fransson et al., 2009; Kaltin & Anderson, 2005). Furthermore, shell dissolution and a range of other negative physiological responses may occur in calcifying planktonic organisms at high partial pressure of $CO_2$ ($pCO_2$), especially in combination with increased temperature. Pteropods (Bednarsek et al., 2014; Bednaršek et al., 2012; Comeau et al., 2009; Lischka et al., 2011) and planktonic foraminifera are considered to be especially vulnerable to ocean acidification (e.g., Davis et al., 2017; Manno et al., 2012; Moy et al., 2009). The reproduction rates of living planktonic foraminifera (LPF) change in response to changes in the environment with higher rates under favorable conditions and vice versa (Kucera, 2007). The global LPF community has changed since preindustrial times in terms of the spatial distribution of assemblages (Jonkers et al., 2019). The shift in the global LPF community is consistent with recent changes in temperature, demonstrating the sensitivity of the LPF to environmental conditions (Jonkers et al., 2019). Yet our understanding of LPF ecology is fragmented, especially in the northern polar regions. Little is known about causes of interannual variability in production in terms of absolute abundance (concentration) and species distribution patterns (e.g., Schiebel, 2002; Schiebel & Hemleben, 2000), the controls of vertical habitat changes (Greco et al., 2019; Kretschmer et al., 2018; Rebotim et al., 2017), and how the vertical habitat varies ontogenetically (Bijma et al., 1990; Hemleben et al., 1989; Schiebel et al., 1997). Also, linkage between the reproduction cycle of the LPF and the lunar cycle is barely known (Bijma et al., 1990; Erez et al., 1991; Hemleben et al., 1989; Jonkers et al., 2015; Schiebel & Hemleben, 2017; Volkmann, 2000). To complicate matters further, the extent to which different ecological parameters affect the production and distribution of LPF vary at species level (Schiebel & Hemleben, 2017). Lastly, it is not known whether or not the dominant Arctic species, *Neogloboquadrina pachyderma*, can overwinter in brine channels in pack and fast ice, as they do in the Southern Ocean (Dieckmann et al., 1991; Spindler, 1996). All of this leads to uncertainties when it comes to using planktonic foraminifers as a proxy for paleoclimate.

In the Arctic, gas hydrate provinces are widespread on the continental shelves (Damm et al., 2005; Graves et al., 2015; Mau et al., 2017; Pisso et al., 2016; Sapart et al., 2017; Shakhova et al., 2010; Westbrook et al., 2009) and are stable under low temperature and high pressure, this stability is threatened under the current climate warming trend. At present, little of the methane ($CH_4$) from the gas hydrate provinces reach the atmosphere (Graves et al., 2015; Pisso et al., 2016; Silyakova et al., 2015). Instead, the $CH_4$ from Arctic subsurface marine hydrate reserves is either anaerobically or aerobically oxidized in the upper layers of the sediments or in the water column by microbial activity (Boetius & Wenzhöfer, 2013; Ruppel & Kessler, 2017). In the water column, microbial aerobic oxidation ($MO_X$) and the less common AOM (anaerobic oxidation of methane) are sinks for $CH_4$; both processes remain poorly understood (Reeburgh, 2013). Following the release of $CH_4$ from the seafloor, these water column processes can change the manner of impact of the $CH_4$ release. For example, model studies have shown that, through the $MO_X$ reaction, $CH_4$ seepage is a potential source of $CO_2$, which can increase ocean acidification (Biastoch et al., 2011; Archer et al., 2008). It has also been hypothesized that $CH_4$ seepage can cause an increase in photosynthetic primary production (Pohlman et al., 2017), making $CH_4$ seepage areas $CO_2$ sinks. There have been several studies in the Arctic focusing on the effects of $CH_4$ seepage on the living benthic communities (Åström et al., 2016, 2018, 2019; Sen, Duperron, et al., 2018, Sen et al., 2019), including living benthic foraminifera, although not exclusive to the Arctic region (Heinz et al., 2005; Herguera et al., 2014; Hill et al., 2004; Rathbun et al., 2000). However, no studies from the Arctic exist that examine the effects of $CH_4$ seepage on the pelagic ecosystem.
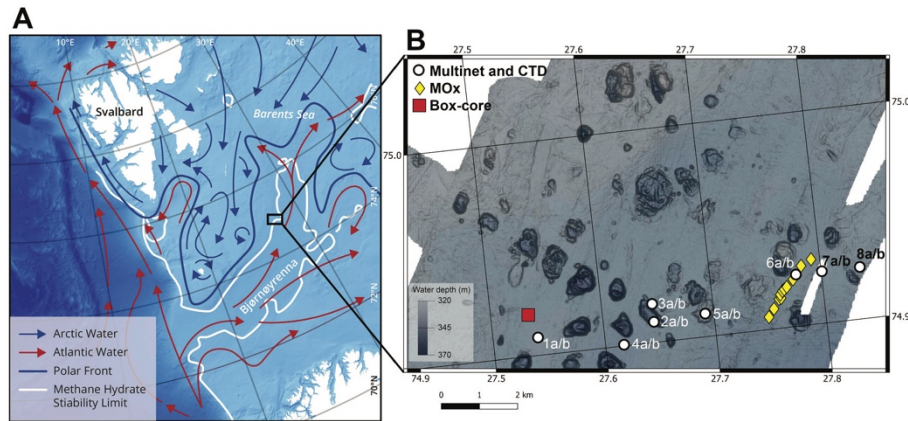
**Figure 1.** (a) Map of study area located in the northern Barents Sea, on the edge of the methane hydrate stability zone. Currents and polar front after Loeng (1991), methane hydrate stability limit after Andreassen et al. (2017). Study area is enclosed in black rectangle. (b) Multibeam bathymetry of the transect area (modified from Andreassen et al., 2017). White dots mark multinet and CTD sampling stations, yellow diamonds $MO_X$ measurement stations, and red square the box-core location.

Here we aim to improve our understanding of the response of LPF and pteropods to seasonal changes and $CH_4$ release to the water column in the Barents Sea with focus on the species compositions, size, and concentration of specimens. This is the first study of LPF in an environment exposed to $CH_4$ seepage from the seafloor. We study the communities between spring (April) and summer (June) to further our knowledge of seasonal variability and eventual impact of $CH_4$ release an extremely variable chemical environment. Changes in size and concentrations of the LPF population are compared to equivalent data from the dominant species of pteropods *Limacina helicina*. We conducted two sampling campaigns in Arctic spring and summer, collecting samples from the Bjørnøyrenna crater area, which is located in the northern Barents Sea. This area is characterized by more than a hundred giant crater-mound systems, with high levels of $CH_4$ release from gas hydrates to the water column, with flares of up to 200 m height (Andreassen et al., 2017).

## 2. Study Area and Sampling Locations

The Barents Sea is a relatively shallow continental shelf sea dominated by the warm north-easterly flowing Atlantic Current, a branch of the Norwegian Atlantic Current called the North Cape Current (Loeng, 1991). The Bjørnøyrenna crater area (referred to in this study as the "crater area") (74.91°N, 27.7°E; Figure 1) is located in shallow water (~340 m depth) on the northern flank of Bear Island Trough, which is on the upper boundary of the gas hydrate stability zone (Andreassen et al., 2017) (Figure 1a). The crater area is ice-free year-round. During our sampling campaigns, the predominant water masses were Atlantic Water (AW, T > 3.0 °C, S > 34.65) (<300 m in April and <250 m in June) and Transformed Atlantic Water (TAW, T = 1.0–3.0 °C, S > 34.65) (>300 m in April and >250 m in June), following the definitions of Cottier et al. (2005). The study site has an area of about 440 km². Streams of gas bubbles entering the water column were visually observed by the ROV 30K during the CAGE 16-5 cruise in June 2016, and by hydroacoustics (EK60) during the CAGE 16-2 cruise in April 2016. Measurements have revealed that the $CH_4$ is primarily of thermogenic origin (Andreassen et al., 2017).

Seasonal sampling took place during two expeditions with *R/V Helmer Hanssen* in spring (CAGE 16-2, 15 April to 22 April) and summer (CAGE 16-5, 16 June 2016 to 4 July) 2016. On 19 April (spring), eight CTD (conductivity, temperature, depth) stations and a stratified plankton net were conducted across a 9 km transect (74.91°N, 27.5–27.9°E) located above several craters and mounds actively releasing $CH_4$ (Figure 1b). The sampling procedures were repeated on 29–30 June (summer), 71 days after the first sampling, with the

addition of aerobic methane oxidation ($MO_X$) rate and $CH_4$ measurements at 11 stations (74.91–74.92°N, 27.74–27.8°E) (Figure 1b). Also in June, three additional water samples were taken from a blade core at station 1b guided by a ROV just above the sediment-water interface for determining the $CO_2$ system (i.e., Total alkalinity ($A_T$) and Dissolved Inorganic carbon (DIC)). A surface sediment sample (position 74.92°N, 27.53° E) was retrieved using a box corer (Figure 1b).

## 3. Material and Methods

### 3.1. Environmental Parameters

Salinity, temperature, and depth in the water column were measured using a CTD (Sea-Bird SBE 19+) equipped with sensors for dissolved oxygen (DO) (Sea-Bird SBE 43) and chlorophyll *a*-fluorescence (chlfluo) (Sea-Bird ECO) (both indicators for primary production), and 12 × 5 L Teflon-lined Niskin bottles for water sampling. Water samples were collected at nine depths (5, 10, 25, 50, 100, 150, 200, 250 m, bottom), and were used for determining $A_T$, DIC, and $CH_4$. The water was transferred into Pyrex borosilicate bottles (250 ml) for the $CO_2$ system, and into crimp-top glass bottles (120 ml) for $CH_4$ concentration. Both parameters were sampled via a Tygon tube to prevent contact with air and to avoid gas bubbles. Samples for $CH_4$ analysis were collected immediately upon recovery of the CTD rosette. Also immediately after sampling, water samples for the $CO_2$ system were preserved with 60 μl of saturated mercury chloride ($HgCl_2$), $CH_4$ samples were amended with 1 ml of 1 M NaOH solution and capped with butyl rubber stoppers and crimped. Water samples were stored in the dark at 2 °C until analysis. The water from the blade core was sampled immediately after retrieval using a Tygon tube and preserved in the same way as the water samples taken by the CTD.

The water samples for the $CO_2$ system were analyzed for $A_T$ and DIC at the Institute of Marine Research (IMR Tromsø, Norway). The method used is described in detail in Dickson et al. (2007). In short, DIC was determined using gas extraction of acidified samples followed by colorimetric titration and photometric detection using a Versatile Instrument for the Determination of Titration Alkalinity (VINDTA 3D, Marianda, Germany). The $A_T$ was determined by potentiometric titration with 0.1 N hydrochloric acid using a Versatile Instrument for the Determination of Titration Alkalinity (VINDTA 3S, Marianda, Germany). Routine analyses of Certified Reference Materials (CRM, provided by A. G. Dickson, Scripps Institution of Oceanography, United States) were used to perform accuracy control. The accuracy of the measurements was better than ±1 and ±2 μmol kg$^{-1}$ for DIC and $A_T$, respectively.

The remaining parameters of the $CO_2$ system of pH, fugacity of $CO_2$ ($fCO_2$), and aragonite saturation ($\Omega_{Ar}$) were calculated using a $CO_2$-chemical speciation model (CO2SYS program, version 01.05) (Lewis & Wallace, 1998; Pierrot & Wallace, 2006) and the DIC and $A_T$ measurements, in combination with temperature, salinity, and depth (pressure). The equilibrium constants K1, K2 from Mehrbach et al. (1973) refitted by Dickson and Millero (1987), and the total hydrogen-ion scale (pHT) were used. We used the $HSO_4^-$ dissociation constant of Dickson (1990), and the boric acid dissociation constant of Uppström (1974).

Methane concentrations were determined using the headspace technique, described in detail in Berndt et al. (2014) and Steinle et al. (2015). In short, 5 ml of pure $N_2$ was added into each of the 120 ml glass bottles and shaken vigorously. Samples were stored in the fridge (2 °C) for 0.5 to 2 hr, allowing the dissolved gas in the seawater to equilibrate with the headspace gas. Following this, 2 ml of gas was extracted and analyzed by a ThermoScientific Trace 1300 gas chromatograph equipped with a flame ionization detector (GC-FID). Methane concentrations were determined according to Wiesenburg and Guinasso (1979).

### 3.2. Aerobic Methane Oxidation Rates

Aerobic methane oxidation ($MO_X$) is mediated by bacteria and proceeds according to the following net reaction:

$$CH_4 + 2O_2 \rightleftharpoons CO_2 + 2H_2O \tag{1}$$

Water samples were taken at 11 stations along a transect (Figure 1b) from eight different water levels, which were at 5, 15, 25 m below the sea surface, 5, 15, 25 m above seafloor, and two additional intermediate levels depending on water depth. Subsamples were taken immediately upon recovery of the sampler. $MO_X$ rates were determined by ex-situ incubations with trace amounts of tritium labeled $CH_4$ ($C^3H_4$), allowing to

trace the label transfer by measuring the activity of substrate ($C^3H_4$) and product pools ($^3H_2O$) after incubation (Berndt et al., 2014; Niemann et al., 2015; Steinle et al., 2015). Briefly, for each sampling depth, six 20-ml crimp-top vials were filled and closed bubble-free with PTFE-coated Bromobutyl rubber stoppers (Wheaton, United States). Each sample was amended with 5 μl gaseous tritium-labeled $CH_4$ ($C^3H_4$) (~20 kBq, American Radiolabeled Chemicals, United States) and incubated for 72 hr at 4 °C in the dark. The incubations were terminated by adding 0.5 ml saturated $HgCl_2$ solution to one triplicate of the six parallel samples (aboard ship) and total activity ($^3H–CH_4 + {}^3H–H_2O$) was determined on a 2-ml aliquot mixed with 3 ml of scintillation cocktail (Ultima Gold, Perkin Elmer) by using a Liquid Scintillation Analyzer Packard TRI-CARB 2300TR (PerkinElmer, IL, United States) at our home laboratory. The remaining triplicate of samples was used to estimate the net amount of $^3H–CH_4$ consumption. Therefore, a 10-ml aliquot of the incubation was amended with aqueous NaCl solution (1 ml, 30%, w/v) and purged for 30 min with air to strip out the remaining $CH_4$. The activity of the produced $^3H_2O$ was determined in our home laboratories by liquid scintillation counting. $MO_X$ rates were calculated from the fractional turnover of labeled $CH_4$ and measured water column $CH_4$ concentration assuming first order kinetics (Reeburgh, 2013):

$$rMO_X = k \times [CH_4], \tag{2}$$

where k is the first-order rate constant (determined from the fractional turnover of labeled $CH_4$ per unit time and corrected for tracer turnover in control samples) and $[CH_4]$ is the concentration of $CH_4$ at the beginning of the incubation. $MO_X$ rates were corrected for insubstantial tracer turnover in control samples, which were taken frequently, fixed with $HgCl_2$ solution immediately after the addition of the tracer.

### 3.3. Plankton Samples Collection and Treatment

Foraminiferal and thecosome pteropod specimens were sampled concurrent with the hydrographic samples using a Multinet with mesh size of 64 μm (net opening 0.5 $m^2$; Hydro-Bios, Kiel, Germany). This mesh size enabled the collection of small specimens, possibly preadults, in order to address seasonality and reproduction between the two sampling campaigns. The nets were towed vertically, collecting plankton at five consecutive depth intervals (300–200, 200–150, 150–100, 100–50, and 50–0 m) (Table S1). The flowmeter attached to the net opening allowed calculation of the volume of water filtered through each net and calculation of concentration of specimens (number individuals/volume ($m^{-3}$)). Once on board, the samples were sieved with sea water through a 63-μm sieve and transferred into plastic bottles (250 ml) where they were immediately fixed and buffered with approximately 230 ml ethanol (98%), a quarter of a teaspoon hexamethylenetetramine (≥99.0%), and stored at 2 °C. Once returned to the home laboratory, the samples were briefly washed with tap water on a 63-μm sieve in order to remove organic particles from the surface of the foraminiferal tests and to break up aggregations of material. Due to the very high concentration of LPF in June, the samples were split by a Motodo plankton sample divider. The number of specimens in resulting aliquots was used to calculate the total concentration of foraminifera in the sample. The foraminifera were manually counted and identified to species level under a Leica MZ12.5 light microscope following the taxonomy of Schiebel and Hemleben (2017) and SCOR WG 138 (http://www.eforams.org/index.php/WG138_Taxonomy).

### 3.4. Planktonic Foraminifera From Surface Sediment

In order to retrieve recently dead adult specimens from the surface sediments, a box-corer (50 × 50 × 50 cm) was deployed from the ship. Immediately after recovering the sediment core, the top layer (1 cm) was scraped off by a spoon, and preserved in approximately 50 ml of ethanol (96%) with rose bengal (2 g $L^{-1}$ of ethanol), and stored at 2 °C. In the home laboratory, the samples were sieved through a 63-μm sieve and dried for at least 24 hr at 40 °C. Once dried, planktonic foraminifera were picked under a light microscope, with a fine brush, and identified to species level.

### 3.5. Planktonic Foraminifera and *Limacina helicina* Morphometrical Parameters

For size measurements, the LPF and *L. helicina* from the water column, in addition to planktonic foraminifera from surface sediments, were uniformly arranged on a slide with the umbilical side facing upward. Images were acquired by a Leica Z16 APO microscope, using the integrated Leica DFC450 camera and LAS version 4.12.0 software. The images were processed using the ruler tool in Adobe Photoshop CS6, with

which the minimum and maximum diameters that bisect the center of the foraminiferal tests were measured in microns always by the same operator to be as accurate as possible.

### 3.6. Stable Isotopes

Stable isotopes of carbon and oxygen from LPF shells were analyzed at The Stable Isotope Laboratory at CAGE—Centre for Arctic Gas Hydrate, Environment and Climate located at UiT—The Arctic University of Norway, Tromsø, Norway. Due to the low concentration and dominance of small shells in April, stable isotope analysis was only performed on the LPF from June. Twenty specimens of *Neogloboquadrina pachyderma* and 20 specimens of *Turborotalita quinqueloba* of the same size class (150–200 μm) were picked from all five sampling depths and placed in 4.5 ml vials. A total of 20 samples were analyzed, 10 for each species. The vials were flushed with He, and five drops of water-free $H_3PO_4$ were added manually with a syringe. After equilibration for more than 3 hr at 50 °C, the samples were analyzed on a Gasbench II and Thermo Scientific MAT253 IRMS. Isotopic values are reported vs. the VPDB scale, which has been normalized by two to three inhouse standards with a wide range of $\delta^{13}C$ and $\delta^{18}O$ values. The inhouse standards have been normalized by several international standards. Instrument uncertainty of $\delta^{13}C$ and $\delta^{18}O$ is standard deviation ≤0.1‰ (ThermoScientific).

### 3.7. Statistical Analyses

To test for difference between the environmental parameters sampled in the surface and bottom waters of April and June, a Mann-Whitney $U$ test (Mann & Whitney, 1947) was conducted on the data. The stations were separated into their surface (0–100 m) and bottom (100–300 m) water samples.

To test for possible significant differences between the LPF population sampled in April and June, we used a Mann and Whitney $U$ test and tried the following hypothesis:

1. Are LPF concentrations (all species together) and test size significantly different between sampling periods?
2. Are specific (species by species) LPF concentrations significantly different between sampling periods?
3. Are LPF concentrations by depth significantly different between sampling periods?
4. Which environmental parameters are significantly different between the sampling periods?

To determine if there is a relationship between the maximum $CH_4$ concentration at each station and LPF concentration in the overlying water column, and primary production indicators, we performed a Pearson's correlation test on both April and June data. Both the Pearson's correlation tests and the Mann-Whitney $U$ tests were performed on the program RStudio (Version 1.2.1335) (RStudio Team: RStudio: Integrated development for R, 2015). In order to compare the species diversity within the LPF population between April and June, the Shannon Index ($H'$) (Shannon & Weaver, 1949) was calculated.

## 4. Results

### 4.1. Environmental Parameters

Temperature and salinity, the $CO_2$ system parameters (DIC, $A_T$, pH, and calcium carbonate saturation states $\Omega$), and primary production indicators along the 9-km transect reveal clear seasonal differences between April and June. In April, the water column is well mixed in terms of temperature and salinity (Figures 2a and 2b), with temperature ranging between 2.77 °C and 3.77 °C, and the salinity between 34.99 and 35.02. In April, the water column is dominated by AW with an occasional presence of TAW in the bottom ~50 m. In June, the temperature ranges from 2.1–7.03 °C, increasing toward the surface, and the salinity between 35 and 35.02. In June, the water column is more thermally stratified, with a surface mixed layer extending to ~50 m water depth. In June, the lower ~100 m of the water column is dominated by the colder TAW, and the upper ~250 m is dominated by AW. Sea surface temperature increased by 3.26 °C from April to June, while the salinity remained almost constant. This allows for the investigation of seasonal changes in thermal stratification on the LPF and *Limacina helicina*. In Figures 2 and 3, all parameters are presented on the same scale, with the exception of $CH_4$, due to the large difference in concentration between the two sampling seasons (Figures 2c and 3c).

In April (Figure 2), our data show two $CH_4$ plumes close to the seafloor (Figure 2c), which also correspond to plumes of elevated DIC and $fCO_2$ (Figures 2d and 2k). These plumes of elevated $CH_4$ and carbon originate
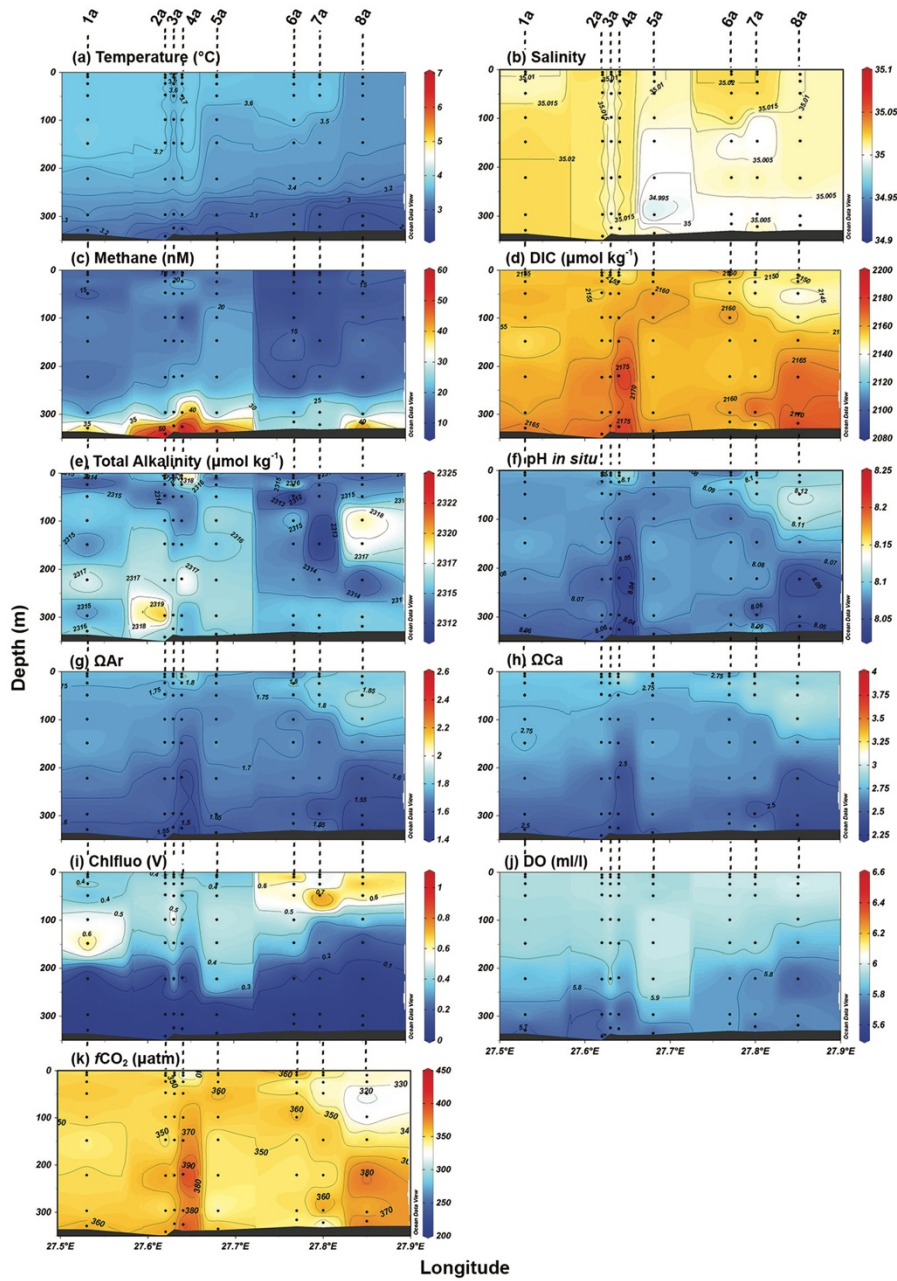
53

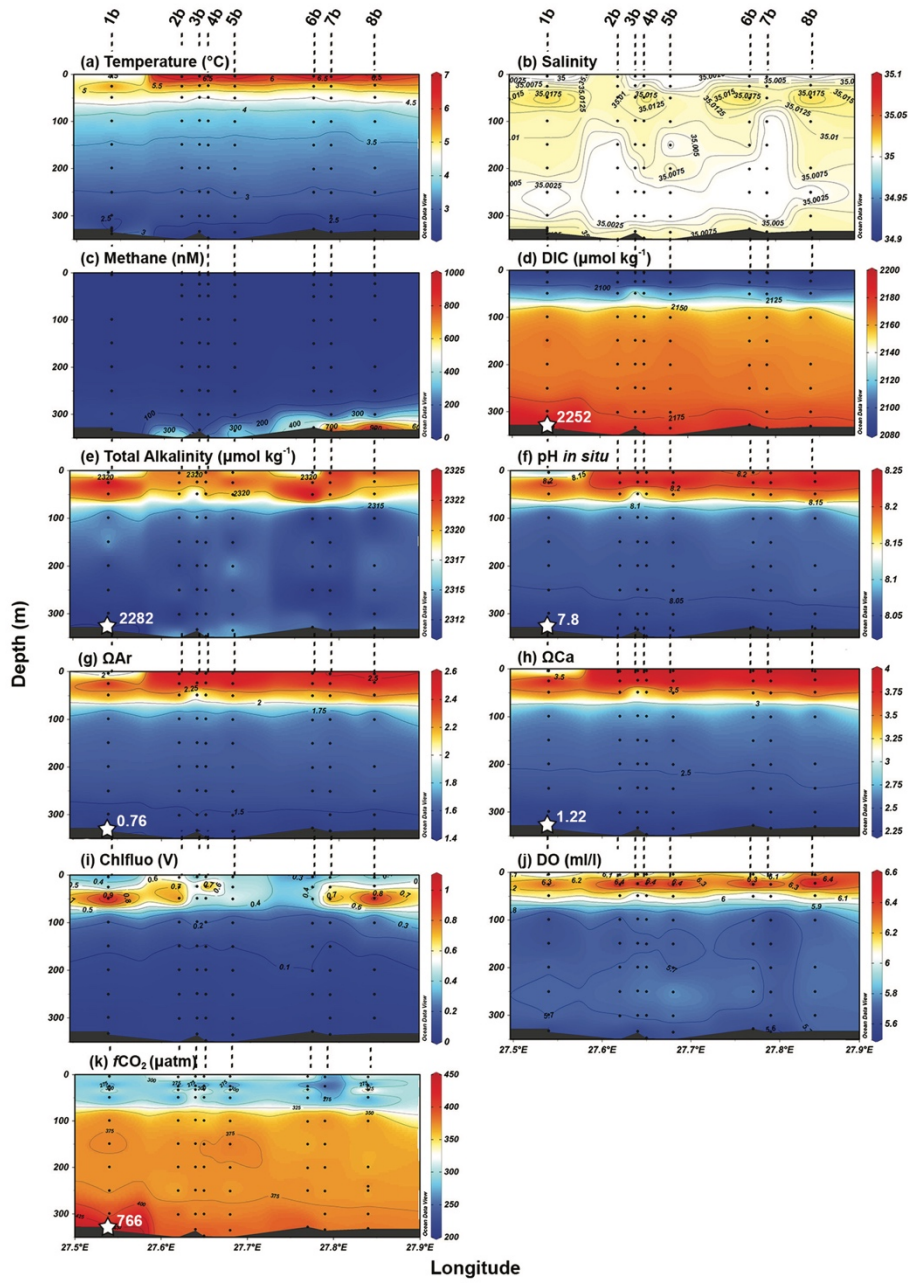**Figure 2.** Vertical sections of (a) temperature (°C), (b) salinity, (c) methane (nM), (d) dissolved inorganic carbon (DIC, µmol kg$^{-1}$), (e) total alkalinity ($A_T$, µmol kg$^{-1}$), (f) pH, (g) aragonite saturation ($\Omega_{Ar}$), (h) calcite saturation ($\Omega_{Ca}$), (i) chlorophyll $a$-fluorescence (chlfluo, V), (j) dissolved oxygen (DO, ml L$^{-1}$), and (k) carbon dioxide fugacity ($f$CO$_2$, µatm) in April 2016. Black dots represent sampling depth for water samples throughout the water column. Station IDs are given on the top of the figure.

54

**Figure 3.** Vertical sections of (a) temperature (°C), (b) salinity, (c) methane (nM), (d) dissolved inorganic carbon (DIC, µmol kg$^{-1}$), (e) total alkalinity (A$_T$, µmol kg$^{-1}$), (f) pH, (g) aragonite saturation ($\Omega_{Ar}$), (h) calcite saturation ($\Omega_{Ca}$), (i) chlorophyll $a$-fluorescence (chlfluo, V), (j) dissolved oxygen (DO, ml L$^{-1}$), and (k) carbon dioxide fugacity ($f$CO$_2$, µatm) in June 2016. Black dots represent sampling depth for water samples throughout the water column. White stars and white text are concentrations from bladecore samples at sediment-water interface. Station IDs are given on the top of the figure.

from the seafloor at 27.65 and 27.85°E and extend upward to approximately 200 m water depth. The maximum $CH_4$ concentration is 57 nM, found at stations 2a and 4a, at 13 and 9 m above the seafloor, respectively (Figure 2c). The $CH_4$ concentration is elevated throughout the entire water column (average concentration = 15.7 nM), with only a slight gradient from the seafloor to the surface. From 300 m water depth to the seafloor, the average $CH_4$ concentration reaches 31.8 nM. The $CH_4$ concentration decreases from 300 to 5 m water depth to reach 15.7 nM. The plumes are also characterized by lower pH, $\Omega_{Ar}$, and $\Omega_{Ca}$ (pH = 8.02, $\Omega_{Ar}$ = 1.4, $\Omega_{Ca}$ = 2.3), compared to surrounding waters (pH = 8.08, $\Omega_{Ar}$ = 1.7, $\Omega_{Ca}$ = 2.7). $A_T$ is slightly elevated at the plume locations, and ranges from 2,311 to 2,321 $\mu$mol kg$^{-1}$.

In June, the $CH_4$ concentrations close to the seafloor are on average more than one order of magnitude higher than in April, with a maximum concentration of 959 nM at station 8b, 1 m above the seafloor (Figure 3c). Elevated $CH_4$ concentrations extend to 150 m, shallower than in April (200 m). From 300 m water depth to the seafloor, the average $CH_4$ concentration is 275 nM, and from 300 to 5 m water depth it is 9.3 nM. Waters at the seafloor were recorded to have $\Omega_{Ar}$ as low as 0.76 at station 1b, this coincides with relatively low temperature (2.5 °C), high DIC (2,252 $\mu$mol kg$^{-1}$) and a pH of 7.8 (Figure 3g). The $f$CO$_2$ in the waters at the seafloor at station 1b is 766 $\mu$atm (Figure 2k). The $A_T$ is elevated at the top 75 m (TA > 2,318 $\mu$mol kg$^{-1}$) compared to the rest of the water column (Figure 3e). In the upper 75 m of the water column, DIC values decreased from about 2,160 $\mu$mol kg$^{-1}$ in April (Figure 2d), to <2,100 $\mu$mol kg$^{-1}$ in June (Figure 3d), coinciding with increased $A_T$, pH, DO, and chlfluo (Figures 3e, 3f, 3i, and 3j). The surface DO and chlfluo are higher in June than in April (DO: 5.8 to 6.5 ml L$^{-1}$ vs. 5.9 to 6 ml L$^{-1}$, chlfluo: 0.3 to 1 ml L$^{-1}$ vs. 0.5 to 0.7 ml L$^{-1}$), suggesting higher primary production in June relative to April. In the layer between 100 and 250 m water depth, the $CO_2$ system parameters (DIC, $A_T$, pH, $\Omega$) are relatively homogenous.

Overall, from April to June we observe a thermal stratification of the water column and an increase in $CH_4$ concentration with increasing water depth. Although the seafloor $CH_4$ concentrations were higher in June compared to April, its global background concentration along the sampled transect was higher in April. The DIC concentrations in the waters at the seafloor increased from April to June and high values of about 2,200 $\mu$mol kg$^{-1}$ encompassed the entire study area.

### 4.2. Microbial Methane Oxidation Activity

The highest microbial methane oxidation activity is found close to the seafloor (0–15 m above seafloor) with a maximum value of 32 nM d$^{-1}$ at station M10 (Figure 4, Table S6). The average MO$_X$ activity close to the seafloor from all stations along the transect is 11 nM d$^{-1}$. At the sea surface and in the water column down to 215 m, MO$_X$ activity was below detection limit. Methane concentrations are highest in the bottom waters (0–25 m above sea floor), and range from 38 (station M8) to 767 nM (Station M5).

### 4.3. Planktonic Foraminiferal Concentrations and Assemblages in the Water Column and Surface Sediments

In April, LPF concentrations are low, ranging from 0 (station 7a, 200–300 m depth) to 6 (station 1a, 0–50 m depth) individuals (ind.) m$^{-3}$ (Figure 5). Also in April, benthic foraminifera occur in the Multinet samples at all of the stations with the exception of 7a. In June, the concentration of planktonic foraminifera is higher compared to April, and ranges from 12 ind. m$^{-3}$ (station 8b, 200–300 m depth) to 436 ind. m$^{-3}$ (station 2b, 50–100 m depth) (Figure 5). In June, benthic foraminifera are only found in the Multinet samples from station 8b. Maximum concentrations of LPF in both seasons are located in surface waters (0–100 m), and the lowest in the 100–300 m water depth interval. The total concentrations of LPF across all stations is 87 ind. m$^{-3}$ in April, and 4,637 ind. m$^{-3}$ in June, with an average per station of 11 and 580 ind. m$^{-3}$, respectively. During both seasons, the five stations to the west (1a/b, 2a/b, 3a/b, 4a/b, 5a/b; Figures 1b and 6) have a higher concentration of LPF compared to the three stations to the east (6a/b, 7a/b, 8a/b) (Figure 5). The concentration of LPF along the 9-km transect is highly variable both in April and June (Figure 6).

There are seven LPF species present in April and 12 in June (Figure 7). The assemblages of April and June are both largely dominated by *Turborotalita quinqueloba* and *Neogloboquadrina pachyderma*, where they together make up to 90.6% and 88.8% of the total LPF community, respectively. This allows for a comparison
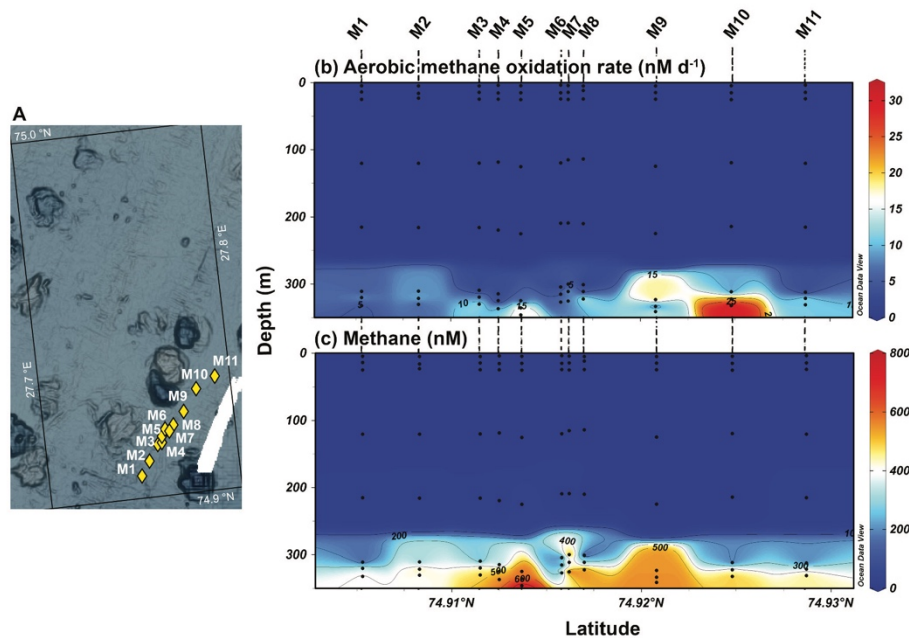
**Figure 4.** (a) Map over $MO_X$ and methane sampling stations, and vertical sections of (b) aerobic methane oxidation rate (nM d$^{-1}$) and (c) methane (nM).

of the size distribution of the *T. quinqueloba* and *N. pachyderma* that were present in April and June (Figure 9).

At most stations and during both sampling periods *T. quinqueloba* is the dominant species reaching maximum concentrations in April and June of 6 and 355 ind. m$^{-3}$, respectively. In April *T. quinqueloba* makes up 77.7% of the community, while *N. pachyderma* makes up 12.9%. In June, *T. quinqueloba* makes up 64.3%, while *N. pachyderma* makes up 24.5% (Figure 7). Two significant differences are the decrease of *Neogloboquadrina incompta* percentages from 5.2% in April to 0.9% in June. The other significant difference between spring and summer is the increase in the *Globigerinita uvula* population from 2.5% to 6.6%. The June LPF community is more diverse ($H' = 1.12$ vs. 0.81), and includes specimens of *Globigerina bulloides*, *Orcadia riedeli*, *Turborotalita humilis*, and *Globigerinoides conglobatus*. None of the LPF specimens from the surface sediments were stained. *Turborotalita quinqueloba* is the most dominant species in the surface sediments, making up 80% of the fauna, while *N. pachyderma* and *G. uvula* make up 16% and 4%, respectively (Figure 7c).

### 4.4. *Limacina helicina* Concentrations

*Limacina helicina* is the only pteropod species found in our samples from the crater area. Similar to the LPF, *L. helicina* specimens are more abundant in summer than in spring, with the highest concentration in the surface waters (0–50 m depth) (Figure 8). However, the increase in overall concentration across all stations from 41 to 127 ind. m$^{-3}$ is not as dramatic compared to the LPF community (37 to 1,971 ind. m$^{-3}$). During both periods, *L. helicina* was absent from some samples. In April, the highest concentration at a single station reaches five ind. m$^{-3}$ (station 1a, 0–50 m depth), while in June it is 10 times higher, reaching 47 ind. m$^{-3}$ (station 2b, 0–50 m depth). The concentration in the 100–300 m depth interval does not change much between the two sampling periods. In April, the average concentration in the 100–300 m depth interval is three ind. m$^{-3}$, while in June it is two ind. m$^{-3}$. The spring vertical distribution of *L. helicina* is quite
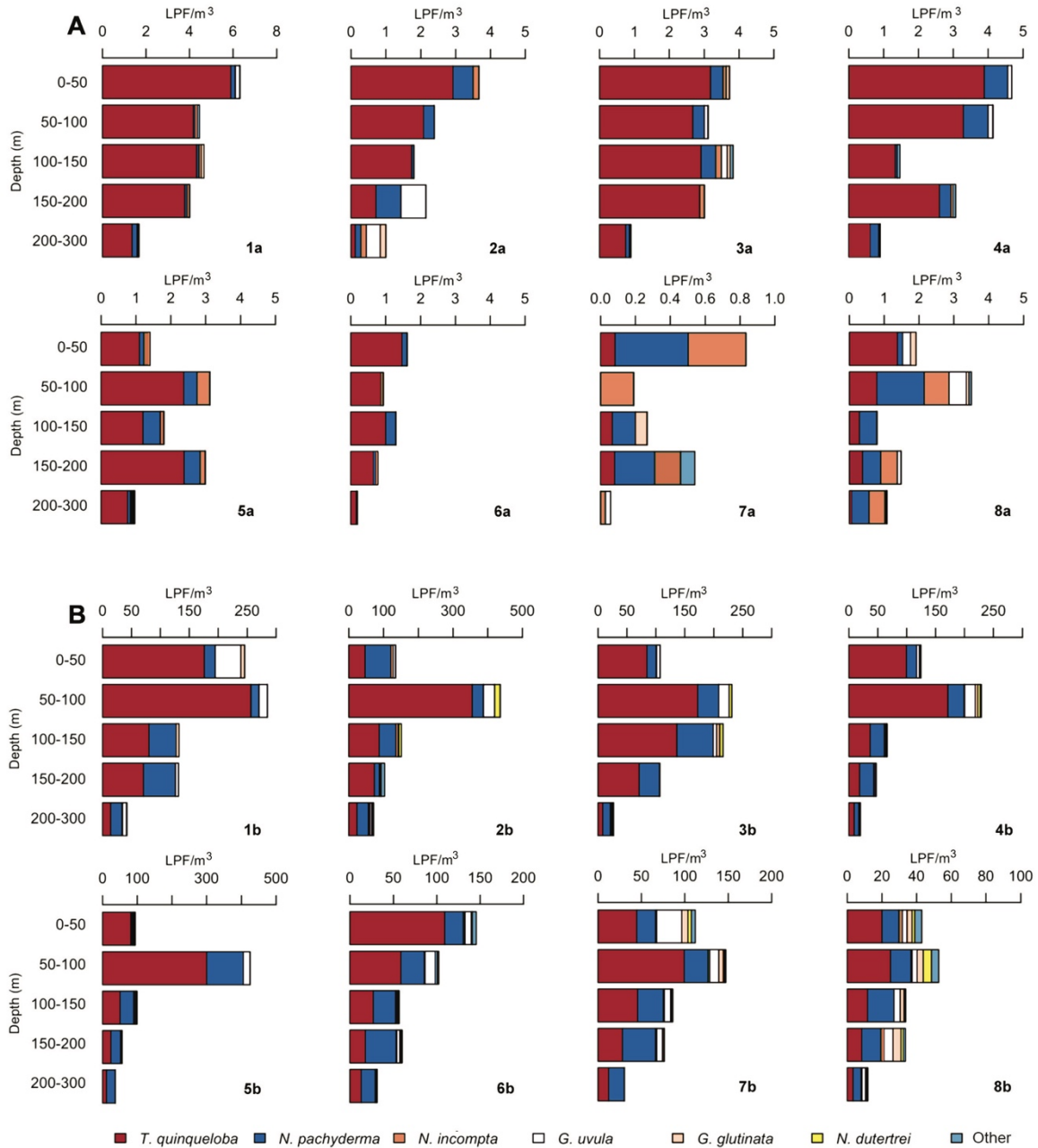
57

**Figure 5.** Planktonic foraminiferal abundances (individual (ind.) m$^{-3}$) per species plotted against water depth (m) for every station sampled in (a) April and (b) June. Bold numbers at the lower right of each graph are station IDs. Please note different *x* axes.
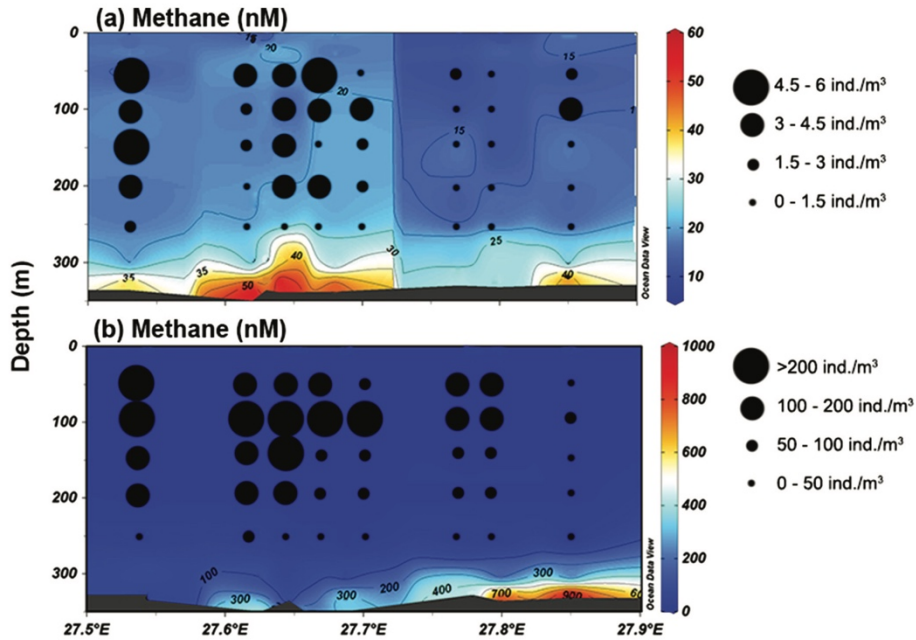
58

**Figure 6.** LPF concentration in the water column overlain on methane concentrations for (a) April and (b) June. Note different scales for both methane and LPF concentration. Station IDs are given on top of each cross section.

homogeneous in the depth interval 0–200 m, while in summer the distribution is characterized by a peak in the surface waters (0–50 m) followed by a sharp decline with depth.

### 4.5. LPF Size Parameters

A total of 1,562 LPF were measured for their diameters, in addition to 56 planktonic foraminifera from surface sediment samples. In April, the test sizes of the LPF assemblages has a mean of 103.3 μm, and are constrained to diameters of 60–200 μm, with the highest frequency of specimens falling in the 100 to 110 μm bin suggesting the community to be largely dominated by small specimens, likely to be juveniles or young adults (Figure 9a). In June, the test sizes have a mean diameter of 188.6 μm and display a larger range with no obvious peak in frequency. The size distribution of June ranges from 80–340 μm (Figure 9a). The June
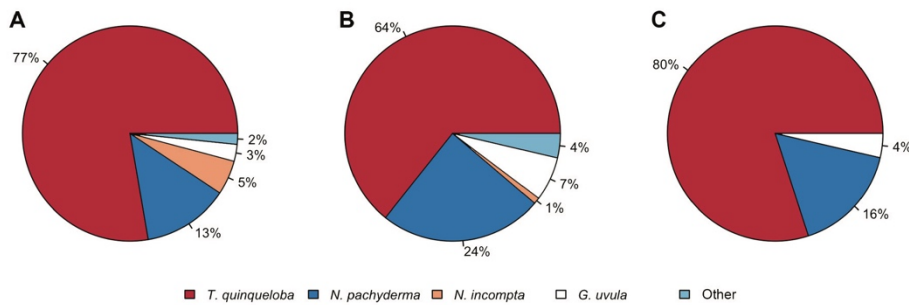


**Figure 7.** Average LPF species composition across all stations, in (a) April, (b) June, and in (c) surface sediments in the crater area.
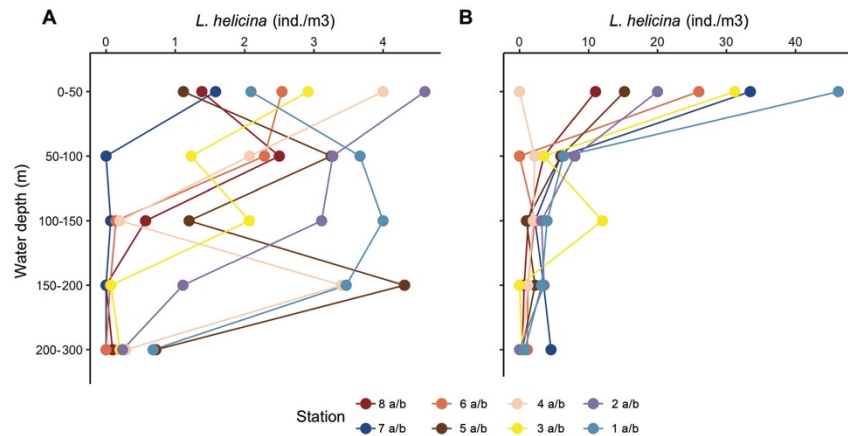
59

**Figure 8.** Vertical concentration of *Limacina helicina* (individuals (ind.) m$^{-3}$) for stations sampled in (a) April and (b) June. Note different scales of *x* axes.

population consists of a mix between small and large specimens, likely to be both adults and juveniles. The recently dead population in the surface sediments has a size distribution of 100–330 μm, with the highest frequency of specimens falling in the 210 to 220 μm bin and in the 230 to 240 μm bin (Figure 9a). The diameters of *N. pachyderma* and *T. quinqueloba* were not found to be significantly different ($p = 0.68$), therefore the increase in LPF diameter from April to June is not a reflection of the increase in the relative concentration of *N. pachyderma* (13% to 24% of the LPF community).

In April, the largest tests are found in the 200–300 m water depth interval, where the average test diameter is 107.95 μm. The smallest tests were in the 0–50 m interval, with an average diameter of 98.85 μm (Figure 9c). In June, the largest tests are in the 150–200 m water depth interval, where the average test diameter is 210.77 μm. The smallest tests are found within the 200–300 m water depth interval, with an average diameter of 157.1 μm (Figure 9d). The difference in test size between April and June at the crater area is statistically significant (Figure 9e).

Seven LPF shell diameters in April ($n = 957$) were found to be smaller than 64 μm, the mesh size of the nets, and none in June ($n = 605$).

### 4.6. *Limacina helicina* Size Parameters

The shell diameter of 331 specimens of *L. helicina* was measured (256 from April and 175 from June). In April, the shell diameters are constrained to 150–300 μm, with the most frequent diameter falling in the 150 to 200 μm bin. As in the LPF population small specimens, in this case, veliger larvae, are dominant. In June, the size distribution widens, ranging from 150–1200 μm with no clear dominant size frequency. The seasonal size trend of *L. helicina* mirrors that of the LPF population, in that the April population is largely dominated by small specimens, likely to be juveniles or young adults, and the June population consists of a mix between small and large specimens, likely to be both adults and juveniles.

### 4.7. Stable Isotopes of LPF

In June, the δ$^{18}$O composition of *N. pachyderma* in the water column ranges from 2.3‰ to 3.17‰ (Figure 10a; Table S2). The highest δ$^{18}$O value is found in the 200–300 m depth interval at station 8b, and the lowest in the 0–50 m interval at stations 8b and 5b. For *T. quinqueloba*, the δ$^{18}$O values range from 1.82‰ to 2.74‰ (Figure 10a; Table S2). The highest δ$^{18}$O value is found in the 100–150 m depth interval at station 5b, and the lowest in the 0–50 m interval at station 8b. For both species, a general trend of decreasing δ$^{18}$O values with shallower water depth is shown by the linear regression line. The linear regressions for *N. pachyderma* and *T. quinqueloba* have $r^2$ values of 0.44 and 0.13, respectively.
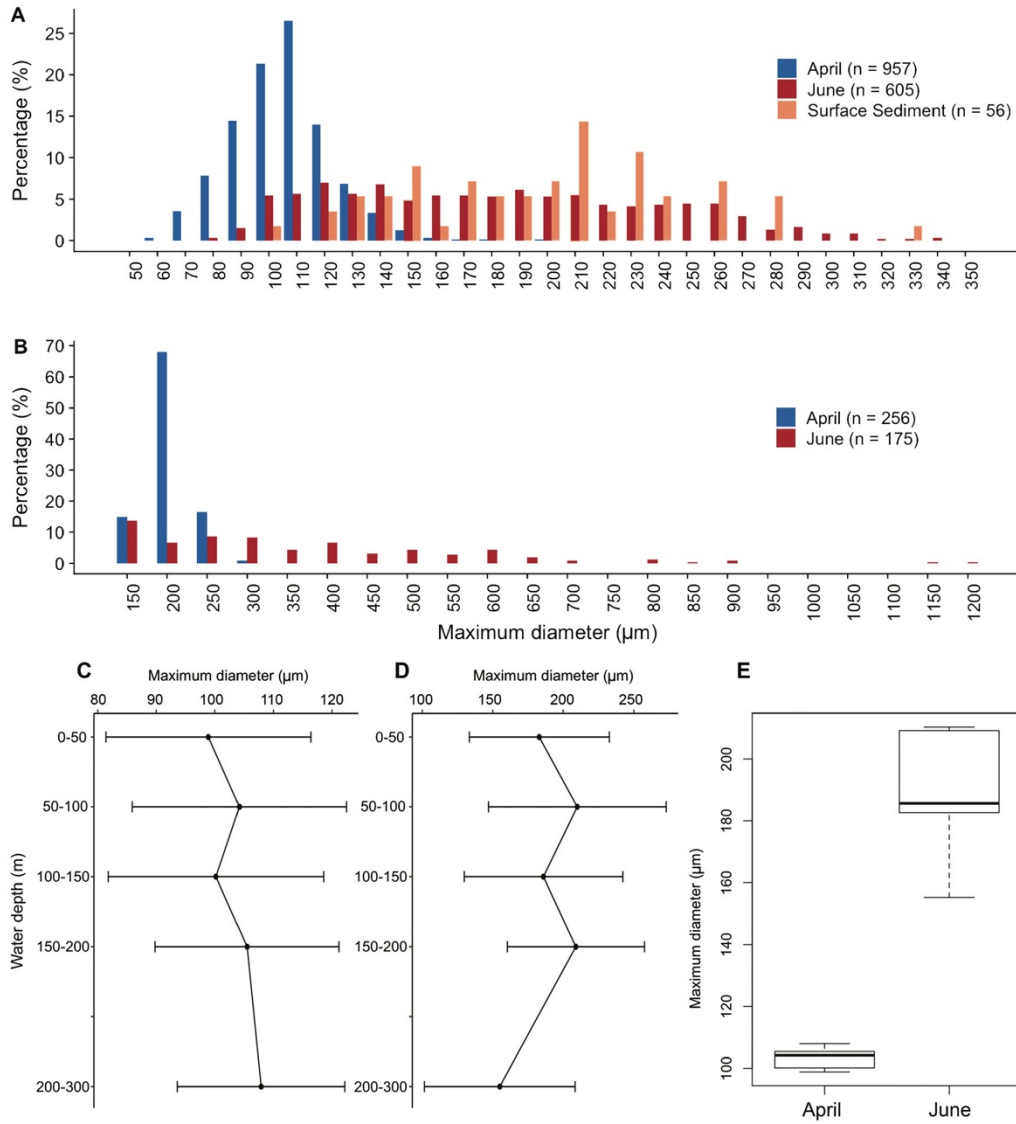
**Figure 9.** Size distribution of (a) LPF and planktonic foraminifera from surface sediments and (b) *Limacina helicina* in the crater area in April (blue) and June (red). Note different scales of *y* axes. Vertical distribution of LPF test sizes in the crater area in (c) April and (d) June, in addition to standard deviation, and (e) a box-and-whisker plot of test size. Note different scales of *x* axes.

The $\delta^{13}C$ composition of *N. pachyderma* in the water column ranges from $-1.02‰$ to $-0.17‰$ (Figure 10b, Table S2). The highest $\delta^{13}C$ value is found in the 200–300 m depth interval at station 5b, and the lowest $\delta^{13}C$ value is found in the 50–100 m interval at stations 8b. For *T. quinqueloba*, the $\delta^{13}C$ values ranged from $-2.39‰$ to $-1.1‰$ (Figure 10b, Table S2). The highest value was found in the 100–150 m depth interval at station 5b, and the lowest in the 0–50 m interval at station 8b. The linear regression line for *N.*
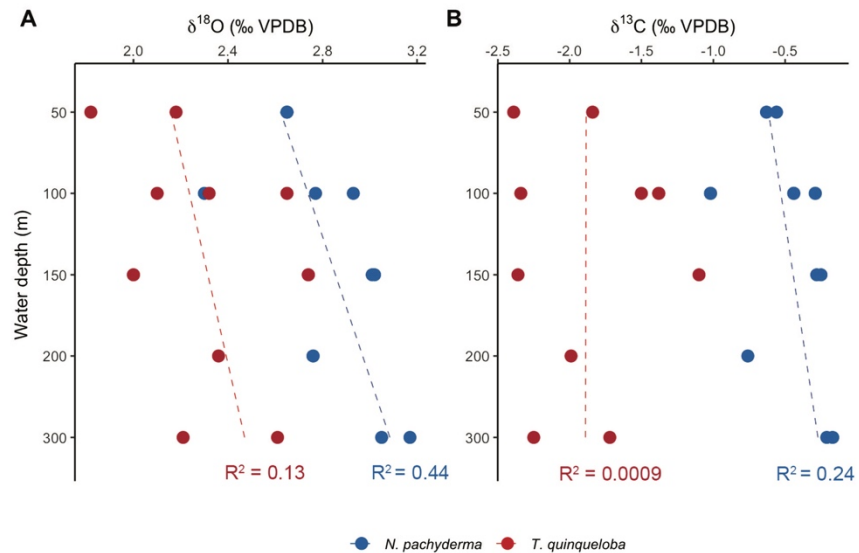
**Figure 10.** (a) $\delta^{18}O$ and (b) $\delta^{13}C$ values of *Neogloboquadrina pachyderma* (blue) and *Turborotalita quinqueloba* (red) in June. Dashed line indicates the linear regression for the respective species.

*pachyderma* shows a general trend of increasing $\delta^{13}C$ values with depth, and an $r^2$ value of 0.24. The $\delta^{13}C$ values of *T. quinqueloba* throughout the water column do not show any trend.

### 4.8. Statistical Analyses

All environmental parameters in the surface (0–100 m) and bottom (100–300 m) waters show a statistically significant difference between the two sampling periods, with the exception of surface water chlfluo ($p = 0.22$) (Table S3). All LPF variables, that is, total concentration, concentration by depth, species-specific concentrations, and test sizes, also show statistically significant differences between the two sampling seasons (Table S4). The Shannon diversity index ($H'$) for the LPF community in spring is 0.81, while in summer, it is 1.12. During both seasons, there is no statistically significant correlation between $CH_4$ concentration and overlying LPF concentration, chlfluo or DO (Table S5).

## 5. Discussion

There are 47 planktonic foraminiferal morphospecies in the modern ocean (SCOR WG 138), but few can be found in any considerable numbers in the Arctic and polar regions. The Arctic and northern polar LPF population shows a low diversity, and is dominated by *Neogloboquadrina pachyderma* and *Turborotalita quinqueloba* (e.g., Carstens et al., 1997; Eynaud, 2011; Jensen, 1998; Pados & Spielhagen, 2014; Volkmann, 2000), similar to our samples from the Barents Sea. In addition, our samples from April and June in the crater area highlight the highly heterogeneous nature of the LPF spatial distribution (Meilland et al., 2019) along the 9 km transect (Figure 6). It has been shown that the zooplankton community in the Barents Sea display strong seasonal variability in terms of their concentration and community composition (Arashkevich et al., 2002). This seasonality is caused by variations in sea surface temperature and phytoplankton biomass. The phytoplankton biomass at a given site is controlled by changes in the mixed layer depth, brought on by thermal stratification. The shoaling of the mixed layer depth enables nutrient pumping (e.g., Bé, 1960) and creates an environment with high nutrient and light levels, marking the start of the phytoplankton bloom. Wind driven mixing supplies nutrients and supports a prolonged primary production into summer and early fall. It has been found that in cold regions, primary productivity serves as a timing cue for when conditions are

suitable for growth and reproduction of the LPF (Kretschmer et al., 2016). Typically, the highest concentrations of LPF occurs during the summer (e.g., Fischer et al., 1988; Kretschmer et al., 2016).

In addition to the potential shift in LPF phenology, a change in the LPF faunal composition at high latitude regions, as a result of ocean warming, has already been observed. For example, the species diversity has increased over the past few decades. There is a higher concentration of the subarctic species *Orcadia riedeli*, *Globigerinita uvula*, and *Neogloboquadrina incompta* (Meilland, 2015; Meilland et al., 2018) in polar regions compared to preindustrial times (Jonkers et al., 2019) (Figures 5 and 7). The observed recent increase in LPF diversity highlights that the Arctic and polar LPF community is changing. Our study shows the current composition of the LPF population in the northern Barents Sea, and its seasonal (spring to summer) development in relation to changes in the environmental conditions, including $CH_4$, in the water column.

### 5.1. LPF Seasonal Variability

We observe significant differences in the LPF community sampled in the Barents Sea crater area between April and June (Table S4) and in all the environmental parameters (Table S3), with salinity being the least variable and surface $CH_4$ being the most (Figures 2b, 2c, 3b, and 3c). Seasonal variations in plankton communities and water properties in the Barents Sea have been intensely studied (e.g., Arashkevich et al., 2002; Loeng et al., 1997; Oziel et al., 2016; Oziel et al., 2017; Reigstad et al., 2002; Wassmann & Slagstad, 1993). March represents the winter season in the central and northern Barents Sea, with very low chlorophyll *a* concentrations in the water column (Reigstad et al., 2002). In the crater area, thermal stratification of the water column starts in April (spring) following the rise in daylight. Although stratification is very subtle in our temperature profile, the two-layered water column (divided at 200 m) can be seen clearly in the chlfluo and DO profiles (Figures 2a, 2i, and 2j). In April, the mean test diameter of the LPF population is 103.3 μm, and 88% of the population has a test equal or smaller than 120 μm. The small test size coincides with low concentration (0–6 ind. $m^{-3}$). This is likely to be the first population of the spring season. The occurrence of small tests in early spring was also found in the Greenland Sea (Jensen, 1998) and the Fram Strait (Gyldenfeldt et al., 2000). The spring bloom in the Barents Sea typically peaks in May and ends in June when nutrients in the surface water layers are depleted and there is stronger zooplankton grazing by planktivorous organisms like chaetognaths and medusae (Arashkevich et al., 2002; Oziel et al., 2017).

In June, the thermal stratification of the water column in the crater area is much more pronounced and the boundary layer is shallower (at 100 m). Above 100 m water depth, we find the highest concentration of LPF and *Limacina helicina* (Figures 5b and 8). The increase in DO and chlfluo coincide with the thermocline and are indicative of primary production in the surface waters (Figures 3a, 3i, and 3j). Since salinity did not change significantly between April and June in the crater area, the decreased DIC of about 60 μmol $kg^{-1}$ is most likely due to $CO_2$ uptake during photosynthesis (Figure 3d). The difference in the surface water chlfluo ($p = 0.22$) between April and June is not significant, suggesting that April represents the start of the spring bloom and in June the end of the spring bloom, where nutrients may already be depleted. By June, the water temperature in the crater area has apparently increased sufficiently to include the thermal range tolerated by the nonpolar species *Orcadia riedeli* and *Globigerinoides conglobatus*. The water temperature at the time of sampling represents also the modeled optimal temperature for *N. pachyderma* (Kretschmer et al., 2018). Only 19.9% of the population has a test diameter equal or smaller than 120 μm, meaning that the relative concentration of juveniles has greatly reduced in June, compared to April. In terms of concentrations, we see a 53-fold increase from April to June (43–436 ind. $m^{-3}$), but there is no dominant size of individuals (test diameter) (Figure 9a), suggesting that we are capturing several cohorts, in contrast to April. Larger tests during times of high flux of LPF are also found in the Fram Strait (Gyldenfeldt et al., 2000). In April, we see an increase in size with depth, while the opposite occurs in June, suggesting that juveniles do not have a preferred habitat depth, or that it is unpredictable.

The seasonal trend in zooplankton biomass is nearly identical to that of the primary productivity (Fulton, 1983), suggesting that zooplankton grazing intensifies simultaneously with increasing phytoplankton productivity. Temperate and cold-water LPF species are characterized by general absence of symbionts, making them reliant on productivity in the water column for food (Jonkers & Kučera, 2015). The changes to the LPF community observed in this study in terms of size and concentration appear to match calanoid copepod seasonality in the same region with spawning of *Calanus finmarchicus* and *Calanus glacialis* in March–April, early adult stages in May, and adult stages in July, which have already started to spawn (Arashkevich

et al., 2002). Our data suggest that *L. helicina* also follows this growth pattern, meaning that LPF and *L. helicina* likely both develop simultaneously with the primary producers (Figure 9b). According to Wang et al. (2017), the life cycle of *L. helicina* comprises two generations per year. The population sampled in April was likely spawned the previous summer and overwintered with minimal to no growth (Figure 9b). By June, the *L. helicina* population had tripled in concentration and increased in test diameter from x̄ = 175.6 μm in spring, to x̄ = 334.6 μm in summer. It is possible that some of the larger *L. helicina* sampled in April had spawned the summer/fall population sampled in June. The small-sized *L. helicina* we captured in June will then likely spawn in late summer/fall to produce the population that will overwinter.

For the LPF, the Shannon-Wiener Index was higher in June than April (1.12 vs 0.81), reflective of a more diverse community. Overall, we see a close similarity in species composition in the surface sediments compared to the Multinet samples, suggesting that the surface sediments accurately represent the LPF fauna in the overlying water column (Figure 7). Planktonic foraminifera in surface sediments can be biased toward large and fast sinking tests (e.g., Berelson, 2002), which could lead to a misrepresentation of the LPF size composition; however, this does not seem to be the case in our study.

Oziel et al. (2017) recorded that a smaller summer bloom in the Barents Sea develops in July–August, and peaks in September. By late summer, the breakdown of the vertical stratification due to surface cooling and wind mixing cause renewed nutrient enrichment of the surface waters, meaning that the summer bloom can be sustained as long as the irradiance in the euphotic zone is high enough (Oziel et al., 2017). If our sampling period would have been extended to include the early autumn (September–October), we would expect the test size distribution of both LPF and *L. helicina* to show two peaks. One peak should be at the larger end of the size spectrum, comprising the specimens that will end their lifecycle before winter, and one peak at the smaller end, which are likely the specimens that are preparing to hibernate and that will seed the next year's population. However, a smaller mesh size (<64 μm) would likely be needed to capture the overwintering LPF and *L. helicina* populations. By using a mesh size of 64 μm, we do not have any data on the concentration of LPF smaller than 64 μm. However, our data show the advantage in using a 64-μm mesh as opposed to a 100-μm mesh, which would have resulted in excluding a large part of the small-sized April population (Figure 9a). Many seasonal studies, and consequently, models, are based solely on >125 or >150 μm fraction. Our results would therefore indicate that they provide limited information on the population structure of the planktonic foraminiferal faunas.

### 5.2. Lunar Cycle

It has been shown that many planktonic foraminiferal species are affected by lunar-phased synchronized reproduction, which is superimposed on seasonal changes in shell flux (e.g., Jonkers et al., 2015). It is conceivable that the population captured in the northern Barents Sea on 19 April probably was spawned during the previous full moon (23 March 2016), since the size distribution strongly suggests that this is a single population (Figure 9a). If they were closely linked to the lunar cycle, the size distribution on 29 June would show two distinct populations, one that spawned after the full moon on 21 May, and one from 20 June (Figure 9a). Juvenile specimens grow rapidly and reach a test size of >100 μm in less than 10 days (Hemleben et al., 1989; Spero & Lea, 1996) making it possible for them to be captured in a 64 μm net 9 days later. They should thus produce a peak in the smaller size frequency. However, the lack of peaks in the test size distribution suggests that these individuals are the result of several spawning events (Figure 9a). The variability we observe in the LPF concentration and size on 29 June does not appear to be linked to the lunar cycle, but rather to seasonality.

### 5.3. Data Comparison to LPF Seasonality in the Greenland Sea and Irminger Sea

There is limited data on the seasonal distribution of LPF in the northern polar and Arctic regions. Global seasonality models are based largely on two sediment trap studies for polar biogeographic regions: Jensen (1998) with two locations (GS/2, 75°N, 0°E and OG5, 72.38°N, 07.72°W) in the Greenland Sea and Jonkers et al. (2010) in the Irminger Sea (59.25°N, 39.66°W). Due to differences in sampling methods, a direct comparison between our Multinet study from the Barents Sea and the sediment trap fluxes from the Greenland Sea and Irminger Sea is not possible. The sediment trap data reflect planktonic foraminifera that have completed their lifecycle and have sunk into the trap, while our multinet data reflect the living community at all stages of their life cycle. However, the sedimentation of specimens tends to follow the

same spatial trends as plankton net samples (Pados & Spielhagen, 2014), meaning relatively high absolute concentration in the water column will be shown as relatively high fluxes to the sediment trap.

There are two prominent peaks in planktonic foraminiferal concentration in the Irminger Sea during the year. Similar to our data from the crater area, in the Irminger Sea, the first population completes their life-cycle by mid-April, while the peak flux into the sediment trap occurs in May–June, and by late June the flux has greatly decreased. Jonkers et al. (2010) show only a slight difference in foraminiferal shell flux to the sediment traps from mid-April to late June. However, small and light shells that completed their life cycle in April may not sink to the sediment trap depths. Due to the 53-fold increase in the LPF population at the crater area between April and June, we would expect the flux to the seafloor in the crater area to be much higher in summer compared to spring. This suggests that the LPF bloom dynamics in the northern Barents Sea may differ from that of the central Irminger Sea. In the Greenland Sea in OG5, the flux of planktonic foraminifera to the sediment trap starts mid-March, and there are still a very low flux of planktonic forami-nifera by late April and restricted to the 63–125 μm size fraction. By late June in the Greenland Sea (OG5), there is an increasing presence of planktonic foraminifera in the 125–250 μm fraction—which is in agree-ment with our size data (Figure 9a), and the overall flux of planktonic foraminifera has doubled. This dou-bling of the flux and increase in size in the Greenland Sea (OG5) is likely due to the increased presence of phytoplankton in the summer, similar to what we observe at the crater area (Figure 3i). However, the overall largest peak in flux at OG5 does not occur until August, suggesting that the highest concentration of LPF at OG5 occurs in late summer. Because the time series from the Greenland Sea is from 1991–1992, the current seasonal trend at OG5 of planktonic foraminifera may be more similar to our current observations in the cra-ter area due to ocean warming and the reduction of sea ice in the Greenland Sea. Warmer waters cause LPF populations to peak earlier in the year and to shift northward in the northern hemisphere (Jonkers et al., 2019; Jonkers & Kučera, 2015). The northern-most time series of LPF, at GS/2 in the Greenland Sea, shows a narrow LPF production period, and lower flux. In contrast to the Irminger Sea and OG5, there is no spring bloom. The first planktonic foraminiferal flux to the sediment trap appears in June and consists of tests with diameters that fall evenly within the 63–125 and 125–150 μm fraction, and peaks in September. However, GS/2 is the only site out of the three, which is dominated by *T. quinqueloba*. If we are considering the spring to summer development of the LPF community in terms of concentration and size, our seasonal data seem to be most in line with OG5 from the southern part of the Greenland Sea.

The data from the Barents Sea is also in agreement with the global seasonality model by Jonkers and Kučera (2015). The model shows that in high latitude waters, which have a surface temperature above 5 °C, the peak in the LPF concentration occurs early in the summer, slightly after or at the same time as the maximum chlorophyll *a* concentration, validating the tight link between primary production and LPF seasonality. This suggests that our samples in June represent the peak in LPF concentration.

It must be emphasized that since these sediment trap experiments were done in 1991–1992 and 1994–1995 by Jensen (1998) and in 2003–2006 by Jonkers et al. (2010), there may have been changes in the hydrography and water mass properties due to ocean warming and ice melt, resulting in a different LPF seasonality. There are also strong interannual variations in productivity at any given site. Finally, the location of the three sedi-ment trap experiments and our sampling site in the crater area are all in different oceanographic settings, so we would not expect to see the exact same seasonal trends and species compositions.

### 5.4. The Effect of Methane on Productivity and LPF Biomass

Methane seep ecosystems are unique, because they host chemosynthesis-based communities resulting in an "oasis effect" on the seafloor, due to enhanced macrofaunal biomass and diversity in comparison to nearby nonseep environments (Åström et al., 2018; Levin, 2005; Levin et al., 2016; Sibuet & Olu, 1998; Sibuet & Olu-Le Roy, 2002; Thomsen et al., 2019). At the crater area, numerous frenulate siboglinid worms, the dominant chemosymbiotrophic megafauna in high latitude seeps, and chemosynthetic bacterial mats are recorded (Sen, Duperron, et al., 2018). The impact of $CH_4$ seepage on benthic productivity and biomass in the Arctic is clear (Åström et al., 2018, 2019), but an effect on the ecosystem in the overlying water column is unknown. Aggregations of various demersal fish have been found at $CH_4$ seeps around the world, although the cause of this remains unclear (Åström et al., 2019; Bowden et al., 2013; Grupe et al., 2015; Sellanes et al., 2008; Sen, Åström, et al., 2018). We hypothesize that planktonic organisms may behave in the same manner in that they aggregate above seeps.

The hypothesis that $CH_4$ seepage enhances primary production and hence biomass in the water column has been discussed previously in the literature (e.g., D'Souza et al., 2016; Pohlman et al., 2017; Rakowski et al., 2015). Enhanced primary production and $CO_2$ uptake has been reported at a site off the west coast of Spitsbergen, which is also characterized by high $CH_4$ flux from the seafloor (Pohlman et al., 2017). The mechanism, which causes this enhancement, is, however, unknown. One of the hypotheses is that the physical bubbling of $CH_4$ gas from the seafloor may cause an upwelling of nutrient rich waters. This mechanism may be present even at depths exceeding 1,000 m, particularly if gas plumes are strong and extend high into the water column (D'souza et al., 2016; Leifer et al., 2009). It is feasible that this upwelling effect of nutrient-rich water, and therefore an enhancement of photosynthetic primary production, also occurs at the crater area where the water depth is only 370 m and intense gas seepage with $CH_4$ bubble streams up to 200 m height were observed (Andreassen et al., 2017).

In addition to the physical bubbling mechanism, potential chemical pathways that could link $CH_4$ seepage and photosynthetic primary production exist as well. Further evidence to support the links between $CH_4$ and planktonic biomass was found in a subterranean estuary ecosystem. It was shown that shrimps were feeding on $CH_4$-derived carbon (Brankovits et al., 2017). Methane-derived carbon could be added to the water column by two mechanisms; first through bubble stripping, which entails gas exchange of $CO_2$ from $CH_4$ bubbles (Vielstädte et al., 2015), and second by $CO_2$ production as a result of active microbial $MO_X$ (equation (1)). An addition of $CO_2$ into the water column may lead to an increase in primary production if nutrient levels are sufficient (Engel et al., 2013). The hypothesis that $CO_2$ is added to the water column by gas exchange from $CH_4$ bubbles is supported by the elevated DIC and $A_T$ in the $CH_4$ plumes in April, relative to the surrounding water (Figures 2d and 2e). In April, the pH, $\Omega_{Ar}$, and $\Omega_{Ca}$ are lower in the plumes than in the surrounding water, likely due to a net $CO_2$ addition from the $CH_4$ plumes (Figures 2f and 2g). In June, the high DIC values in waters just above the seafloor are no longer confined in plumes and has likely been accumulating and dispersing since April (Figure 3d). Since $A_T$ is relatively constant between the seasons, $CO_2$ has most likely caused the elevated DIC. $MO_X$ data from June (Figure 4c) show 14 times higher rates compared to rates measured at another Arctic $CH_4$ seepage location at Storfjorden, east of Spitzbergen (Mau et al., 2013). It could therefore be possible that plankton are feeding on carbon sourced from methanotrophic bacteria.

Statistical analyses revealed that the $CH_4$ concentration in the surface water (0–100 m) in our study area showed a significantly higher variability, compared to the temperature changes between the two sampling periods (Figures 2c and 3c), probably controlled by lateral advection. April shows a nearly four-times higher $CH_4$ concentration in the surface water (Figure 2c), with an average of 16.3 nM compared to 4.4 nM in June. Furthermore, nearly all multinet samples from April contained benthic foraminifera, which also indicates strong lateral advection and increasing the likelihood that $CH_4$ could be resuspended in the water column. Higher wind stress and lower temperatures in April may have resulted in stronger currents and well-mixed water masses and consequently a stronger vertical redistribution of $CH_4$ after its release from the seafloor. This vertical redistribution of $CH_4$ causes less of a vertical gradient in $CH_4$ concentration in the water column in April compared to June. Currents also dictate the concentration of methanotrophic bacteria in the water column; the stronger the current, the wider the methanotrophic bacteria community gets spread that lowers the quantity of present methanotrophs per sampling point (Steinle et al., 2015). In June, we see a direct correlation between $CH_4$ concentration and $MO_X$ activity. It is likely that $MO_X$ activity, as well as the concentration of methanotrophic bacteria, would be lower in April, as we see in the $CH_4$ distribution pattern.

The LPF concentration at the crater area cannot be explained by the concentration of $CH_4$ in the water just above seafloor as a result of seepage (Table S5) during both sampling seasons (Figure 6). Similarly, we also do not find a positive correlation between $CH_4$ and the primary production indicators chlfluo and DO (Table S5). Methane appears to be more confined to the bottom waters in June (Figure 3c), perhaps due to the strong thermal stratification, or the high $MO_X$ rates causing the $CH_4$ to be utilized before it reaches the upper water column. This could eliminate the possibility of direct contact between $CH_4$ and the LPF in June. The $\delta^{13}C$ values of *N. pachyderma* and *T. quinqueloba* in the water column in June do not show anomalously negative values, indicating no incorporation of $CH_4$-derived carbon in their tests. Both $\delta^{13}C$ and $\delta^{18}O$ values of *N. pachyderma* and *T. quinqueloba* are comparable to those reported in the Fram Strait (Pados et al., 2015)

and Nordic Seas (Simstich et al., 2003). However, it has been demonstrated that benthic foraminiferal species do not always record the influence of $CH_4$ in their tests (Hill et al., 2004). Although our data from the crater area does not suggest a link between $CH_4$ seepage and LPF concentration, the physical and chemical mechanisms, i.e., upwelling of nutrient-rich wasters by gas flares, or the addition of $CO_2$ to the surface waters by bubble stripping or $MO_X$, are all plausible in the crater area.

## 6. Conclusions

We found significant differences in concentration, species composition, and test size between the LPF and *Limacina helicina* sampled at the beginning (April) and toward the end (June) of the spring bloom. The LPF and *L. helicina* seasonal development follows that of calanoid copepods in the same region. Test size and concentrations of both groups increased from April to June potentially as a response to the thermal stratification and increase in food availability, but without any clear link to the lunar cycle. The observation of smaller specimens of LPF and *L. helicina* in spring also suggests the occurrence of only one population/generation in April, while in June several generations and a larger species diversity are displayed. Seasonal studies on LPF, and consequently, models, are based solely on >125 or >150 μm fraction, as opposed to our data which uses the >64 μm fraction. Our results indicate that they provide limited information on the population structure of the planktonic foraminiferal faunas. Isotopic measurements on LPF shells revealed no direct influence of $CH_4$ flares on their $\delta^{18}O$ and $\delta^{13}C$ composition. Seepage of $CH_4$ therefore does not directly influence LPF. We, however, speculate that it could indirectly enhance primary production and therefore an increase in biomass in the overlying water column, either through upwelling of nutrient-rich waters or by the addition of $CO_2$, owing to gas exchange from $CH_4$ bubbles or through $MO_X$ activity. We believe that the potential fertilizing effect that $CH_4$ seepage has on the water column might be significant on a regional scale. Future research focusing on $CH_4$ seepage in marine environments should investigate the linkages between $CH_4$ input and its uptake by planktonic organisms through the mapping of trophic interactions. This could help to understand how the species or assemblages may benefit from enhanced $CH_4$ supply.

## Data Set

Total foraminiferal and pteropod counts, species concentrations, and filtered volumes are available on the PANGAEA database (https://doi.pangaea.de/10.1594/PANGAEA.904463). The CTD data are available on Norwegian Marine Data Center (https://doi.org/10.21335/NMDC-225800978).

## Competing Interests

The authors declare that there are no competing interests.

## References

AMAP: AMAP assessment (2013). Arctic Ocean acidification., 2013.
AMAP: AMAP Assessment (2018). Arctic Ocean Acidification, Arctic Monitoring and Assessment Programme (AMAP), Tromsø, Norway (www.amap.no), Tromsø, Norway., 2018.
Andreassen, K., Hubbard, A., Winsborrow, M. C. M., Patton, H., Vadakkepuliyambatta, S., Plaza-Faverola, A., et al. (2017). Massive blow-out craters formed by hydrate-controlled methane expulsion from the Arctic seafloor. *Science* (80-.), *356*(6341), 948–953. https://doi.org/10.1126/science.aal4500
Arashkevich, E., Wassmann, P., Pasternak, A., & Wexels Riser, C. (2002). Seasonal and spatial changes in biomass, structure, and development progress of the zooplankton community in the Barents Sea. *Journal of Marine Systems*, *38*(1–2), 125–145. https://doi.org/10.1016/S0924-7963(02)00173-2
Archer, D., Buffett, B., & Brovkin, V. (2008). Ocean methane hydrates as a slow tipping point in the global carbon cycle. *Proceedings of the National Academy of Sciences*, *106*(49), 2059620601. 10.1073/pnas.0800885105
Arrigo, K. R., & van Dijken, G. L. (2011). Secular trends in Arctic Ocean net primary production. *Journal of Geophysical Research, Oceans*, *116*(C9), 1, C09011–15. https://doi.org/10.1029/2011JC007151
Arrigo, K. R., & van Dijken, G. L. (2015). Continued increases in Arctic Ocean primary production. *Progress in Oceanography*, *136*, 60–70. https://doi.org/10.1016/j.pocean.2015.05.002
Åström, E. K. L., Carroll, M. L., Ambrose, W. G., & Carroll, J. (2016). Arctic cold seeps in marine methane hydrate environments: Impacts on shelf macrobenthic community structure offshore Svalbard. *Marine Ecology Progress Series*, *552*, 1–18. https://doi.org/10.3354/meps11773
Åström, E. K. L., Carroll, M. L., Ambrose, W. G., Sen, A., Silyakova, A., & Carroll, J. L. (2018). Methane cold seeps as biological oases in the high-Arctic deep sea. *Limnology and Oceanography*, *63*(S1), S209–S231. https://doi.org/10.1002/lno.10732

Åström, E. K. L., Carroll, M. L., Sen, A., Niemann, H., Ambrose, W. G., Lehmann, M. F., & Carroll, J. (2019). Chemosynthesis influences food web and community structure in high-Arctic benthos. *Marine Ecology Progress Series*, *629*(October), 19–42. https://doi.org/10.3354/meps13101

Bates, N. R., & Mathis, J. T. (2009). The Arctic Ocean marine carbon cycle: Evaluation of air-sea $CO_2$ exchanges, ocean acidification impacts and potential feedbacks. *Biogeosciences*, *6*(11), 2433–2459. https://doi.org/10.5194/bg-6-2433-2009

Bé, A. W. H. (1960). Ecology of Recent planktonic foraminifera—Part 2, Bathymetric and seasonal distributions in the Sargasso Sea off Nermuda. *Micropaleontology*, *6*(4), 373–392. https://doi.org/10.2307/1484218

Bednaršek, N., Tarling, G. A., Bakker, D. C. E., Fielding, S., Cohen, A., Kuzirian, A., et al. (2012). Description and quantification of pteropod shell dissolution: A sensitive bioindicator of ocean acidification. *Global Change Biology*, *18*(7), 2378–2388. https://doi.org/10.1111/j.1365-2486.2012.02668.x

Bednarsek, N., Tarling, G. A., Bakker, D. C. E., Fielding, S., & Feely, R. A. (2014). Dissolution dominating calcification process in polar pteropods close to the point of aragonite undersaturation. *PLoS ONE*, *9*(10), e109183. https://doi.org/10.1371/journal.pone.0109183

Berelson, W. M. (2002). Particle settling rates increase with depth in the ocean. *Deep-Sea Research Part II: Topical Studies in Oceanography*, *49*(1-3), 237–251. https://doi.org/10.1016/S0967-0645(01)00102-3

Biastoch, A., Treude, T., Rüpke, L. H., Riebesell, U., Roth, C., Burwicz, E. B., ... Wallmann, K. (2011). Rising Arctic Ocean temperatures cause gas hydrate destabilization and ocean acidification. *Geophysical Research Letters*, *38*(8), 16. https://doi.org/10.1029/2011gl047222

Bijma, J., Erez, J., & Hemleben, C. (1990). Lunar and semi-lunar reproductive cycles in some spinose planktonic foraminifers. *Journal of Foraminiferal Research*, *20*(2), 117–127. https://doi.org/10.2113/gsjfr.20.2.117

Bjørklund, K. R., Kruglikova, S. B., & Anderson, O. R. (2012). Modern incursions of tropical Radiolaria into the Arctic Ocean. *Journal of Micropalaeontology*, *31*(2), 139–158. https://doi.org/10.1144/0262-821X11-030

Boetius, A., & Wenzhöfer, F. (2013). Seafloor oxygen consumption fuelled by methane from cold seeps. *Nature Geoscience*, *6*(9), 725–734. https://doi.org/10.1038/ngeo1926

Bowden, D. A., Rowden, A. A., Thurber, A. R., Baco, A. R., Levin, L. A., & Smith, C. R. (2013). Cold seep epifaunal communities on the Hikurangi Margin, New Zealand: Composition, succession, and vulnerability to human activities. *PLoS ONE*, *8*(10), e76869. https://doi.org/10.1371/journal.pone.0076869

Berndt, C., Feseker, T., Treude, T., Krastel, S., Liebetrau, V., Niemann, H., et al. (2014). Temporal Constraints on Hydrate-Controlled Methane Seepage off Svalbard. *Science*, *343*(6168), 284287. https://doi.org/10.1126/science.1246298

Brankovits, D., Pohlman, J. W., Niemann, H., Leigh, M. B., Leewis, M. C., Becker, K. W., et al. (2017). Methane-and dissolved organic carbon-fueled microbial loop supports a tropical subterranean estuary ecosystem. *Nature Communications*, *8*(1), 1835. https://doi.org/10.1038/s41467-017-01776-x

Caldeira, K., & Wickett, M. (2005). Ocean model predictions of chemistry changes from carbon dioxide emissions to the atmosphere and ocean. *Journal of Geophysical Research, C: Oceans*, *110*(C9), 1, C09S04–12. https://doi.org/10.1029/2004JC002671

Carstens, J., Hebbeln, D., & Wefer, G. (1997). Distribution of planktic foraminifera at the ice margin in the Arctic (Fram Strait). *Marine Micropaleontology*, *29*(3–4), 257–269. https://doi.org/10.1016/S0377-8398(96)00014-X

Comeau, S., Gorsky, G., Jeffree, R., Teyssi, J., Villefranche, D. and Cedex, V.: Impact of ocean acidification on a key Arctic pelagic mollusc. pdf, 1877–1882, 2009.

Cottier, F., Tverberg, V., Inall, M., Svendsen, H., Nilsen, F., & Griffiths, C. (2005). Water mass modification in an Arctic fjord through cross-shelf exchange: The seasonal hydrography of Kongsfjorden, Svalbard. *Journal of Geophysical Research, Oceans*, *110*(C12), 1, C12005–18. https://doi.org/10.1029/2004JC002757

Damm, E., Mackensen, A., Budéus, G., Faber, E., & Hanfland, C. (2005). Pathways of methane in seawater: Plume spreading in an Arctic shelf environment (SW-Spitsbergen). *Continental Shelf Research*, *25*(12–13), 1453–1472. https://doi.org/10.1016/j.csr.2005.03.003

Davis, C. V., Rivest, E. B., Hill, T. M., Gaylord, B., Russell, A. D., & Sanford, E. (2017). Ocean acidification compromises a planktic calcifier with implications for global carbon cycling. *Scientific Reports*, *7*(1), 1–8. https://doi.org/10.1038/s41598-017-01530-9

Dickson, A., & Millero, F. (1987). A comparison of the equilibrium constants for the dissociation of carbonic acid in seawater media. *Deep Sea Research Part A, Oceanographic Research Papers*, *34*(10), 1733–1743.

Dickson, A. G. (1990). Thermodynamics of the dissociation of boric acid in synthetic seawater from 273.15 to 318.15 K. *Deep-Sea Research Part I: Oceanographic Research Papers*, *37*(5), 755–766. https://doi.org/10.1016/0198-0149(90)90004-F

Dickson, A. G., Sabine, C. L. and Christian, J. R.: *Guide to best practices for ocean CO2 measurements.*, 2007.

Dieckmann, G. S., Spindler, M., Lange, M. A., Ackley, S. F., & Eicken, H. (1991). Antarctic sea ice: A habitat for the foraminifer Neogloboquadrina pachyderma. *Journal of Foraminiferal Research*, *21*(2), 182–189. https://doi.org/10.2113/gsjfr.21.2.182

Dlugokencky, E. J. & Tans, P. P., (2019). NOAA/ESRL.

D'souza, N. A., Subramaniam, A., Juhl, A. R., Hafez, M., Chekalyuk, A., Phan, S., et al. (2016). Elevated surface chlorophyll associated with natural oil seeps in the Gulf of Mexico. *Nature Geoscience*, *9*(3), 215–218. https://doi.org/10.1038/ngeo2631

Engel, A., Borchard, C., Piontek, J., Schulz, K. G., Riebesell, U., & Bellerby, R. (2013). $CO_2$ increases 14C primary production in an Arctic plankton community. *Biogeosciences*, *10*(3), 12911308. https://doi.org/10.5194/bg-10-1291-2013

Erez, J., Almogi-Labin, A., & Avraham, S. (1991). On the life history of planktonic foraminifera: Lunar reproduction cycle in Globigerinoides sacculifer (Brady). *Paleoceanography*, *6*(3), 295–306. https://doi.org/10.1029/90PA02731

Eynaud, F. (2011). Planktonic foraminifera in the arctic: Potentials and issues regarding modern and quaternary populations. *IOP Conference Series: Earth and Environmental Science*, *14*(1). https://doi.org/10.1088/1755-1315/14/1/012005

Fischer, G., Fütterer, D., Gersonde, R., Honjo, S., Ostermann, D., & Wefer, G. (1988). Seasonal variability of particle flux in the Weddell Sea and its relation to ice cover. *Nature*, *335*(6189), 426–428. https://doi.org/10.1038/335426a0

Fossheim, M., Primicerio, R., Johannesen, E., Ingvaldsen, R. B., Aschan, M. M., & Dolgov, A. V. (2015). Recent warming leads to a rapid borealization of fish communities in the Arctic. *Nature Climate Change*, *5*(7), 673–677. https://doi.org/10.1038/nclimate2647

Fransson, A., Chierici, M., & Nojiri, Y. (2009). New insights into the spatial variability of the surface water carbon dioxide in varying sea ice conditions in the Arctic Ocean. *Continental Shelf Research*, *29*(10), 1317–1328. https://doi.org/10.1016/j.csr.2009.03.008

Fulton, J. (1983). Seasonal and annual variations of net zooplankton at Ocean Station P, 1959–1980. *Canadian Data Report Fisheries and Aquatic Sciences*, *374*, 65.

Graves, C. A., Steinle, L., Rehder, G., Niemann, H., Connelly, D. P., Lowry, D., et al. (2015). Fluxes and fate of dissolved methane released at the seafloor at the landward limit of the gas hydrate stability zone offshore western Svalbard. *Journal of Geophysical Research, Oceans*, *120*(9), 6185–6201. https://doi.org/10.1002/2015JC011084

68

Greco, M., Jonkers, L., Kretschmer, K., Bijma, J., & Kucera, M. (2019). Variable habitat depth of the planktonic foraminifera Neogloboquadrina pachyderma in the northern high latitudes explained by sea-ice and chlorophyll concentration. *Biogeosciences Discussions*. https://doi.org/10.5194/bg-2019-79

Grupe, B. M., Krach, M. L., Pasulka, A. L., Maloney, J. M., Levin, L. A., & Frieder, C. A. (2015). Methane seep ecosystem functions and services from a recently discovered southern California seep. *Marine Ecology*, *36*(S1), 91–108. https://doi.org/10.1111/maec.12243

Gyldenfeldt, A.-B. V., Carstens, J., & Meincke, J. (2000). Estimation of the catchment area of a sediment trap by means of current meters and foraminiferal tests. *Deep-Sea Research Part II: Topical Studies in Oceanography*, *47*(9–11), 1701–1717. https://doi.org/10.1016/S0967-0645(00)00004-7

Haine, T. W. N., Curry, B., Gerdes, R., Hansen, E., Karcher, M., Lee, C., et al. (2015). Arctic freshwater export: Status, mechanisms, and prospects. *Global and Planetary Change*, *125*, 13–35. https://doi.org/10.1016/j.gloplacha.2014.11.013

Heinz, P., Sommer, S., Pfannkuche, O., & Hemleben, C. (2005). Living benthic foraminifera in sediments influenced by gas hydrates at the Cascadia convergent margin, NE Pacific. *Marine Ecology Progress Series*, *304*, 77–89. https://doi.org/10.3354/meps304077

Hemleben, C., Spindler, M., & Anderson, O. R. (1989). *Modern planktonic foraminifera*, (1st ed.). New York: Springer-Verlag.

Herguera, J. C., Paull, C. K., Perez, E., Ussler, W., & Peltzer, E. (2014). Limits to the sensitivity of living benthic foraminifera to pore water carbon isotope anomalies in methane vent environments. *Paleoceanography*, *29*(3), 273–289. https://doi.org/10.1177/0091270004269562

Hill, T. M., Kennett, J. P., & Valentine, D. L. (2004). Isotopic evidence for the incorporation of methane-derived carbon into foraminifera from modern methane seeps, Hydrate Ridge, Northeast Pacific. *Geochimica et Cosmochimica Acta*, *68*(22), 4619–4627. https://doi.org/10.1016/j.gca.2004.07.012

IPCC: Climate change (2013). The physical science basis. In T. F. Stocker, D. Qin, G.-K. Plattner, M. Tignor, S. K. Allen, J. Boschung, et al. (Eds.), *Contribution of Working Group I to the Fifth Assessment Report of the Intergovernmental Panel on Climate Change*. (Chapter 8, p. 1535). Cambridge, United Kingdom and New York, NY, USA: Cambridge University Press.

Jensen, S. (1998). Planktische Foraminiferen im Europäischen Nordmeer: Verbreitung und Vertikalfluß sowie ihre Entwicklung während der letzten 15000 Jahre, Berichte Sonderforschungsbereich 313, Univ. Kiel, *75*(75), 1–105.

Jonkers, L., Brummer, G. J. A., Peeters, F. J. C., Van Aken, H. M., & De Jong, M. F. (2010). Seasonal stratification, shell flux, and oxygen isotope dynamics of leftcoiling N. pachyderma and T. quinqueloba in the western subpolar North Atlantic. *Paleoceanography*, *25*, PA2204. https://doi.org/10.1029/2009PA001849

Jonkers, L., Hillebrand, H., & Kučera, M. (2019). Global change drives modern plankton communities away from the preindustrial state. *Nature*, *570*(7761), 372–375. https://doi.org/10.1038/s41586-019-1230-3

Jonkers, L. and Kučera, M.: Global analysis of seasonality in the shell flux of extant planktonic Foraminifera, *Biogeosciences*, *12*(7), 2207–2226, doi:https://doi.org/10.5194/bg-12-2207-2015, PA22042015.

Jonkers, L., Reynolds, C. E., Richey, J., & Hall, I. R. (2015). Lunar periodicity in the shell flux of planktonic foraminifera in the Gulf of Mexico. *Biogeosciences*, *12*(10), 3061–3070. https://doi.org/10.5194/bg-12-3061-2015

Kaltin, S., & Anderson, L. G. (2005). Uptake of atmospheric carbon dioxide in Arctic shelf seas: Evaluation of the relative importance of processes that influence pCO2 in water transported over the Bering-Chukchi Sea shelf. *Marine Chemistry*, *94*(1–4), 67–79. https://doi.org/10.1016/j.marchem.2004.07.010

Kretschmer, K., Jonkers, L., Kucera, M., & Schulz, M. (2018). Modeling seasonal and vertical habitats of planktonic foraminifera on a global scale. *Biogeosciences*, *15*(14), 4405–4429. https://doi.org/10.5194/bg-15-4405-2018

Kretschmer, K., Kucera, M., & Schulz, M. (2016). Modeling the distribution and seasonality of Neogloboquadrina pachyderma in the North Atlantic Ocean during Heinrich Stadial 1. *Paleoceanography and Paleoclimatology*, 986–1010. https://doi.org/10.1002/2015PA002819

Kucera, M. (2007). Chapter six planktonic foraminifera as tracers of past oceanic environments. *Developments in Marine Geology*, *1*(07), 213–262. https://doi.org/10.1016/S1572-5480(07)01011-1

Leifer, I., Jeuthe, H., Gjøsund, S. H., & Johansen, V. (2009). Engineered and natural marine seep, bubble-driven buoyancy flows. *Journal of Physical Oceanography*, *39*(12), 3071–3090. https://doi.org/10.1175/2009jpo4135.1

Levin, L. A. (2005). Ecology of cold seep sediments: Interactions of fauna with flow, chemistry and microbes. *Oceanography and Marine Biology: An Annual Review*, *43*, 1–46. https://doi.org/10.1201/9781420037449.ch1

Levin, L. A., Baco, A. R., Bowden, D. A., Colaco, A., Cordes, E. E., Cunha, M. R., et al. (2016). Hydrothermal vents and methane seeps: Rethinking the sphere of influence. *Frontiers in Marine Science*, *3*(May), 1–23. https://doi.org/10.3389/fmars.2016.00072

Lewis, E. & Wallace, D. W. R. (1998). CO2SYS-Program developed for CO2 system calculations, ORNL/CDIAC-105, Carbon Dioxide Inf. Anal. Cent., Oak Ridge Natl. Lab., Oak Ridge, Tenn.

Lischka, S., Büdenbender, J., Boxhammer, T., & Riebesell, U. (2011). Impact of ocean acidification and elevated temperatures on early juveniles of the polar shelled pteropod Limacina helicina: Mortality, shell degradation, and shell growth. *Biogeosciences*, *8*(4), 919–932. https://doi.org/10.5194/bg-8-919-2011

Loeng, H. (1991). Features of the physical oceanographic conditions of the Barents Sea. *Polar Research*, *10*(1), 5–18. https://doi.org/10.1111/j.1751-8369.1991.tb00630.x

Loeng, H., Ozhigin, V., & Ådlandsvik, B. (1997). Water fluxes through the Barents Sea. *ICES Journal of Marine Science*, *54*(3), 310–317. https://doi.org/10.1006/jmsc.1996.0165

Mann, H. B., & Whitney, D. R. (1947). On a test of whether one of two random variables is stochastically larger than the other. *Annals of Mathematical Statistics*, *18*(1), 50–60.

Manno, C., Morata, N., & Bellerby, R. (2012). Effect of ocean acidification and temperature increase on the planktonic foraminifer Neogloboquadrina pachyderma (sinistral). *Polar Biology*, *35*(9), 1311–1319. https://doi.org/10.1007/s00300-012-1174-7

Mau, S., Blees, J., Helmke, E., Niemann, H., & Damm, E. (2013). Vertical distribution of methane oxidation and methanotrophic response to elevated methane concentrations in stratified waters of the Arctic fjord Storfjorden (Svalbard, Norway). *Biogeosciences*, *10*(10), 6267–6268. https://doi.org/10.5194/bg-10-6267-2013

Mau, S., Römer, M., Torres, M. E., Bussmann, I., Pape, T., Damm, E. & Geprägs, P. (2017). Widespread methane seepage along the continental margin off Svalbard—From Bjørnøya to Kongsfjorden, Nat. Publ. Gr., (January), 1–13, doi:https://doi.org/10.1038/srep42997.

Mehrbach, C., Culberson, C. H., Hawley, J. E., & Pytkowicx, R. M. (1973). Measurement of the apparent dissociation constants of carbonic acid in seawater at atmospheric pressure1. *Limnology and Oceanography*, *18*(6), 897–907. https://doi.org/10.4319/lo.1973.18.6.0897

Meilland, J. (2015). Rôle des foraminifères planctoniques dans le cycle du carbone marin des hautes latitudes (Océan Indien Austral), Université d'Angers, 2015. Français.

Meilland, J., Schiebel, R., Sanchez, S., & Howa, H. (2018). Abundances and test weights of living planktic foraminifers across the Southwest Indian Ocean: Implications for carbon fl uxes. *Deep Sea Research Part I*, *131*(March 2017), 27–40. https://doi.org/10.1016/j.dsr.2017.11.004

69

Meilland, J., Siccha, M., Weinkauf, M. F. G., Jonkers, L., & Morard, R. (2019). Highly replicated sampling reveals no species-specific vertical habitats in diurnal vertical migration but stable planktonic foraminifera. *Journal of Plankton Research*, *00*, 1–15. https://doi.org/10.1093/zoolinnean/zly093

Moy, A. D., Howard, W. R., Bray, S. G., & Trull, T. W. (2009). Reduced calcification in modern Southern Ocean planktonic foraminifera. *Nature Geoscience*, *2*(4), 276–280. https://doi.org/10.1038/ngeo460

Niemann, H., Steinle, L., Blees, J., Bussmann, I., Treude, T., Krause, S., et al. (2015). Toxic effects of lab-grade butyl rubber stoppers on aerobic methane oxidation. *Limnology and Oceanography: Methods*, *13*(1), 40–52. https://doi.org/10.1002/lom3.10005

Orr, J. C., Fabry, V. J., Aumont, O., Bopp, L., Doney, S. C., Feely, R. A., et al. (2005). Anthropogenic ocean acidification over the twenty-first century and its impact on calcifying organisms. *Nature*, *437*(7059), 681–686. https://doi.org/10.1038/nature04095

Oziel, L., Neukermans, G., Ardyna, M., Sirven, J., Ruiz-Pino, D., Gascard, J.-C., et al. (2017). Role for Atlantic inflows and sea ice loss on shifting phytoplankton blooms in the Barents Sea. *Journal of Geophysical Research, Oceans*, *122*, 5121–5139. https://doi.org/10.1002/2016JC012582

Oziel, L., Sirven, J., & Gascard, J. C. (2016). The Barents Sea frontal zones and water masses variability (1980-2011). *Ocean Science*, *12*(1), 169–184. https://doi.org/10.5194/os-12-169-2016

Pados, T., & Spielhagen, R. F. (2014). Species distribution and depth habitat of recent planktic foraminifera in Fram Strait, Arctic Ocean. *Polar Research*, *33*(1), 22483. https://doi.org/10.3402/polar.v33.22483

Pados, T., Spielhagen, R. F., Bauch, D., Meyer, H., & Segl, M. (2015). Oxygen and carbon isotope composition of modern planktic foraminifera and near-surface waters in the Fram Strait (Arctic Ocean)—A case study. *Biogeosciences*, *12*(6), 1733–1752. https://doi.org/10.5194/bg-12-1733-2015

Pierrot, D. E. & Wallace, D. W. R. (2006). MS Excel program developed for CO2 system calculations.

Pisso, I., Myhre, C. L., Platt, S. M., Eckhardt, S., Hermansen, O., Schmidbauer, N., et al. (2016). Constraints on oceanic methane emissions west of Svalbard from atmospheric in situ measurements and Lagrangian transport modeling. *Journal of Geophysical Research – Atmospheres*, *121*(23), 14,188–14,200. https://doi.org/10.1002/2016JD025590

Pohlman, J. W., Greinert, J., Ruppel, C., Silyakova, A., Vielstädte, L., Casso, M., et al. (2017). Enhanced CO 2 uptake at a shallow Arctic Ocean seep field overwhelms the positive warming potential of emitted methane. *Proceedings of the National Academy of Sciences*, *19*, 201618926. https://doi.org/10.1073/pnas.1618926114

Rabe, B., Karcher, M., Schauer, U., Toole, J. M., Krishfield, R. A., Pisarev, S., et al. (2011). An assessment of Arctic Ocean freshwater content changes from the 1990s to the 2006-2008 period. *Deep-Sea Research Part I: Oceanographic Research Papers*, *58*(2), 173–185. https://doi.org/10.1016/j.dsr.2010.12.002

Rakowski, C. V., Magen, C., Bosman, S., Rogers, K. L., Gillies, L. E., Chanton, J. P., & Mason, O. U. (2015). Methane and microbial dynamics in the Gulf of Mexico water column. *Frontiers in Marine Science*, *2*, 1–10. https://doi.org/10.3389/fmars.2015.00069

Rathburn, A. E., Levin, L. A., Held, Z., & Lohmann, K. C. (2000). Benthic foraminifera associated with cold seeps on the northern California margin: Ecology and stableisotopic composition. *Marine Micropaleontology*, *38*, 247–266. https://doi.org/10.1016/S0377-8398(00)00005-0

Rebotim, A., Voelker, A. H. L., Jonkers, L., Waniek, J. J., Meggers, H., Schiebel, R., et al. (2017). Factors controlling the depth habitat of planktonic foraminifera in the subtropical eastern North Atlantic. *Biogeosciences*, *14*(4), 827–859. https://doi.org/10.5194/bg-14-827-2017

Reeburgh, W. S. (2013). Global methane biogeochemistry. In *Treatise Geochemistry*, (Second ed., Vol. 5, pp. 71–94). University of California, Irvine, CA, USA: Elsevier Science. https://doi.org/10.1016/B978-0-08-095975-7.00403-4

Reigstad, M., Wassmann, P., Wexels Riser, C., Øygarden, S., & Rey, F. (2002). Variations in hydrography, nutrients and chlorophyll *a* in the marginal ice-zone and the central Barents Sea. *Journal of Marine Systems*, *38*(1–2), 9–29. https://doi.org/10.1016/S0924-7963(02)00167-7

RStudio Team: RStudio: Integrated development for R (2015). RStudio, Inc.

Ruppel, C. D., & Kessler, J. D. (2017). The interaction of climate change and methane hydrates. *Reviews of Geophysics*, *55*(1), 126–168. https://doi.org/10.1002/2016RG000534

Sapart, C. J., Shakhova, N., Semiletov, I., Jansen, J., Szidat, S., Kosmach, D., ... Röckmann, T. (2017). The origin of methane in the East Siberian Arctic Shelf unraveled with triple isotope analysis. *Biogeosciences*, *14*(9), 22832292. https://doi.org/10.5194/bg-14-2283-2017

Schiebel, R. (2002). Planktic foraminiferal sedimentation and the marine calcite budget. *Global Biogeochemical Cycles*, *16*(4), 1065. https://doi.org/10.1029/2001GB001459

Schiebel, R., Bijma, J., & Hemleben, C. (1997). Population dynamics of the planktic foraminifer Globigerina bulloides from the eastern North Atlantic. *Deep-Sea Research Part I: Oceanographic Research Papers*, *44*(9–10), 1701–1713. https://doi.org/10.1016/S0967-0637(97)00036-8

Schiebel, R., & Hemleben, C. (2000). Interannual variability of planktic foraminiferal populations and test flux in the eastern North Atlantic Ocean (JGOFS). *Deep-Sea Research Part II: Topical Studies in Oceanography*, *47*(9–11), 1809–1852. https://doi.org/10.1016/S0967-0645(00)00008-4

Schiebel, R., & Hemleben, C. (2017). *Planktic foraminifers in the modern ocean*. Berlin Heidelberg.: Springer-Verlag.

Sellanes, J., Quiroga, E., & Neira, C. (2008). Megafauna community structure and trophic relationships at the recently discovered Concepción Methane Seep Area, Chile, ∼36°S. *ICES Journal of Marine Science*, *65*(7), 1102–1111. https://doi.org/10.1093/icesjms/fsn099

Sen, A., Aström, E. K. L., Hong, W. L., Portnov, A., Waage, M., Serov, P., et al. (2018). Geophysical and geochemical controls on the megafaunal community of a high Arctic cold seep. *Biogeosciences*, *15*(14), 4533–4559. https://doi.org/10.5194/bg-15-4533-2018

Sen, A., Duperron, S., Hourdez, S., Piquet, B., Léger, N., Gebruk, A., et al. (2018). Cryptic frenulates are the dominant chemosymbiotrophic fauna at Arctic and high latitude Atlantic cold seeps. *PLoS ONE*, *13*(12), e0209273. https://doi.org/10.1371/journal.pone.0209273

Sen, A., Himmler, T., Hong, W. L., Chitkara, C., Raymond, W., Ferré, B., et al. (2019). Atypical biological features of a new cold seep site on the Lofoten-Vesterålen continental margin (northern Norway). *Scientific Reports*, 1–14. https://doi.org/10.1038/s41598-018-38070-9

Shakhova, N., Semiletov, I., Salyuk, A., Yusupov, V., Kosmach, D., & Gustafsson, Ö. (2010). Extensive methane venting to the atmosphere from sediments of the East Siberian Arctic Shelf. *Science*, *327*(5970), 1246–1250.

Shannon, C. E., & Weaver, W. (1949). *The mathematical theory of communication*. Urbana.: University of Illinois press.

Sibuet, M., & Olu, K. (1998). Biogeography, biodiversity and fluid dependence of deep-sea cold-seep communities at active and passive margins. *Deep-Sea Research Part II: Topical Studies in Oceanography*, *45*(1–3), 517–567. https://doi.org/10.1016/S0967-0645(97)00074-X

Sibuet, M., & Olu-Le Roy, K. (2002). Cold seep communities on continental margins: Structure and quantitative distribution relative to geological and fluid venting patterns. In G. Wefer, D. Billett, D. Hebbeln, B. B. Jørgensen, M. Schlüter, & T. C. E. van Weering (Eds.), *Ocean Margin Systems*, (pp. 235–251). Berlin, Heidelberg: Springer.

70

Silyakova, A., Greinert, J., Jansson, P. & Ferré, B. (2015). Methane from shallow seep areas of the NW Svalbard Arctic margin does not reach the sea surface, 17(223259), 223259.

Simstich, J., Sarnthein, M., & Erlenkeuser, H. (2003). Paired δ18O signals of Neogloboquadrina pachyderma (s) and Turborotalita quinqueloba show thermal stratification structure in Nordic Seas. *Marine Micropaleontology*, *48*(1–2), 107–125. https://doi.org/10.1016/S0377-8398(02)00165-2

Spero, H. J., & Lea, D. W. (1996). Experimental determination of stable isotope variability in Globigerina bulloides: Implications for paleoceanographic reconstructions. *Marine Micropaleontology*, *28*(3–4), 231–246.

Spindler, M. (1996). On the salinity tolerance of the planktonic foraminifer neogloboquadrina pachyderma from antarctic sea ice. *Proceedings of the NIPR Symposium on Polar Biology*, *9*, 85–91. https://doi.org/10.2113/gsjfr.21.2.182

Steinle, L., Graves, C. A., Treude, T., Ferré, B., Biastoch, A., Bussmann, I., et al. (2015). Water column methanotrophy controlled by a rapid oceanographic switch. *Nature Geoscience*. https://doi.org/10.1038/NGEO2420

Stouffer, R. J., Manabe, S., & Bryan, K. (1989). Interhemispheric asymmetry in climate response to a gradual increase of atmospheric CO2. *Nature*, *342*(6250), 660–662. https://doi.org/10.1038/342660a0

Stroeve, J. C., Serreze, M. C., Holland, M. M., Kay, J. E., Malanik, J., & Barrett, A. P. (2012). The Arctic's rapidly shrinking sea ice cover: A research synthesis. *Climatic Change*, *110*(3–4), 1005–1027. https://doi.org/10.1007/s10584-011-0101-1

Thomsen, E., Rasmussen, T. L., Sztybor, K., Hanken, N., Tendal, O. S., & Uchman, A. (2019). Cold-seep fossil macrofaunal assemblages from Vestnesa Ridge, eastern Fram Strait, during the past 45 000 years. *Polar Research*, *38*(3310), 1–20. https://doi.org/10.33265/polar.v38.3310

Uppström, L. R. (1974). The boron/chlorinity ratio of deep-sea water from the Pacific Ocean. *Deep-Sea Research and Oceanographic Abstracts*, *21*(2), 161–162. https://doi.org/10.1016/0011-7471(74)90074-6

Vielstädte, L., Karstens, J., Haeckel, M., Schmidt, M., Linke, P., Reimann, S., et al. (2015). Quantification of methane emissions at abandoned gas wells in the Central North Sea. *Marine and Petroleum Geology*, *68*, 848–860. https://doi.org/10.1016/j.marpetgeo.2015.07.030

Volkmann, R. (2000). Planktic foraminifers in the outer Laptev Sea and the Fram Strait—Modern distribution and ecology. *Journal of Foraminiferal Research*, *30*(3), 157–176. https://doi.org/10.2113/0300157

Wang, K., Hunt, B. P. V., Liang, C., Pauly, D., & Pakhomov, E. A. (2017). Reassessment of the life cycle of the pteropod Limacina helicina from a high resolution interannual time series in the temperate North Pacific. *ICES Journal of Marine Science*, *74*(7), 1906–1920. https://doi.org/10.1093/icesjms/fsx014

Wassmann, P., & Slagstad, D. (1993). Seasonal and annual dynamics of particulate carbon flux in the Barents Sea—A model approach. *Polar Biology*, *13*(6), 363–372. https://doi.org/10.1007/BF01681977

Westbrook, G. K., Thatcher, K. E., Rohling, E. J., Piotrowski, A. M., Osborne, A. H., Nisbet, E. G., et al. (2009). Escape of methane gas from the seabed along the West Spitsbergen continental margin. *Geophysical Research Letters*, *36*, L15608. https://doi.org/10.1029/2009GL039191

Wiesenburg, D. A., & Guinasso, N. L. (1979). Equilibrium solubilities of methane, carbon monoxide, and hydrogen in water and sea water. *Journal of Chemical & Engineering Data*, *24*(4), 356–360.
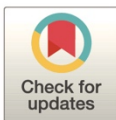
Paper II

# PLOS ONE

# Shell density of planktonic foraminifera and pteropod species *Limacina helicina* in the Barents Sea: Relation to ontogeny and water chemistry

**Siri Ofstad** [1] *, **Katarzyna Zamelczyk**[1], **Katsunori Kimoto**[2], **Melissa Chierici**[3], **Agneta Fransson**[4], **Tine Lander Rasmussen**[1]

**1** CAGE–Centre for Arctic Gas Hydrate, Environment and Climate, Department of Geosciences, UiT, The Arctic University of Norway, Tromsø, Norway, **2** Japan Agency for Marine-Earth Science and Technology (JAMSTEC), Yokosuka, Japan, **3** Institute of Marine Research, Fram Centre, Tromsø, Norway, **4** Norwegian Polar Institute, Fram Centre, Tromsø, Norway

* siri.ofstad@uit.no

## Abstract

Planktonic calcifiers, the foraminiferal species *Neogloboquadrina pachyderma* and *Turborotalita quinqueloba*, and the thecosome pteropod *Limacina helicina* from plankton tows and surface sediments from the northern Barents Sea were studied to assess how shell density varies with depth habitat and ontogenetic processes. The shells were measured using X-ray microcomputed tomography (XMCT) scanning and compared to the physical and chemical properties of the water column including the carbonate chemistry and calcium carbonate saturation of calcite and aragonite. Both living *L. helicina* and *N. pachyderma* increased in shell density from the surface to 300 m water depth. *Turborotalita quinqueloba* increased in shell density to 150–200 m water depth. Deeper than 150 m, *T. quinqueloba* experienced a loss of density due to internal dissolution, possibly related to gametogenesis. The shell density of recently settled (dead) specimens of planktonic foraminifera from surface sediment samples was compared to the living fauna and showed a large range of dissolution states. This dissolution was not apparent from shell-surface texture, especially for *N. pachyderma*, which tended to be both thicker and denser than *T. quinqueloba*. Dissolution lowered the shell density while the thickness of the shell remained intact. *Limacina helicina* also increase in shell size with water depth and thicken the shell apex with growth. This study demonstrates that the living fauna in this specific area from the Barents Sea did not suffer from dissolution effects. Dissolution occurred after death and after settling on the sea floor. The study also shows that biomonitoring is important for the understanding of the natural variability in shell density of calcifying zooplankton.

## 1. Introduction

The Arctic is particularly sensitive to global warming, and this warming is greatly amplified in the Barents Sea, a large and productive shelf sea bordering the Arctic Ocean [1,2]. The Barents

72

Sea is influenced by inflow of Atlantic Water (AW) from the south and Polar Water from the Arctic Ocean in the north, making it a hydrologically dynamic region. The two water masses mix and generate the Polar Front, a zone of very high-productivity [3]. In the northern Barents Sea there has been a substantial shift in water mass properties over the past several decades [4]. The water column in the northern Barents Sea has become warmer and more saline, and stratification has weakened [4]. This shift is due to an increase of AW water transport, and an increase in temperature and salinity of the AW [5,6]. This 'Atlantification' of the water column will impact the productivity and structure of the Barents Sea ecosystems by displacing the Polar Front north-eastward, and allowing the advection of temperate species further into the Arctic domain [6–8]. A poleward shift of species in the Barents Sea has already been documented [9–11]. The large volume of warm and saline AW is also thought to be the main cause of the rapid decline of the winter sea ice cover [1].

The Barents Sea is one of the largest $CO_2$ sink areas in the Arctic region, which is mainly caused by the year-round $CO_2$ undersaturation and high biological production [12,13] despite the formation of sea-ice in winter. The Barents Sea $CO_2$ sink is predicted to double by 2065 with an associated pH decrease of up to 0.25 pH units [14]. A significant proportion of the observed $CO_2$ increase in the Barents Sea has been from the inflow of AW, which is rich in anthropogenic $CO_2$ [15]. The meltwater from sea ice or glaciers lowers the saturation state of seawater with respect to calcite ($\Omega_{Ca}$) and aragonite ($\Omega_{Ar}$), the two most common polymorphs of $CaCO_3$ formed by marine organisms [16–18]. The volume of meltwater is predicted to increase as a result of the progressing global warming [19]. Ocean acidification (OA) may lead to adverse effects on the ability of marine calcifiers to produce $CaCO_3$ shells [20].

Planktonic foraminifera (PF) and thecosome pteropods are the major calcifiers among marine zooplankton [20]. Marine calcifiers, in particular pteropods, are important prey in many marine food webs [21–24]. In addition, both PF and pteropods contribute significantly to the biological carbon pump [25–29]. Only few studies of PF and pteropod faunas for the high Arctic exists and in particular for the Barents Sea [30–32]. Planktonic foraminifera build their shells of calcite, while the polar pteropod species *Limacina helicina* build their shells of aragonite. The crystal structure of calcite is more stable than aragonite, and the tendency for the crystal structure to dissolve is linked to the $\Omega$ in the surrounding environment of the particular mineral phase. The crystal structures of aragonite and calcite are thermodynamically stable when $\Omega > 1$. Both PF and *L. helicina* are sensitive to the carbonate chemistry in their environment and the extent of their calcification is commonly used as an indicator for OA [33–40]. Furthermore, due to their long sedimentary record PF shell density has been used for paleoceanographic studies of OA and atmospheric $CO_2$ [41–44].

In a previous study, we documented the seasonal variability in the distribution patterns of PF and polar pteropod *L. helicina* and their environments in the northern Barents Sea [30]. Test size and abundance of both groups increased drastically from spring to summer, and in summer there was a clearer depth zonation of the individuals, possibly related to the thermal stratification [30]. Here, we extend our analysis on PF and *L. helicina* to study the shell density of the summer population.

In OA research there are few studies with focus on how the shell density of calcareous planktonic organisms varies with ontogeny. In contrast to the pteropod *L. helicina*, PF do not perform diel vertical migration [45]. However, their shell density and depth habitat may be linked due to the possibility of ontogenetic vertical migration meaning that they descend to a deeper habitat as their life cycle progresses, likely in order to reproduce at certain water depths [46–49]. It should be noted that this concept is still disputed and is difficult to document. We thus hypothesize that the shell density of PF is related to its depth habitat in the upper water column. As PF grow and add chambers, they add layers of calcite onto the existing shell

through secondary calcification. It is unknown how the shell density of PF changes with increasing water depth. Following the assumption that calcification is linear, it will be assumed that denser shells found deeper in the water column are older.

Furthermore, processes like ontogenetic secondary calcification, gametogenic calcite addition following gametogenesis, and diagenetic encrustation will influence how well PF are preserved in the sedimentary record, which is significant for the accuracy of studies of fossil faunas. Knowledge on the natural variability in shell density across a population of calcareous planktonic organisms will improve our ability to better document biological effects of OA. In this study, we aim to show 1) the variability in shell density of the living planktonic foraminiferal species *N. pachyderma* and *T. quinqueloba* and the pteropod *L. helicina* with shell size and water depth, 2) the interspecies differences in shell density of *N. pachyderma* and *T. quinqueloba*, 3) if any changes in the observed patterns in shell density can be related to seawater carbonate chemistry, and 4) how shell density and ontogenetic processes affect the preservation of foraminifera in the surface sediments. This study is based on X-ray microcomputed tomography (XMCT) scanning of their shells. This is a pioneer study to provide the first shell density measurements of specimens of planktonic foraminifera and *Limacina helicina* from the Arctic region.

## 2. Material and methods

### 2.1 Study and sample collection

The Barents Sea is a relatively shallow continental shelf sea adjacent to the Nordic Seas and the Arctic Ocean with a mean depth of 250 m. The Bjørnøyrenna crater area (referred to in this study as the 'crater area') (74.91˚N, 27.7˚E; Fig 1) is located in relatively deep water (~340 m depth) on the northern flank of Bear Island Trough and is characterized by high levels of methane emission [50]. The Barents Sea is mainly influenced by the inflow of warm and saline Atlantic water transported in the north-eastern flowing Norwegian Atlantic current (NwAC) and the cold Arctic water transported in the East Spitsbergen current (ESC) from the north to the south [3] (Fig 1). Once the NwAC enters the Bear Island Through it splits into two branches. A substantial part of the NwAC forms a northeast flowing current, the North Cape current, which enters the southern Barents Sea, while the remainder forms the northwest flowing West Spitsbergen current (WSC).

Samples were collected onboard *R/V Helmer Hanssen* during the expedition CAGE 16–5, on June 29th 2016 at three stations located at 74.9˚N, 27.7˚E–27.8˚E. No sampling permission was required at this location. This is because the study area is outside of the 12-mile limit of the Norwegian coast, meaning it is not in territorial waters, and the sampling causes no harm to the environment. The plankton sampled from the water column are not endangered or protected species. The PF and *L. helicina* were sampled with a stratified plankton net with mesh size of 64 µm (net opening 0.5 m$^2$; Hydro-Bios, Kiel, Germany), from five consecutive depth intervals (0–50 m, 50–100 m, 100–150 m, 150–200 m, and 200–300 m). Parallel measurements and sampling for the study of physical and chemical environment in the water column were performed at the same location using a Conductivity-Temperature-Depth (CTD)-Rosette system with seawater sampling for determination of carbonate chemistry. Empty shells found in the water column >150 m are assumed to represent recently dead specimens. Their shells were transparent, well preserved and similar to the shells of the live specimens containing protoplasm.

### 2.2 Sampling of marine calcifiers

Once the plankton tows were retrieved, the samples were sieved with sea water through a 63-µm sieve and transferred into plastic bottles (250 ml) and fixed and buffered with
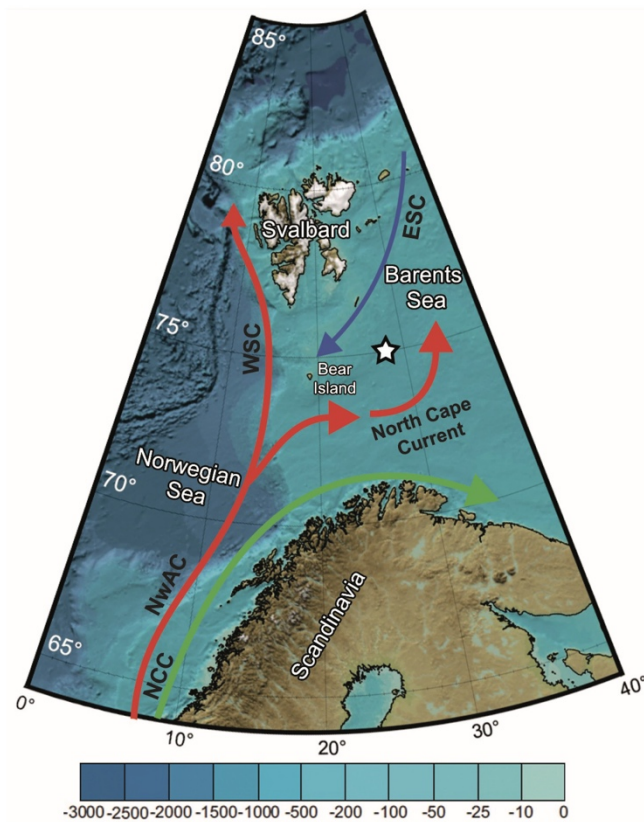
74

**Fig 1. Schematic map of study area and main current systems in the Nordic Seas.** White star indicates the crater area where plankton tows, box-cores and water sampling were conducted, detailed bathymetry can be found in Ofstad et al. [30]. Red lines are Atlantic Water inflows, blue line is Arctic Water outflows, and the green line is a coastal current. Abbreviations: *NwAC* Norwegian Atlantic current, *WSC* West Spitsbergen current, *ESC* East Spitsbergen current, *NCC* Norwegian Coastal Current. Current systems are based on Loeng [3]. Basemap from IBCAO 3.0 [51].

approximately 230 ml ethanol (98%), a quarter of a teaspoon hexamethylenetetramine ($\geq$99.0%), and stored at 2°C. Once in the laboratory, the samples were washed over a 63-μm sieve in order to remove organic particles from the surface of the foraminiferal tests and to break up aggregations of material. All PF and *L. helicina* from the >63-μm size fraction were picked with a fine brush under a light microscope. Live (cytoplasm-bearing) planktonic foraminifera specimens were counted for each depth.

Recently settled planktonic foraminifera were collected from two box-cores located within the same area as the plankton tow stations (74.92°N, 27.77°E and 27.53°E). The water depth at both box-core stations was 330 m, and the $\Omega_{Ca}$ directly above the sediments was 1.22 [30]. The PF were collected by sampling the top sediment layer (1 cm) of the boxcore. The samples were preserved in approximately 50 ml of ethanol (96%) with rose bengal (2 g L$^{-1}$ of ethanol), and stored at 2°C. In the home laboratory, the samples were washed over a 63-μm sieve and dried in a 40°C for at least 24 hr. Once dried, PF were picked under a light microscope with a fine

75

brush and identified to species level. There were large pteropods in the sediment samples, but they were broken, and therefore not included in the study. The complete description of sample collection, treatment, and analysis is described in Ofstad et al. [30].

## 2.3 XMCT

An XMCT system (ScanXmate-DF160TSS105, Comscantecno Co. Ltd., Kanagawa, Japan) was used to quantify the shell density of individual specimens. A high-resolution setting (X-ray focus spot diameter of 0.8 μm, X-ray tube voltage of 80 kV, detector array size of 1024x1024 for the pteropods and 992x992 for the foraminifera, spatial resolution of 0.833 μm for *Limacina helicina* and 0.964 μm for the foraminifera, 1200 projections/360˚, 4 s/projection) was used for 3-D quantitative densitometry of the foraminiferal and pteropod tests. One to three samples (depending on the shell size) were placed on a stage made of a quartz glass bar. Tests were mounted on the sample stage with urethane glue. A calcite crystal ball was used to standardize the computed tomography (CT) number of each test sample and enabled us to distinguish the density distributions in the foraminiferal and pteropod tests with high resolution. In this study, a limestone particle (diameter of approximately 130 μm; 1000 in mean CT number; NIST RM8544 (NBS19)) was embedded in the sample stage, and all of the test samples were scanned with the same calcite standard. ConeCTexpress software (White Rabbit Corp., Tokyo, Japan) was used to correct and reconstruct tomography data, and the general principle of Feldkamp cone beam reconstruction was followed to reconstruct image cross sections based on filtered back projections. In order to avoid the beam hardening effect (selective attenuation of X-ray) during scan, we put the metal filter (Aluminium, 0.2 um thickness) in front of X-ray detector. Mean shell thickness was calculated by dividing the $CaCO_3$ volume by the shell surface area, both of which are parameters measured by the XMCT. The shell surface area includes both the outer areas and the surfaces of the internal chambers. A caveat with the calculated mean shell thickness is that values will decrease, when the shell material is more porous. High porosity of the shell material increases the surface area, resulting in a decrease in mean shell thickness.

Well-preserved specimens to be scanned with the XMCT were selected at random, but with the intention of having a representative size range. The complete size range of the PF and *L. helicina* specimens sampled in June 2016 from the crater area can be found in Ofstad et al. [30]. A total of 226 planktonic foraminifera shells from the water column (*N. pachyderma* n = 120, *T. quinqueloba* n = 115), 30 recently settled planktonic foraminifera shells (*N. pachyderma* n = 12, *T. quinqueloba* n = 18), and 25 *Limacina helicina* shells from all depth intervals (0–50 m, 50–100 m, 100–150 m, 150–200 m, and 200–300 m) were scanned with the XMCT (S1 Table in S1 File; Fig 2). All scanned pteropod shells were either veligers, *Limacina* spp. (<300 μm, n = 7), or juveniles *L. helicina* (300–4000 μm, n = 18) [52].

## 2.4 CT number

From the 3-D scanning data of planktonic foraminiferal and *L. helicina* tests, we obtained a CT number of each volumetric pixel—referred to as a voxel, and volume ($μm^3$) of each individual test. The 3-D imaging software Molcer Plus (White Rabbit Corp., version 1.35) and the following equation were used to calculate the calcite CT number:

$$\text{CT number} = [(\mu_{\text{sample}} - \mu_{\text{air}})/(\mu_{\text{calcite STD}} - \mu_{\text{air}})] \times 1000 \qquad (1)$$

where $\mu_{\text{sample}}$, $\mu_{\text{air}}$, and $\mu_{\text{calciteSTD}}$ are the X-ray attenuation coefficients of the sample, calcite, and air, respectively.
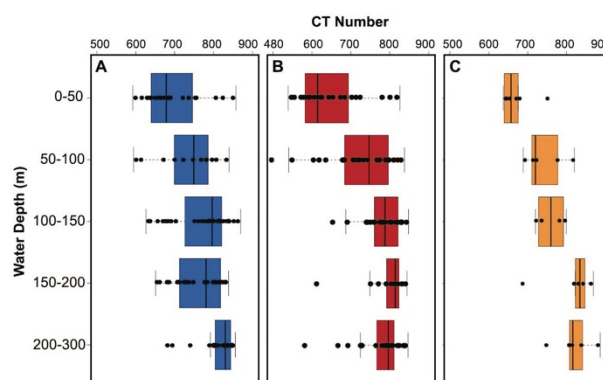
76

**Fig 2.** Box-and-whisker plot of shell density with water depth for A) *Neogloboquadrina pachyderma* (n = 120), B) *Turborotalita quinqueloba* (n = 115) and c) *Limacina helicina* (n = 25) sampled from the crater area in 2016. Boxes extend from the lower to upper quartile values of the data, with a line at the median. Whiskers indicate 1.5 times the inter-quartile distance. Black dots are single measurements.

The mean CT number for an entire test was calculated with the following equations:

$$\text{Mean CT number} = \frac{1}{T} \sum_{n=230}^{1000} n T_n \qquad (2)$$

where n is the CT number, $T_n$ is the total number of voxels with a specific CT number (n), and T is the total number of voxels in the whole test. The mean CT number indicates the mean density of an individual test.

## 2.5 CT data analysis

The shell thickness of the apex of *L. helicina* was measured by creating cross-sections using the Molcer Plus software (Version 1.35). A whorl is a single 360˚ revolution of the shell spiral structure. The shell apex of 16 shells of *L. helicina* were measured at four locations, twice on the protoconch (first whorl), and twice on the second whorl (S1 Fig). Careful consideration was made to take measurements at the same location for each shell for ease of comparison. Following the methods outlined by Janssen [53], the *L. helicina* shell diameters were measured and the total number of whorls were counted to the nearest quarter (S1 Fig). Additional *L. helicina* from the sampling station were measured for their shell diameter. Images were acquired by a Leica Z16 APO microscope, using the integrated Leica DFC450 camera and LAS version 4.12.0 software. The images were processed using the ruler tool in Adobe Photoshop CS6. All measurements of shell diameter and thickness performed this study are the result of three repeated measurements to diminish inaccuracies.

In order to calculate area density (area normalised weight), 111 PF shells (*T. quinqueloba* n = 54, *N. pachyderma* n = 57) shells were weighed individually using a Sartorius microbalance (model M2P, 0.1µg sensitivity). The given weight measurements are based on three repeated measurements of the single specimen. Area density is given by shell weight divided by surface area.

Isolation of the penultimate and final chamber was done on a select number of shells in order to validate the relationship with the overall CT number of the shell.

77

## 2.6 Statistical analyses

To test the relationship between any two parameters (e.g., water depth and mean shell density), a simple linear regression model was applied to the data. To test significance of correlation of shell density of the marine calcifiers with sampling intervals, a Mann-Whitney-U test was performed using Version 1.2.1335 of the program R [54]. When testing variables against water depth, the maximum depth in the plankton tow sampling intervals was used, e.g., 50 m for the sampling interval 0–50 m. When testing against environmental parameters, the mean of all measurements taken in the sampling interval was used. Typically, two water samples were taken with the CTD within a plankton tow sampling interval, once at the shallowest point, and once at the deepest. We believe using the mean of those two measurements within the sampling interval would give the most representative value.

## 2.7 Ocean carbonate chemistry

The water chemistry data were published in Ofstad et al. [30], here we give a brief overview of the methods. Dissolved inorganic carbon (DIC) was determined using gas extraction of acidified sample followed by coulometric titration and photometric detection using a Versatile Instrument for the Determination of Titration carbonate (VINDTA 3C, Marianda, Germany). Routine analyses of Certified Reference Materials (CRM, from A. G. Dickson, Scripps Institution of Oceanography, USA) ensured the accuracy and precision of the measurements. Average standard deviation from triplicate CRM analyses was within $\pm 1$ $\mu$mol kg$^{-1}$ for all samples. Total alkalinity ($A_T$) was determined from potentiometric titration with 0.1 N hydrochloric acid in a closed cell using a Versatile Instrument for the Determination of Titration Alkalinity (VINDTA, Marianda, Germany). Average standard deviation for $A_T$, determined from triplicate CRM measurements was $\pm 2$ $\mu$mol kg$^{-1}$. We used DIC, $A_T$, salinity, temperature, and depth for each sample as input parameters in a $CO_2$-chemical speciation model (CO2SYS program, version 01.05) [55,56] to calculate other parameters in the carbonate system such as carbonate-ion concentration ([$CO_3^{2-}$]), aragonite saturation ($\Omega_{Ar}$) and calcite saturation ($\Omega_{Ca}$). We used the $HSO_4^-$ dissociation constant of Dickson [57], and the $CO_2$-system dissociation constants (K$^*$1 and K$^*$2) estimated by Mehrbach et al. [58], and modified by Dickson and Millero [59].

## 3. Results

### 3.1 Hydrography and water chemistry

During the time of sampling, the predominant water masses were Atlantic Water (AW, T > 3.0°C, S > 34.65) in the top 250 m of the water column, and Transformed Atlantic Water (TAW, T = 1.0–3.0°C, S > 34.65) below 250 m, following the definitions of Cottier et al. [60] (S2 Fig). Both $\Omega_{Ar}$ and $\Omega_{Ca}$ were supersaturated ($\Omega$>1) throughout the entire water column, with the highest values in the surface water and lowest at the bottom (Figs 3D and 8B). The water column had two distinct layers (Figs 3D and 8B). The upper layer is from the sea surface to approximately 75 m water depth (S2 Fig); here, the $\Omega_{Ar}$ is 2.1–2.5, and the $\Omega_{Ca}$ is 4.0–3.0 (Figs 3D and 8B). Between 75 m and 300 m water depth the $\Omega_{Ar}$ is 1.5–2.1, and the $\Omega_{Ca}$ is 2.4–3.0, where the lowest values were observed at the bottom (Figs 3D and 8B). The [$CO_3^{2-}$] ranged between 168 $\mu$mol kg$^{-1}$ at the surface and 105 $\mu$mol kg$^{-1}$ at 300 m water depth. The pH ranged between 8.03 and 8.22.

### 3.2 Shell density from CT number

For both *Neogloboquadrina pachyderma* and *Turborotalita quinqueloba*, the average CT number increases steadily from 684 and 632 in the 0–50 m depth interval to 762 and 793 in the
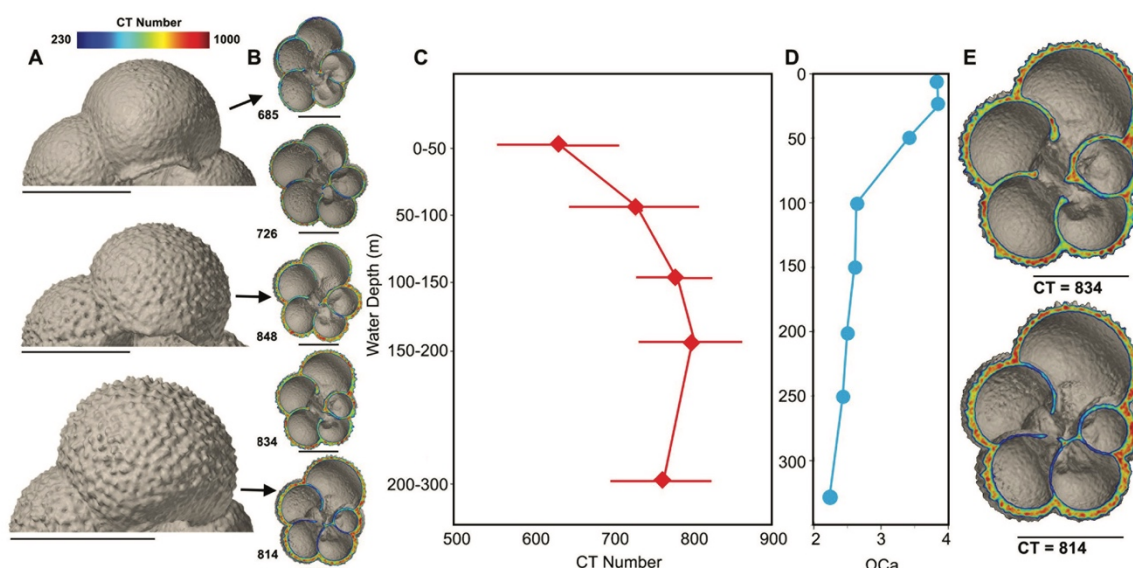
78

**Fig 3. *Turborotalita quinqueloba* from water column.** A) Texture of test surface of *Turborotalita quinqueloba* at three different depth intervals; 0–50 m, 100–150 m and 200–300 m. B) Variation in inner and outer shell density of *T. quinqueloba* as mean CT number of entire shell measured by XMCT increases. C) Mean CT number of *T. quinqueloba* (n = 115), with error bars, plotted against water depth. D) Calcite saturation at sampling site plotted against water depth. E) *T. quinqueloba* cross-section before and after assumed gametogenesis. Scale bars measure 100 μm.

150–200 m depth interval, respectively (Fig 2A and 2B). The difference in CT number between the layer of elevated Ω saturation at 0–50 m and the underlying water column when normalized for shell volume, is also significant for both PF species (p < 0.01), but not *L. helicina* (p = 0.25). For *L. helicina* the difference in shell density between the specimens in the shallow layer (0–50 m) and those found beneath is significant when not size normalized (S10 Table in S1 File). *Turborotalita quinqueloba* reaches its peak shell density of 793 in the 150–200 m depth interval. Below the 150–200 m depth interval, the shell density of *T. quinqueloba* decreases. In the 200–300 m depth interval, the average shell density of *T. quinqueloba* is 766. The outer shell walls are thick and dense, while the CT number is lower in the internal walls (Fig 3E and S3 Fig). In contrast, the shell density of *N. pachyderma* continues to increase until 200–300 m, where it reaches a peak shell density of, on average, 813 (Fig 4C). Similar to *N. pachyderma*, the shell density of *L. helicina* increases with depth. At 0–50 m, *L. helicina* have an average CT number of 670, and by 200–300 m they reach a peak average density of 819 (Fig 2C). Collectively, we found that the difference in shell density between sampling intervals were most significant between the shallowest (0–50 m) and deepest (200–300 m) interval (S8-S10 Tables in S1 File). *Turborotalita quinqueloba* showed the most significant variation between net tows, and *L. helicina* the least.

Although we found a general increase in CT number and shell thickness with depth, we note a range in CT numbers (Fig 2 and S2 Table in S1 File) and mean shell thickness (S2 Table in S1 File) at each sampling depth interval. This is particularly true for *T. quinqueloba* in the shallowest depth interval 0–50 m where the CT numbers of individual specimens are evenly distributed from 539 to 826, and the mean shell thickness ranges from 2.02 to 3.25 μm. Furthermore, in the 0–50 m depth interval the average CT numbers for *N. pachyderma* and *L.*
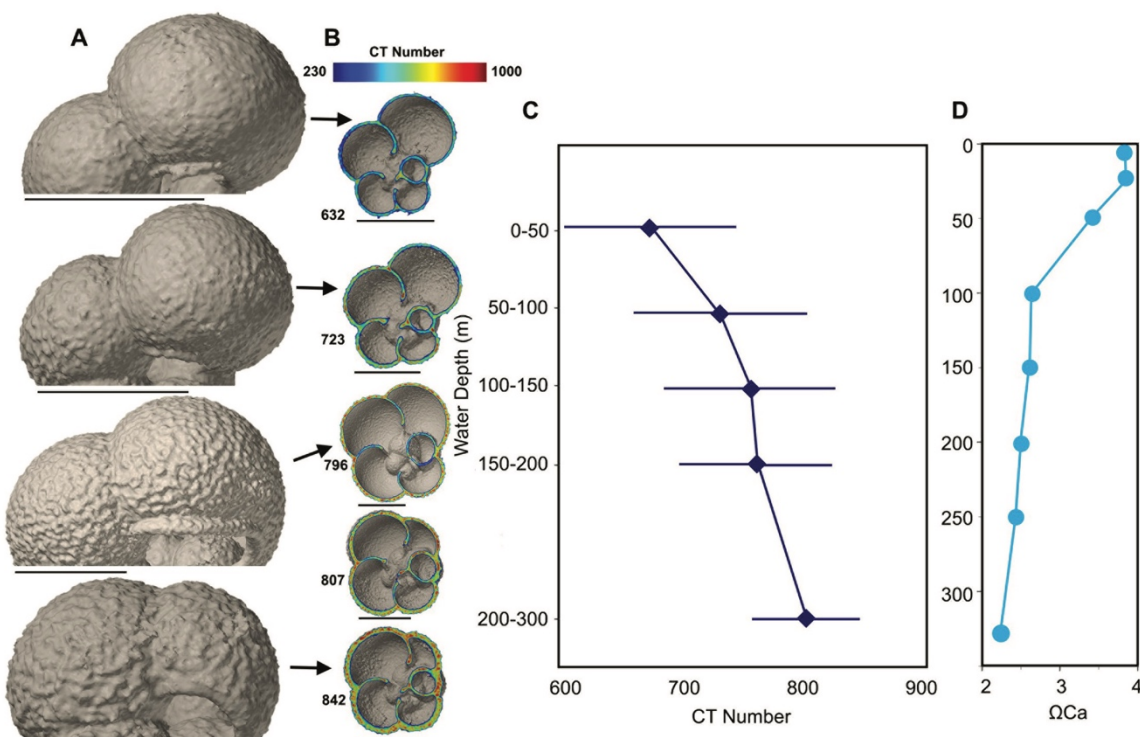
79

**Fig 4. *Neogloboquadrina pachyderma* from water column.** A) Texture of test surface of *Neogloboquadrina pachyderma* at four different depth intervals; 0–50 m, 50–100 m, 100–150 m and 200–300 m. B) Variation in inner and outer shell density of *N. pachyderma* with mean CT number of entire shell measured by XMCT. C) Mean CT number of *N. pachyderma* (n = 120), with error bars, plotted against water depth and calcite saturation. D) Calcite saturation at sampling site plotted against water depth. Scale bars measure 100 μm.

*helicina* ranges from 592 to 857, and 637 to 751, respectively. The shell thickness of *N. pachyderma* and *L. helicina* at the 0–50 m depth interval ranged from 1.94 to 5.28 μm, and 1.98 to 2.75 μm, respectively.

### 3.3 Planktonic foraminifera

**3.3.1 Planktonic foraminifera from the water column.** Both *N. pachyderma* and *T. quinqueloba* show a statistically significant positive correlation between individual shell weight, CT number, mean shell thickness and area density with water depth (S4, S5 Tables in S1 File). Cytoplasm-bearing specimens of both species are found in each sampling depth interval and constitute 80–100% of XMCT-scanned shells from the top 150 m (S7 Table in S1 File). Below 150 m the percentage of live specimens decreases to 75% and 78.6% for *N. pachyderma* in the 150–200 m and 200–300 m depth interval, respectively (S7 Table in S1 File). For *T. quinqueloba* there is a greater decrease in the percentage of live specimens below 150 m, with 14.3% and 23.5% containing a cytoplasm in the 150–200 m and 200–300 m depth interval, respectively (S7 Table in S1 File). For both *T. quinqueloba* and *N. pachyderma* there is increasing formation of a layer of secondary calcite crust on the outer shell with depth. The texture of the

80

shells in the shallowest samples are smooth without any calcite crust. Thereafter ridges appear that become increasingly "rough" with depth and increase in CT number (Figs 3A and 4A).

Both species undergo gradual shell thickening with depth. At 0–50 m water depth the average shell thickness of *N. pachyderma* and *T. quinqueloba* is 2.5±0.8 μm (n = 15) and 2±0.5 μm (n = 28), respectively. *Neogloboquadrina pachyderma* reaches peak thickness at 200–300 m, where the average shell thickness is 4.3±0.7 μm (n = 29). *Turborotalita quinqueloba* reaches peak thickness at 150–200 m, where the average shell thickness is 3.5±0.7 μm (n = 13). In the 200–300 m depth interval the shell thickness of *T. quinqueloba* has decreased to 3.1±0.8 μm (n = 24). Collectively, the shell walls of *N. pachyderma* and *T. quinqueloba* thicken by 40.8% and 35.1%, respectively, from their thinnest at the 0–50 m sampling interval to their peak shell thickness.

The mean shell thickness shows a strong correlation with the CT number (Fig 5; S4, S5 Tables in S1 File). The mean shell thickness of individual *T. quinqueloba* and *N. pachyderma* have an exponential relationship with their respective CT numbers (Fig 5). The exponential curve for *N. pachyderma* is steeper than the curve for *T. quinqueloba*. Furthermore, *N. pachyderma* (n = 120) tend to be larger, denser, and thicker than *T. quinqueloba* (n = 115), based on mean CT numbers and calcite volume (S1, S2 Tables in S1 File).

**3.3.2 Planktonic foraminifera from the surface sediments.** In the top 1 cm of the sediments, both *N. pachyderma* and *T. quinqueloba* are found in a wide range of dissolution states. Some of the planktonic foraminiferal specimens found in the surface sediments have similar shell densities as those found in the overlying water column (Figs 6A, 6C, 7A and 7C), while
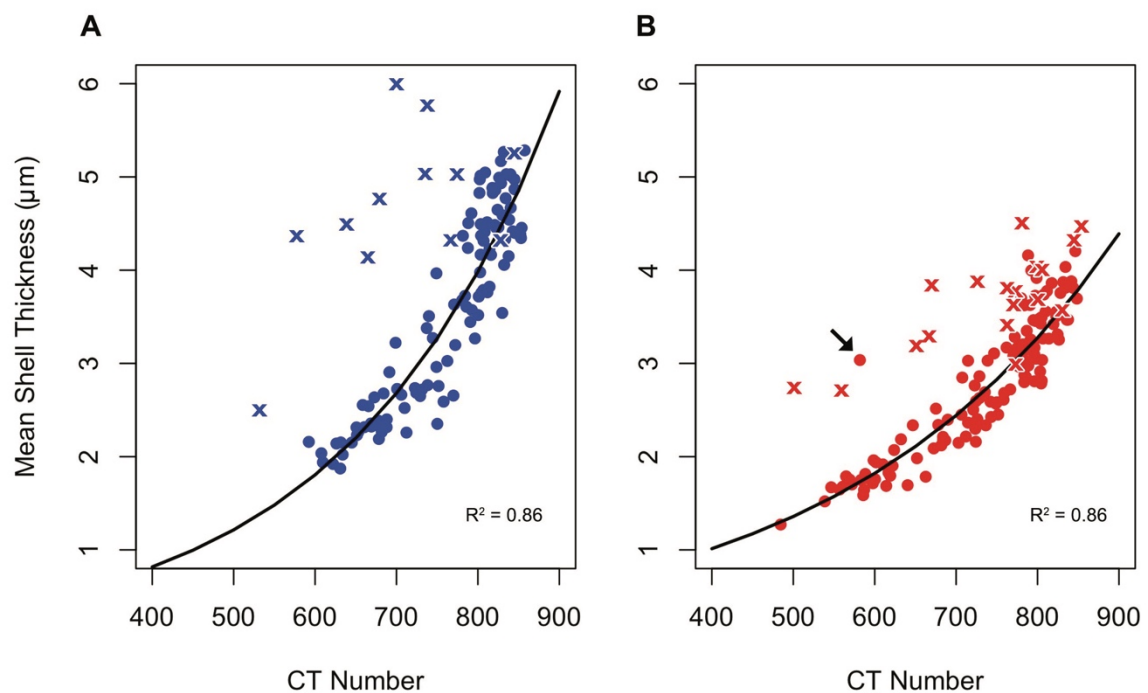


**Fig 5. Shell thickness versus shell density.** Mean shell thickness of A) *Neogloboquadrina pachyderma* and B) *Turborotalita quinqueloba* plotted versus mean shell density in the form of a CT number, fitted with an exponential model. Shells from water column samples are represented by circles, while crosses represent shells from surface sediments. Exponential model is only fitted to shells from water column. Arrow in B) is pointing to an outlier.

https://doi.org/10.1371/journal.pone.0249178.g005

81

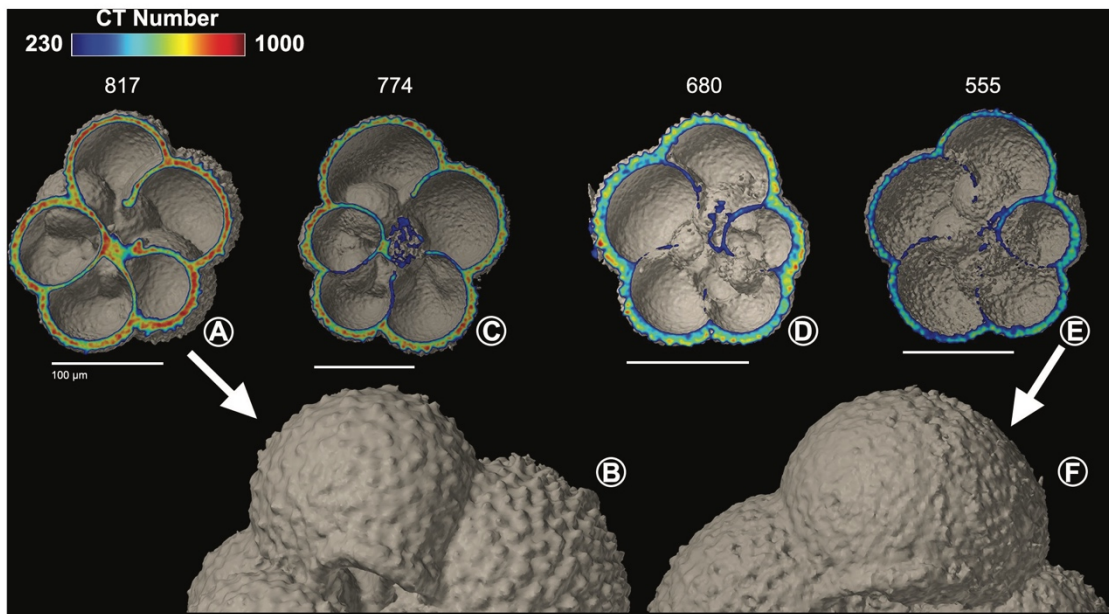**Fig 6. *Turborotalita quinqueloba* from surface sediments.** Cross-sections of *Turborotalita quinqueloba* specimens (A,C,D,E) from surface sediment sample (0–1 cm), including surface texture of a B) high-density (n = 11) and a F) low-density specimen (n = 7). Scale bars measure 100 μm.

other specimens have undergone dissolution (Figs 6D, 6E, 7E and 7F). Out of all of the *N. pachyderma* shells found in the surface sediments, there is a high proportion of low-density shells (9 out of 12, 75%), i.e., shells which can be regarded as outliers in the thickness versus density plot (Fig 5A). In contrast, low-density *T. quinqueloba* shells are in the minority (7 out of 18, 39%) (Fig 5B). The surface texture of *N. pachyderma* and *T. quinqueloba* vary in terms of CT number (Figs 6 and 7). In *T. quinqueloba*, the loss of the base features of the prominent spines is evident as the CT number reduces from 817 to 555, and the surface texture takes on a smoother appearance (Fig 6B and 6F). The surface texture of *N. pachyderma* appears to be mostly unaffected by post-depositional dissolution (Fig 7B and 7G). In the low-density shells, the calcite ridges are more prominent, giving it a more rugose texture overall (Fig 7G). In *N. pachyderma* we see a two-layered dissolution pattern (Fig 7F). There is a clear divide between the less dense (CT number ~ 400) inner calcite, and the denser outer crust (CT number ~ 650) (Fig 7F). Shells of both species from the surface sediments that have undergone post-depositional dissolution plot to the left of the exponential trendline (Fig 5). The external shell walls of the dissolved specimens remain at a similar thickness to those with a high-density shell (Figs 5–7). Dissolution primarily affects the CT number (Fig 5).

### 3.4 *Limacina helicina*

In *L. helicina* we see the same trend in the shell density with water depth as we do with the PF (Fig 2). *Limacina helicina* show a statistically significant positive correlation between shell diameter, CT number, and mean shell thickness with water depth (S6 Table in S1 File). On average, the shell density of *L. helicina* increases with depth (Fig 8A). The mean density given
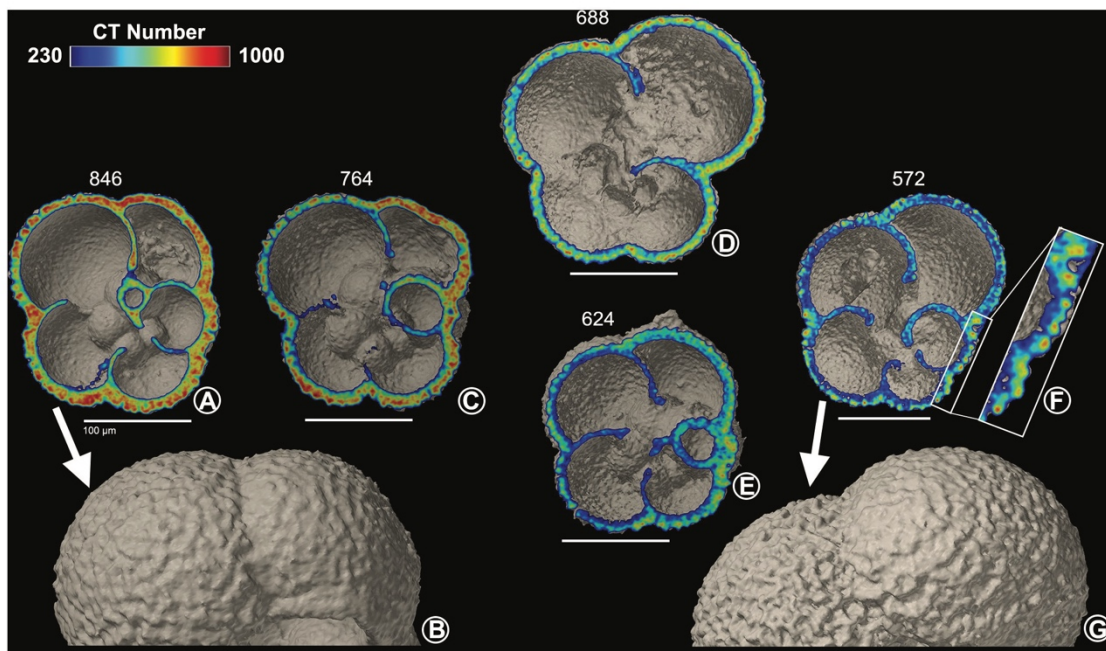
82

**Fig 7. *Neogloboquadrina pachyderma* from surface sediments.** Cross-sections of *Neogloboquadrina pachyderma* specimens (A,C,D,E,F) from surface sediment sample (0–1 cm), including surface texture of a B) high-density (n = 3) and a G) low-density specimen (n = 9). F) Close-up of shell wall cross-section. Scale bars measure 100 µm.

by the CT number starts at a minimum, at 670, in the shallowest sampling interval (0–50 m) (Fig 8A). There is a steady increase until the deepest sampling interval where the mean CT number is 819 (Fig 8A). In contrast to the PF in the crater area, *L. helicina* generally increase in shell diameter with depth (Fig 8A; S6 Table in S1 File). In the 0–50 m depth interval, the shells have the narrowest size range (131–457 µm), and an average size of 274 µm. The 150–200 m water depth interval has the largest range of shell sizes, 124–1190 µm (Fig 8A). The largest shells, on average, are found in the 200–300 m water depth interval and are 511 µm (Fig 8A). The number of whorls varied between 0.6 and 3.6 and is strongly correlated to the shell diameter (p < 0.001).

The distribution of *L. helicina* in the water column in terms of shell density results in an inverse relationship with $\Omega_{Ar}$ ($R^2$ = 0.54, p < 0.001, Fig 8A and 8B). The mean shell thickness also increases with depth, starting at 2.2 µm at 0–50 m water depth, to 2.8 µm at 200–300 m water depth. As the number of whorls increases, the shell apex thickens. The sum of four measurements done on the central-top part of the shell show that shells with 2.5 to 3.5 whorls is 25.9±3.1 µm, while shells with 1.5 to 2.25 whorls has a sum of 19.4±2 µm (Fig 8D).

## 4. Discussion

### 4.1 Distribution of PF, life cycles and shell density

Calcified shells are thought to have evolved as a mean for protection, and is widely found throughout the animal phyla [61]. Calcification intensity, the term often used to refer to shell
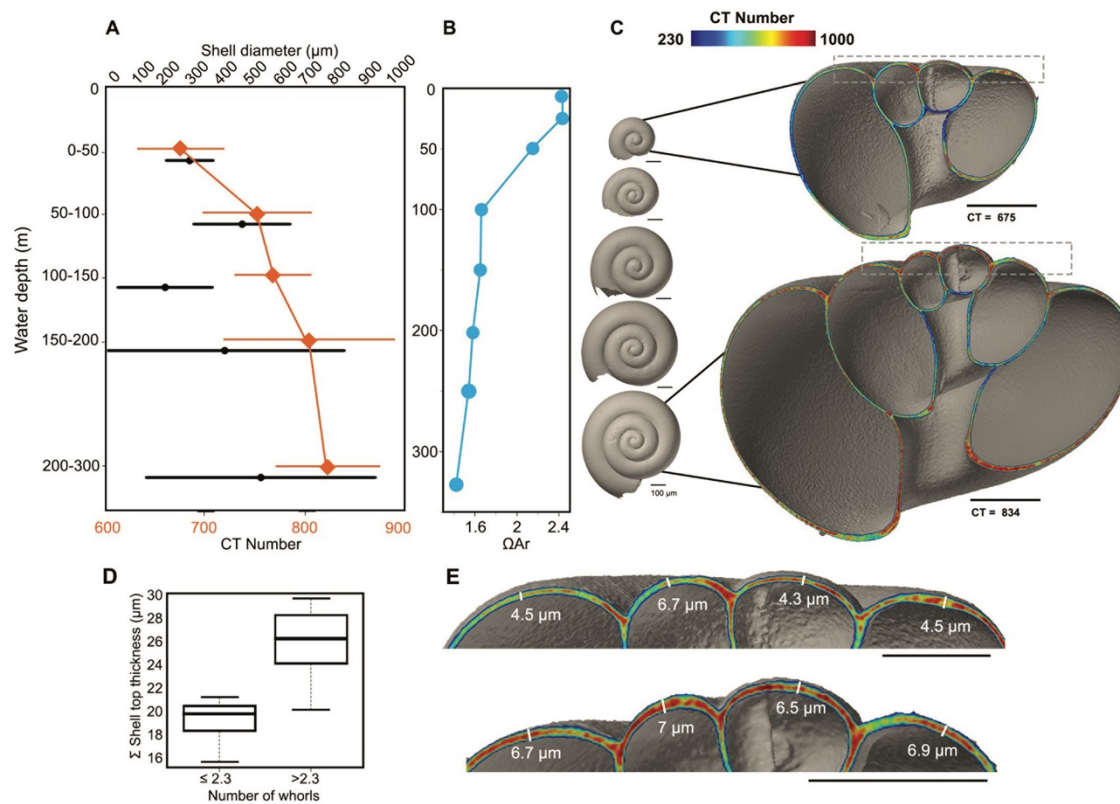
**Fig 8. *Limacina helicina* from water column.** A) *Limacina helicina* shell diameter (n = 175) and density (n = 25) (given by CT number) with depth. B) Aragonite saturation at sampling site plotted against water depth. C) Generalized shell size with depth (left) and cross-sections of *L. helicina* specimens from 0–50 m (2 whorls), and 150–200 m (2.75 whorls) water depth interval. Grey boxes are shown as close-ups in E. D) Boxplot of Mann-Whitney *U* test on top shell thickness of *L. helicina* as a function of whorl number. E) Top of *L. helicina* specimens shown in C, schematic of shell thickness measurements performed on all shells. Scale bars measure 100 μm.

density is believed to be primarily controlled by ambient seawater $[CO_3^{2-}]$ [38,62], and hence $\Omega$, which is largely dictated by absolute $[CO_3^{2-}]$. In addition, the shell size of PF appears to be controlled by temperature and food availability [36,38,63]. *Globigerina bulloides* when growing in favourable conditions, but with low $\Omega_{Ca}$ (~1.5), were found to grow large in size, with low density tests characterised by large and porous crystalline structures, suggesting that PF in some cases may prioritize shell size over shell density [36]. Furthermore, shell thickening by secondary calcification during ontogeny and/or gametogenic calcite addition is poorly understood and exhibit inter-species variation [64,65]. In polar waters, *N. pachyderma* with and without a thick calcite crust generated by secondary calcification were found to be concentrated in different parts of the water column. They were also found to add the calcite crust primarily at 50–200 m water depth, and an increase in secondary calcification of *N. pachyderma* was shown to occur with depth [66]. The degree of ontogenetic crust formation in *N. pachyderma* is highly variable,

84

it can amount to 50–70% of the total shell weight, and there is no consensus to which factors control the crust formation [66–68].

**4.1.1 Comparison of *N. pachyderma* and *T. quinqueloba* in the water column and their preservation patterns.** The dominant living planktonic foraminiferal species in the polar region are *N. pachyderma* and *T. quinqueloba* [69–73], which is reflected in our sampling area [30]. The differences in the shell density depth profile between *N. pachyderma* and *T. quinqueloba* can be explained in part by the differences in depth habitat and depth of reproduction (Fig 2A and 2B) [74,75]. Another factor, which may affect their calcification is that *T. quinqueloba* is a spinose species, while *N. pachyderma* is not. *Turborotalita quinqueloba* calcify within 25–75 m water depth, while *N. pachyderma* calcify within the much wider range of 25–280 m [74,75]. Our interpretation of the shell density profile is that *Neogloboquadrina pachyderma* continue to calcify and apparently grow denser as they migrate to deeper depths throughout their lifecycle (Fig 4), an observation consistent with previous studies [66,76]. Not all *N. pachyderma* shells develop a secondary calcite crust with depth, and these thin non-encrusted shells can be found throughout the water column [66,77]. In the North Pacific, shell parameters of *G. bulloides* such as the area density and outermost chamber wall thickness increase 20% from the 0–50 m to the 100–150 m water depth interval [36]. We find similar results in the northern Barents Sea; the area density of *T. quinqueloba* increases by 50.1% from the 0–50 m to the 100–150 m water depth interval, while the mean area density of *N. pachyderma* increases by 29.5%. Furthermore, the CT numbers of *N. pachyderma* and *T. quinqueloba* increase by 10.2% and 20.3%, respectively, from the 0–50 m to the 150–200 m water depth interval. By the deepest sampling interval, 200–300 m, the CT number of *N. pachyderma* has increased by a further 6.6% (n = 32), resulting in a total increase in CT number by 15.8%. Below the 150–200 m water depth interval (n = 38), *T. quinqueloba* decrease in density by 3.4%. The shallower and narrower depth habitat in the water column of *T. quinqueloba* compared to *N. pachyderma* is reflected in the faster rate of both increasing shell density and shell thickening per meter. However, we find thin low-density shells and thick high-density shells of both species in the entire water column (Fig 2A and 2B). If we use thick high-density shells as a proxy for reproduction, then reproduction occurs in the entire water column. Cytoplasm-bearing specimens are also present in the entire water column (S7 Table in S1 File), although in lower abundance in the deepest sampling intervals, especially *T. quinqueloba*. The increasing density curve with water depth may partly be the result of a higher presence of dead shells that have already released gametes.

The decrease in the CT number of *T. quinqueloba* from the 150–200 m depth interval to the 200–300 m depth interval likely reflects the dissolution of their internal shell walls (S3 Fig). This internal dissolution may be due to gamete formation and release (Fig 3E), which has been documented to occur in certain PF species [67]. Early culture studies on PF also showed that dissolution starts in the internal shell walls [78,79]. In preparation for the release of gametes, PF increase the $\Omega_{Ca}$ of the microenvironment adjacent to their shell [80]. Some foraminifera may do so by discharging alkaline seawater vacuoles, which would result in the internal environment of the foraminifera to become less basic [81]. Another explanation for the internal dissolution is the oxidation of internal organic matter, documented in the pteropod species *Limacina retroversa* and *L. helicina antarctica* [82]. However, this is less likely in PF shells, because they are made of calcite, which is more robust than aragonite and the proportion of soft tissue to shell size is significantly smaller than in pteropods [83]. The $\Omega_{Ca}$ is supersaturated throughout the water column ($\Omega_{Ca}$ = 2.4–4), yet there are no known $\Omega_{Ca}$ thresholds for PF. The presence of *T. quinqueloba* shells in the deepest sampling interval may also reflect a relic population. The internally dissolved shells may have a slower sinking rate than the specimens without dissolved internal walls, making them more likely to be sampled.

85

At our study site, PF shell density is strongly related to shell volume (S4, S5 Tables in S1 File). In general, the larger the shell volume, the more dense it is. However, the increase in CT number with depth after size-normalization is still significant (p < 0.01). This means that the increase in shell density with depth is not a function of shell volume.

Our results highlight the importance of comparing PF in the same life stage, because the shell thickness and density gradually increases as they mature. The same size is not enough to eliminate ontogenetic effects (Figs 3 and 4), therefore it is also advisable to compare shells from the same sampling depth. In a study showing shell thinning in PF due to OA by comparing pre-industrial and modern shells, sampling depth may not have been the same [37]. A discrepancy in sampling depth may mean that the results simply show natural variation in shell thickness with depth.

The PF sampled from the water column in our study area did not show any signs of dissolution, both in the outer and inner shell wall (Fig 5). The only exceptions are some specimens of *T. quinqueloba* found below 150 m water depth (S3 Fig). There is a clear depth zonation in individual abundance [30], and shell density in both species. The increase in shell density with depth is in agreement with observations in the North Pacific [36], and is believed to be driven by ontogeny.

**4.1.2 Comparison *N. pachyderma* and *T. quinqueloba* from the sediment and species-specific dissolution.** The sedimentation rate in the northern Barents Sea ranges from 0.5–1.3 mm/yr [84], meaning that it takes anywhere from 8 to 20 years to accumulate 1 cm of sediment. The top 1 cm of sediments will therefore host PF that have settled at different times and thus can show a variable degree of dissolution (Figs 6 and 7). When PF from sediment samples are used in geochemical studies, it is often stated that the samples do not show any evidence of dissolution. The surface texture of *T. quinqueloba*, and especially that of *N. pachyderma* undergo only slight changes in their external appearance as they dissolve. The subtle dissolution in the surface texture may go undetected under a light microscope if all chambers are intact, which was the case for the samples used in this study. The post-depositional dissolution found in some of the specimens (Figs 6D, 6E and 7D–7F) is likely to alter the original chemical composition of their tests, mainly the Mg/Ca ratio, and the oxygen and carbon isotopic composition [85,86]. The higher percentage of low-density *N. pachyderma* shells (75%) compared to *T. quinqeloba* (39%) suggests that fewer low-density *T. quinqeuloba* shells remain intact in the surface sediments, which may lead to an underrepresentation of *T. quinqueloba* in the sediment records. Selective dissolution of *T. quinqueloba* is also likely because of the extensive internal dissolution in the low-density shells (Fig 6D and 6E), which could lead to a collapse of the entire shell resulting in fragmentation.

The inter-species differences in the manifestation of post-depositional dissolution is thought to be primarily due to the magnesium content in the calcite structure [87], thus also suggesting that the calcification process is species-specific. *Neogloboquadrina pachyderma* consistently rank as one of the planktonic foraminiferal species most resistant to dissolution, regardless of the region they are found, while *T. quinqueloba* has a low resistance to dissolution [87,88]. The exponential curve for *N. pachyderma* shell thickness versus CT number (Fig 5A) is steeper than that of *T. quinqueloba* (Fig 5B). The steeper *N. pachyderma* curve suggests that they calcify more than *T. quinqueloba*, leading to a thicker secondary crust. The ability to build a thicker and denser crust may have a number of different explanations. Firstly, there could be a difference in lifecycle length between *N. pachyderma* and *T. quinqueloba*. *Neogloboquadrina pachyderma* may have a longer lifecycle than *T. quinqueloba* meaning that they could calcify over a longer period of time and build thicker and denser shells. Individuals of *N. pachyderma* have been kept alive in culture for up to 200 days [89,90]. The tendency of *N. pachyderma* to build thicker and denser shells may be due to a naturally higher calcification rate, rather than a

86

longer lifecycle compared to *T. quinqueloba*. The two species may also have very different calcification strategies because, unlike *N. pachyderma*, *T. quinqueloba* builds numerous spines on most of its chambers at the expense of chamber walls resulting in thinner shells.

The two-layered dissolution pattern seen in *N. pachyderma* highlights their higher degree of resistance to dissolution (Fig 7F). A similar pattern was also found in *G. bulloides* [91]. The denser outer calcite of *G. bulloides* was resistant to dissolution and remained well preserved in water undersaturated with respect to calcite, while the Mg-rich inner calcite dissolved [91]. This mechanism of selective dissolution likely skews the sediment record to favor species with a dense outer calcite layer. Following dissolution in the surface sediments, the thickness of the shell walls remains intact while the whole shell gets a more porous crystalline structure, resulting in a lower mean CT number (Figs 6 and 7). In our study, the dissolved shells from the surface sediments plotted to the left of the trend line showcase this phenomenon (Fig 5A and 5B), suggesting that the comparison between CT number and shell thickness can be used as a tool to identify shells which have undergone either post-depositional dissolution or calcified in low $\Omega_{Ca}$ waters [92]. However, outliers may occur if specimens have an unusual morphology. A *T. quinqueloba* specimen with an abnormally large and low-density final chamber plotted significantly to the left of the other shells from the water column (Fig 5B). Large, yet low-density shells may be found when PF calcify in low $\Omega_{Ca}$ waters, and shift their ecological strategy to favor shell size over shell density [36], although, *T. quinqueloba* has been shown to present a large phenotypic variation related to changes in sea surface temperature [93].

## 4.2 *Limacina helicina*

**4.2.1 Distribution in the water column and shell density.** In contrast to PF, *L. helicina* perform diel vertical migrations. Mature individuals diurnally migrate in the upper 200 m of the water column, while veligers and juveniles migrate in the top 50 m [94]. Like PF, it is also not known how the shell density of *L. helicina* changes with depth and increasing number of whorls. There is a skewness towards numerous small individuals at the surface, which is in agreement with previous findings in the polar region [95]. Because they migrate vertically, *L. helicina* showed less of a vertical zonation in shell density through the water column (S8-S10 Tables in S1 File). The statistical significance in the increase in shell density with depth is driven by the low-density, smaller specimens in the 0–50 m depth interval (S10 Table in S1 File). This is an observation consistent with their distribution in the water column [94]. The dominance of small individuals at the surface is likely because they have not developed their swimming wings and must therefore stay in the food-rich layer for growth. Once they have developed their wings they are able to migrate deeper in order to avoid predators, and this predation risk is likely what controls the vertical distribution of *Limacina helicina* [96].

**4.2.2 Dissolution of *L. helicina*, ontogeny, and future outlook.** The connection between low $\Omega_{Ar}$ and shell damage in *L. helicina* has been confirmed by observations from marine environments with large natural gradients in the carbonate chemistry [97,98]. However, recent studies on the periostracum of *L. helicina* suggests that they may not be as sensitive to OA as previously claimed [99,100]. Further, an increased food supply may reduce or even negate the effects of living in low-$\Omega$ waters [101,102]. In the Arctic, *L. helicina* juveniles may experience waters with lowest $[CO_3^{2-}]$ and $\Omega_{Ar}$ during fall and winter, and it is unclear whether they calcify during this time or await elevated saturation states at the onset of $CO_2$ uptake by phytoplankton production in spring [18]. Seasonal decline in carbonate parameters was found to coincide with a higher proportion of pteropod shell dissolution in the North Sea [101]. *Limacina helicina* shell dissolution has been recorded at a $\Omega_{Ar}$ of 1.4 [97], and greatly reduced calcification at $\Omega_{Ar} < 1.2$ [102]. An $\Omega_{Ar}$ of 1.4 is close to the values we observe at the bottom waters

87

in our study area. Moreover, our saturation states are based on a summer situation when the surface water has higher saturation states than what we would expect in fall and winter.

The increase in the thickness of their shell apex with growth could mean that they are more resistant to dissolution if the $\Omega_{Ar}$ at out study site decreases in fall and winter (Fig 8D and 8E), and their depth habitat deepens with growth. In the surface water (0–50 m) during the summer, the $\Omega_{Ar}$ conditions are favourable (Fig 8B), allowing the small, low-density individuals to prioritize the growth of their muscles. Their thin and delicate shells during this stage of their life cycle will be less compromised with the higher $\Omega_{Ar}$. It is possible that the thickening of the shell apex with increasing whorl number could be linked to re-directing the energy to calcification after finalizing the development of their soft body. It has been demonstrated that *L. helicina* can add new shell material after damage [99], and as long as the $\Omega_{Ar}$ is $\geq 1.2$ ongoing thickening can occur over the entire shell, including the protoconch [102]. The repair mechanism of *L. helicina* and ongoing thickening means that they can choose specific areas of their shell to thicken after the initial calcification as part of a resilience strategy to environmental stress. Instances of over-calcification as a reaction to low $\Omega$ values have been found in barnacles [103] and coccolithophores [104,105], further suggesting that some calcifiers can re-direct energy for calcification when their shells are vulnerable. However, a study from an upwelling area in the northern California Current Ecosystem suggests that *L. helicina* produce thinner shells as an adaptation mechanism to lower $\Omega_{Ar}$ water [98].

Longer term studies using the techniques described here could shed light on the natural variability in the shell properties of *L. helicina* throughout their life cycle. Topics which could be addressed are to what extent calcification intensity varies with $\Omega_{Ar}$ and nutrients, and if specimens living in low $\Omega_{Ar}$ environments have adapted by building of thicker and denser shells. One could also investigate if there are geographical variations in whorl thickness depending on seasonality and chemical environment. Furthermore, with the ongoing climate change, water temperatures in the Barents Sea have increased [4] and are projected to continue to increase globally [106]. Synergistic effects of OA and warming have been demonstrated to be especially lethal for juvenile *L. helicina* [107,108], highlighting the need for a better understanding of the *L. helicina* calcification strategy.

## 5. Conclusions

The application of the XMCT scanning technique on the extant planktonic calcifying foraminiferal (PF) species *Neogloboquadrina pachyderma* and *Turborotalita quinqueloba* and the pteropod species *Limacina helicina* retrieved from stratified plankton net samples from the northern Barents Sea have provided us with a unique dataset to better understand the shell density distribution with depth and ontogeny of these species at high Arctic latitudes. We found that both PF and *L. helicina* increase in shell density with depth, however there were inter-species differences in the PF due to depth habitat and reproduction. *Neogloboquadrina pachyderma* tends to be both thicker and denser than *T. quinqueloba*, and continues to increase in density until the deepest sampling interval 200–300 m. *Turborotalita quinqueloba* decrease in shell density below the depth interval 150–200 m, this loss may be due to internal dissolution associated with gamete release or bacterial degradation of the cytoplasm. Our results highlight the importance of sampling at the same water depth interval when comparing PF calcification intensity. In the surface sediments (0–1 cm), the shell preservation state was highly variable in both planktonic foraminiferal species with little alteration of the surface shell texture or shell thickness. Only the average CT number that reflects the average shell density revealed that dissolution had occurred. In the surface sediments, *N. pachyderma* appeared more resilient towards post-depositional dissolution. In this area from the Barents Sea, the

88

living PF did not suffer from dissolution effects. Dissolution occurred after death and after settling on the sea floor. We observed that *L. helicina* thickens their shell apex as the number of whorls increase. There was a weaker zonation in shell density through the water column compared to PF, which is probably due to vertical migration. We recommend longer-term studies on planktonic calcifiers using the XMCT scanning technique. Longer studies in different carbonate chemistry environments would provide even greater insight on the natural variability in shell density. This knowledge is important in order to use PF and *L. helicina* as biological indicators for ocean acidification and to predict future developments in food webs. It is also important in the use of PF as paleo-proxies.

## Supporting information

**S1 Fig. Annotated *Limacina helicina* to demonstrate measurement of physical parameters.** Wall thickness measurements were done along a cross-section (blue), and diameter measured along white stippled line. Black circles show location of shell thickness measurements. The shell in the figure has 3.5 whorls. More details on whorl counting method can be found in Janssen [53].
(TIF)

**S2 Fig. Temperature and salinity profile at study area.**
(TIF)

**S3 Fig. Cross-sections of *Turborotalita quinqueloba* found in the 200–300 m water depth interval.** Scale bars measure 100 μm.
(TIF)

**S1 File.**
(XLSX)

## Acknowledgments

## Author Contributions

**Conceptualization:** Siri Ofstad.

**Data curation:** Siri Ofstad.

**Formal analysis:** Siri Ofstad, Katsunori Kimoto.

**Funding acquisition:** Katsunori Kimoto, Melissa Chierici, Agneta Fransson, Tine Lander Rasmussen.

**Investigation:** Siri Ofstad, Katarzyna Zamelczyk, Katsunori Kimoto.

**Resources:** Katsunori Kimoto, Melissa Chierici, Agneta Fransson, Tine Lander Rasmussen.

**Supervision:** Katarzyna Zamelczyk, Tine Lander Rasmussen.

89

**Validation:** Katarzyna Zamelczyk, Katsunori Kimoto, Melissa Chierici, Agneta Fransson, Tine Lander Rasmussen.

**Visualization:** Siri Ofstad.

**Writing – original draft:** Siri Ofstad.

**Writing – review & editing:** Siri Ofstad, Katarzyna Zamelczyk, Katsunori Kimoto, Melissa Chierici, Agneta Fransson, Tine Lander Rasmussen.

## References

1. Årthun M, Eldevik T, Smedsrud LH, Skagseth Ø, Ingvaldsen RB. Quantifying the Influence of Atlantic Heat on Barents Sea Ice Variability and Retreat. J Clim. 2012; 25(13): 4736–4743. https://doi.org/10. 1175/JCLI-D-11-00466.1

2. Smedsrud LH, Esau I, Ingvaldsen RB, Eldevik T, Haugan PM, Li C, et al. The role of the Barents Sea in the Arctic climate system. 2013; 5(2012): 415–449. https://doi.org/10.1002/rog.20017.1. INTRODUCTION

3. Loeng H. Features of the physical oceanographic conditions of the Barents Sea. Polar Res. 1991; 10 (1): 5–18. https://doi.org/10.1111/j.1751-8369.1991.tb00630.x

4. Lind S, Ingvaldsen RB, Furevik T. Arctic warming hotspot in the northern Barents Sea linked to declining sea-ice import. Nat Clim Chang. 2018; 8(7): 634–639. https://doi.org/10.1038/s41558-018-0205-y

5. Skagseth Ø, Furevik T, Ingvaldsen R, Loeng H, Mork KA, Orvik KA, et al. Volume and Heat Transports to the Arctic Ocean Via the Norwegian and Barents Seas. In: Dickson RR, Meincke J, Rhines P, editors. Arctic-Subarctic Ocean Fluxes: Defining the Role of the Northern Seas in Climate. Dordrecht: Springer Netherlands; 2008. pp. 45–64. https://doi.org/10.1007/978-1-4020-6774-7_3.

6. Oziel L, Sirven J, Gascard JC. The Barents Sea frontal zones and water masses variability (1980–2011). Ocean Sci. 2016; 12(1): 169–184. https://doi.org/10.5194/os-12-169-2016

7. Wassmann P, Kosobokova KN, Slagstad D, Drinkwater KF, Hopcroft RR, Moore SE, et al. The contiguous domains of Arctic Ocean advection: Trails of life and death. Prog Oceanogr. 2015; 139: 42–65. https://doi.org/10.1016/j.pocean.2015.06.011

8. Dalpadado P, Ingvaldsen RB, Stige LC, Bogstad B, Knutsen T, Ottersen G, et al. Climate effects on Barents Sea ecosystem dynamics. ICES J Mar Sci. 2012; 69(7): 1303–1316. https://doi.org/10.1093/icesjms/fss063

9. Neukermans G, Oziel L, Babin M. Increased intrusion of warming Atlantic water leads to rapid expansion of temperate phytoplankton in the Arctic. Glob Chang Biol. 2018; 24(6): 2545–2553. https://doi.org/10.1111/gcb.14075 PMID: 29394007

10. Fossheim M, Primicerio R, Johannesen E, Ingvaldsen RB, Aschan MM, Dolgov A V. Recent warming leads to a rapid borealization of fish communities in the Arctic. Nat Clim Chang. 2015; 5(7): 673–677. https://doi.org/10.1038/nclimate2647

11. Bjørklund KR, Kruglikova SB, Anderson OR. Modern incursions of tropical Radiolaria into the Arctic Ocean. J Micropalaeontology. 2012; 31(2): 139–158. https://doi.org/10.1144/0262-821X11-030

12. Fransson A, Chierici M, Anderson LG, Bussmann I, Kattner G, Peter Jones E, et al. The importance of shelf processes for the modification of chemical constituents in the waters of the Eurasian Arctic Ocean: Implication for carbon fluxes. Cont Shelf Res. 2001; 21(3): 225–242. https://doi.org/10.1016/S0278-4343(00)00088-1.

13. Bates NR, Mathis JT. The Arctic Ocean marine carbon cycle: evaluation of air-sea CO2 exchanges, ocean acidification impacts and potential feedbacks. Biogeosciences. 2009; 6(11): 2433–2459. https://doi.org/10.5194/bg-6-2433-2009

14. Skogen MD, Olsen A, Børsheim KY, Sandø AB, Skjelvan I. Modelling ocean acidification in the Nordic and Barents Seas in present and future climate. J Mar Syst. 2014; 131: 10–20. https://doi.org/10.1016/j.jmarsys.2013.10.005

15. Omar A, Johannessen T, Kaltin S, Olsen A. Anthropogenic increase of oceanic pCO2 in the Barents Sea surface water. J Geophys Res Ocean. 2003; 108(C12): 1–8. https://doi.org/10.1029/2002JC001628

16. Evans W, Mathis JT, Cross JN. Calcium carbonate corrosivity in an Alaskan inland sea. Biogeosciences. 2014; 11: 365–379. https://doi.org/10.5194/bg-11-365-2014

90

17. Fransson A, Chierici M, Nomura D, Granskog MA, Kristiansen S, Martma T, et al. Effect of glacial drainage water on the CO2 system and ocean acidification state in an Arctic tidewater-glacier fjord during two contrasting years. J Geophys Res Ocean. 2015;120. https://doi.org/10.1002/2014JC010320

18. Fransson A, Chierici M, Hop H, Findlay HS, Kristiansen S, Wold A. Late winter-to-summer change in ocean acidification state in Kongsfjorden, with implications for calcifying organisms. Polar Biol. 2016; 39(10): 1841–1857. https://doi.org/10.1007/s00300-016-1955-5

19. Yamamoto A, Kawamiya M, Ishida A, Yamanaka Y, Watanabe S. Impact of rapid sea-ice reduction in the Arctic Ocean on the rate of ocean acidification. Biogeosciences. 2012; 9(6): 2365–2375. https://doi.org/10.5194/bg-9-2365-2012

20. Fabry VJ, Seibel BA, Feely RA, Orr JC. Impacts of ocean acidification on marine fauna and ecosystem processes. ICES J Mar Sci. 2008; 65(3): 414–432. https://doi.org/10.1093/icesjms/fsn048

21. Larson RJ, Harbison GR. Source and Fate of Lipids in Polar Gelatinous Zooplankton. Arctic. 1989; 42 (4): 339–346. https://doi.org/10.14430/arctic1675

22. Hunt BPV, Pakhomov EA, Hosie GW, Siegel V, Ward P, Bernard K. Pteropods in Southern Ocean ecosystems. Prog Oceanogr. 2008; 78(3): 193–221. https://doi.org/10.1016/j.pocean.2008.06.001

23. Weslawski JM, Hacquebord L, Stempniewicz L, Malinga M. Greenland whales and walruses in the Svalbard food web before and after exploitation. Oceanologia. 2000; 42(1): 37–56.

24. Willette TM, Cooney RT. Ecological processes influencing mortality of juvenile pink salmon (Oncorhynchus gorbuscha) in Prince William Sound, Alaska. Fish Oceanogr. 2001; 10: 14–41. https://doi.org/10.1046/j.1054-6006.2001.00043.x

25. Bathmann U V., Noji TT, von Bodungen B. Sedimentation of pteropods in the Norwegian Sea in autumn. Deep Res. 1991; 38(10): 1341–1360. https://doi.org/10.1016/0198-0149(91)90031-A

26. Schiebel R. Planktic foraminiferal sedimentation and the marine calcite budget. Global Biogeochem Cycles. 2002; 16(4): 1–21. https://doi.org/10.1029/2001GB001459

27. Meilland J, Schiebel R, Lo Monaco C, Sanchez S, Howa H. Abundances and test weights of living planktic foraminifers across the Southwest Indian Ocean: Implications for carbon fluxes. Deep Res Part I Oceanogr Res Pap. 2018; 131(March 2017): 27–40. https://doi.org/10.1016/j.dsr.2017.11.004

28. Meilland J, Fabri-Ruiz S, Koubbi P, Monaco C Lo, Cotte C, Hosie GW, et al. Planktonic foraminiferal biogeography in the Indian sector of the Southern Ocean: Contribution from CPR data. Deep Res Part I Oceanogr Res Pap. 2016; 110: 75–89. https://doi.org/10.1016/j.dsr.2015.12.014

29. Manno C, Accornero A, Umani SF. Importance of the contribution of Limacina helicina faecal pellets to the carbon pump in Terra Nova Bay (Antarctica). J Plankton Res. 2010; 32(2): 145–152. https://doi.org/10.1093/plankt/fbp108

30. Ofstad S, Meilland J, Zamelczyk K, Chierici M. Development, Productivity, and Seasonality of Living Planktonic Foraminiferal Faunas and Limacina helicina in an Area of Intense Methane Seepage in the Barents Sea. J Geophys Res Biogeosciences. 2020; 125(2): 1–24. https://doi.org/10.1029/2019JG005387

31. Meilland J, Howa H, Hulot V, Demangel I, Salaün J, Garlan T. Population dynamics of modern planktonic foraminifera in the western Barents Sea. Biogeosciences. 2020; 17(6): 1437–1450.

32. Kacprzak P, Panasiuk A, Wawrzynek J, Weydmann A. Distribution and abundance of pteropods in the western Barents Sea. Oceanol Hydrobiol Stud. 2017; 46(4): 393–404. https://doi.org/10.1515/ohs-2017-0039

33. Howes EL, Eagle RA, Gattuso JP, Bijma J. Comparison of Mediterranean pteropod shell biometrics and ultrastructure from historical (1910 and 1921) and present day (2012) samples provides baseline for monitoring effects of global change. PLoS One. 2017; 12(1): 1–23. https://doi.org/10.1371/journal.pone.0167891 PMID: 28125590

34. Oakes RL, Sessa JA. Assessing annual variability in the shell thickness of the pteropod Heliconoides inflatus in the Cariaco Basin using micro-CT scanning. 2019(October).

35. Beer CJ, Schiebel R, Wilson PA. Testing planktic foraminiferal shell weight as a surface water [CO2-3] proxy using plankton net samples. Geology. 2010; 38(2): 103–106. https://doi.org/10.1130/G30150.1

36. Iwasaki S, Kimoto K, Sasaki O, Kano H, Uchida H. Sensitivity of planktic foraminiferal test bulk density to ocean acidification. 2019;(June): 1–9. https://doi.org/10.1038/s41598-019-46041-x PMID: 31278289

37. Fox L, Stukins S, Hill T, Miller CG. Quantifying the Effect of Anthropogenic Climate Change on Calcifying Plankton. Sci Rep. 2020; 10(1620): 1–9. https://doi.org/10.1038/s41598-020-58501-w PMID: 32005920

38. Osborne EB, Thunell RC, Marshall BJ, Holm JA, Tapa EJ, Benitez-Nelson C, et al. Calcification of the planktonic foraminifera Globigerina bulloides and carbonate ion concentration: Results from the Santa Barbara Basin. Paleoceanography. 2016; 31(8): 1083–1102. https://doi.org/10.1002/2016PA002933

91

39. Marshall BJ, Thunell RC, Henehan MJ, Astor Y, Wejnert KE. Planktonic foraminiferal area density as a proxy for carbonate ion concentration: A calibration study using the Cariaco Basin ocean time series. Paleoceanography. 2013; 28(2): 363–376. https://doi.org/10.1002/palo.20034

40. de Moel H, Ganssen GM, Peeters FJC, Jung SJA, Kroon D, Brummer GJA, et al. Planktic foraminiferal shell thinning in the Arabian Sea due to anthropogenic ocean acidification? Biogeosciences. 2009; 6 (9): 1917–1925. https://doi.org/10.5194/bg-6-1917-2009

41. Barker S, Elderfield H. Foraminiferal Calcification Response to Glacial-Interglacial Changes in Atmospheric CO2. Science. 2002; 297(5582): 833–836. https://doi.org/10.1126/science.1072815 PMID: 12161653

42. Todd C. Planktic foraminiferal test size and weight response to the late Pliocene environment Planktic Foraminiferal Test Size and Weight Response to the Late Pliocene Environment. Paleoceanogr Paleoclimatology. 2020; 35(1): e2019PA003738. https://doi.org/10.1029/2019PA003738

43. Naik SS, Naidu PD, Govil P, Godad S. Relationship between weights of planktonic foraminifer shell and surface water CO3 = concentration during the Holocene and Last Glacial Period. Mar Geol. 2010; 275(1–4): 278–282. https://doi.org/10.1016/j.margeo.2010.05.004

44. Gonzalez-Mora B, Sierro FJ, Flores JA. Controls of shell calcification in planktonic foraminifers. Quat Sci Rev. 2008; 27: 956–961. https://doi.org/10.1016/j.quascirev.2008.01.008

45. Meilland J, Siccha M, Weinkauf MFG, Jonkers L, Morard R. Highly replicated sampling reveals no species-specific vertical habitats in diurnal vertical migration but stable planktonic foraminifera. J Plankton Res. 2019; 41(2): 127–141. https://doi.org/10.1093/zoolinnean/zly093

46. Erez J, Almogi-Labin A, Avraham S. On the Life History of Planktonic Foraminifera: Lunar Reproduction Cycle in Globigerinoides Sacculifer (Brady). Paleoceanography. 1991; 6(3): 295–306. https://doi.org/10.1029/90PA02731

47. Bijma J, Erez J, Hemleben C. Lunar and semi-lunar reproductive cycles in some spinose planktonic foraminifers. J Foraminifer Res. 1990; 20(2): 117–127. https://doi.org/10.2113/gsjfr.20.2.117

48. Hemleben C, Spindler M, Anderson OR. Modern Planktonic Foraminifera. 1st ed. Springer-Verlag New York; 1989. https://doi.org/10.1007/978-1-4612-3544-6

49. Schiebel R, Bijma J, Hemleben C. Population dynamics of the planktic foraminifer Globigerina bulloides from the eastern North Atlantic. Deep Res Part I Oceanogr Res Pap. 1997; 44(9–10): 1701–1713. https://doi.org/10.1016/S0967-0637(97)00036-8

50. Andreassen K, Hubbard A, Winsborrow MCM, Patton H, Vadakkepuliyambatta S, Plaza-Faverola A, et al. Massive blow-out craters formed by hydrate-controlled methane expulsion from the Arctic seafloor. Science. 2017; 356(6341): 948–953. https://doi.org/10.1126/science.aal4500 PMID: 28572390

51. Jakobsson M, Mayer L, Coakley B, Dowdeswell JA, Forbes S, Fridman B, et al. The International Bathymetric Chart of the Arctic Ocean (IBCAO) Version 3.0. Geophys Res Lett. 2012; 39(12). https://doi.org/10.1029/2012GL052219

52. Lalli CM, Wells FE. Reproduction in the genus Limacina (Opisthobranchia Thecosomata). J Zool. 1978; 186(1): 95–108. https://doi.org/10.1111/j.1469-7998.1978.tb03359.x

53. Janssen AW. Holoplanktonic Mollusca (Gastropoda: Pterotracheoidea, Janthinoidea, Thecosomata and Gymnosomata) from the Pliocene of Pangasinan (Luzon, Philippines). Scr Geol. 2007; 135: 29–177.

54. Team RStudio. RStudio: Integrated Development for R. RStudio, Inc. Boston, MA; 2015. Available: http://www.rstudio.com/.

55. Pierrot DE, Wallace DWR. MS Excel program developed for CO2 system calculations. Oak Ridge, Tenn.: ORNL/CDIAC-105, Carbon Dioxide Inf. Anal. Cent., Oak Ridge Natl. Lab., U.S. Dep. of Energy; 2006.

56. Lewis E, Wallace DWR. CO2SYS-Program developed for CO2 system calculations, ORNL/CDIAC-105. Oak Ridge, Tenn.: Carbon Dioxide Inf. Anal. Cent., Oak Ridge Natl. Lab.; 1998. https://doi.org/10.2172/639712

57. Dickson AG. Thermodynamics of the dissociation of boric acid in synthetic seawater from 273.15 to 318.15 K. Deep Sea Res Part A Oceanogr Res Pap. 1990; 37(5): 755–766. https://doi.org/10.1016/0198-0149(90)90004-F

58. Mehrbach C, Culberson CH, Hawley JE, Pytkowicx RM. Measurement of the Apparent Dissociation Constants of Carbonic Acid in Seawater At Atmospheric Pressure. Limnol Oceanogr. 1973; 18(6): 897–907. https://doi.org/10.4319/lo.1973.18.6.0897

59. Dickson A, Millero F. A Comparison of the Equilibrium Constants for the Dissociation of Carbonic Acid in Seawater Media. Deep Sea Research Part A. Oceanographic Research Papers. 1987. https://doi.org/10.1016/0198-0149(87)90021-5

92

**60.**   Cottier F, Tverberg V, Inall M, Svendsen H, Nilsen F, Griffiths C. Water mass modification in an Arctic fjord through cross-shelf exchange: The seasonal hydrography of Kongsfjorden, Svalbard. J Geophys Res Ocean. 2005; 110(12): 1–18. https://doi.org/10.1029/2004JC002757

**61.**   Bengtson S. The advent of skeletons. Early life on earth.  New York, NY: Nobel symposium No. 84. Columbia University Press; 1994. pp. 412–425.

**62.**   Weinkauf MFG, Moller T, Koch MC, Kucera M. Calcification intensity in planktonic foraminifera reflects ambient conditions irrespective of environmental stress. Biogeosciences. 2013; 10(10): 6639–6655. https://doi.org/10.5194/bg-10-6639-2013

**63.**   Manno C, Morata N, Bellerby R. Effect of ocean acidification and temperature increase on the planktonic foraminifer Neogloboquadrina pachyderma (sinistral). Polar Biol. 2012; 35(9): 1311–1319. https://doi.org/10.1007/s00300-012-1174-7

**64.**   Steinhardt J, Nooijer LJ De, Brummer GJ, Reichart G. Profiling planktonic foraminiferal crust formation. Geochemistry Geophys Geosystems. 2015; 18(1–2): 1541–1576. https://doi.org/10.1002/2014GC005684.Key

**65.**   Caron DA, Anderson OR, Lindsey JL, Faber WW, Lin EE. Effects of Gametogenesis on Test Structure and Dissolution of Some Spinose Planktonic Foraminifera and Implications for Test Preservation. Mar Micropaleontol. 1990; 16(1–2): 93–116. https://doi.org/10.1016/0377-8398(90)90031-G

**66.**   Kohfeld KE, Fairbanks RG, Smith SL, Walsh ID. Neogloboquadrina pachyderma (sinistral coiling) as paleoceanographic tracers in polar oceans: Evidence from Northeast Water Polynya plankton tows, sediment traps, and surface sediments. Paleoceanography. 1996; 11(6): 679–699. https://doi.org/10.1029/96PA02617

**67.**   Arikawa R. Distribution and Taxonomy of Globigerina pachyderma (Ehrenberg) off the Sanriku Coast, Northeast Honshu, Japan. Tohoku Univ Sci Rep Ser Geol. 1983; 53: 103–157.

**68.**   Stangeew E. Distribution and Isotopic Composition of Living Planktonic Foraminifera N. pachyderma (sinistral) and T. quinqueloba in the High Latitude North Atlantic. Christian-Albrechts-Universität, Kiel. 2001. Available: https://macau.uni-kiel.de/rsc/thumbnail/diss_mods_00000464.png.

**69.**   Carstens J, Hebbeln D, Wefer G. Distribution of planktic foraminifera at the ice margin in the Arctic (Fram Strait). Mar Micropaleontol. 1997; 29(3–4): 257–269. https://doi.org/10.1016/S0377-8398(96)00014-X

**70.**   Eynaud F. Planktonic foraminifera in the arctic: Potentials and issues regarding modern and quaternary populations. IOP Conf Ser Earth Environ Sci. 2011; 14(1). https://doi.org/10.1088/1755-1315/14/1/012005

**71.**   Jensen S. Planktische Foraminiferen im Europäischen Nordmeer: Verbreitung und Vertikalfluß sowie ihre Entwicklung während der letzten 15000 Jahre. Berichte Sonderforschungsbereich 313, Univ Kiel. 1998; 75(75): 1–105.

**72.**   Pados T, Spielhagen RF. Species distribution and depth habitat of recent planktic foraminifera in Fram Strait, Arctic Ocean. Polar Res. 2014; 33(1): 22483. https://doi.org/10.3402/polar.v33.22483

**73.**   Volkmann R. Planktic Foraminifers in the Outer Laptev Sea and the Fram Strait-Modern Distribution and Ecology. J Foraminifer Res. 2000; 30(3): 157–176. https://doi.org/10.2113/0300157

**74.**   Simstich J, Sarnthein M, Erlenkeuser H. Paired δ18O signals of Neogloboquadrina pachyderma (s) and Turborotalita quinqueloba show thermal stratification structure in Nordic Seas. Mar Micropaleontol. 2003; 48(1–2): 107–125. https://doi.org/10.1016/S0377-8398(02)00165-2

**75.**   Greco M, Jonkers L, Kretschmer K, Bijma J, Kucera M. Variable habitat depth of the planktonic foraminifera Neogloboquadrina pachyderma in the northern high latitudes explained by sea-ice and chlorophyll concentration. Biogeosciences. 2019; 16(17): 3425–3437. https://doi.org/10.5194/bg-16-3425-2019

**76.**   Carstens J, Wefer G. Recent distribution of planktonic foraminifera in the Nansen Basin, Arctic Ocean. Deep Res. 1992; 39.

**77.**   Kozdon R, Ushikubo T, Kita NT, Spicuzza M, Valley JW. Intratest oxygen isotope variability in the planktonic foraminifer N. pachyderma: Real vs. apparent vital effects by ion microprobe. Chem Geol. 2009; 258(3–4): 327–337. https://doi.org/10.1016/j.chemgeo.2008.10.032

**78.**   Brown SJ, Elderfield H. Variations in Mg/Ca and Sr/Ca ratios of planktonic foraminifera caused by postdepositional dissolution: Evidence of shallow Mg-dependent dissolution. Paleoceanography. 1996; 11(5): 543–551. https://doi.org/10.1029/96PA01491

**79.**   Hecht AD, Eslinger E V, Garmon LB. Experimental studies on the dissolution of planktonic foraminifera. In: Sliter W V, Bé AWH, Berger WH, editors. Dissolution of Deep-sea Carbonates.  Cushman Foundation for Foraminiferal Research; 1975. pp. 59–69.

93

80. Hamilton CP, Spero HJ, Bijma J, Lea DW. Geochemical investigation of gametogenic calcite addition in the planktonic foraminifera Orbulina universa. Mar Micropaleontol. 2008; 68(3–4): 256–267. https://doi.org/10.1016/j.marmicro.2008.04.003

81. Erez J. The Source of Ions for Biomineralization in Foraminifera and Their Implications for Paleoceanographic Proxies. Rev Mineral Geochemistry. 2003; 54(1): 115–149. https://doi.org/10.2113/0540115

82. Oakes RL, Peck VL, Manno C, Bralower TJ. Degradation of Internal Organic Matter is the Main Control on Pteropod Shell Dissolution After Death. Global Biogeochem Cycles. 2019; 33(6): 749–760. https://doi.org/10.1029/2019GB006223

83. Watanabe E, Onodera J, Harada N, Honda MC, Kimoto K, Kikuchi T, et al. Enhanced role of eddies in the Arctic marine biological pump. Nat Commun. 2014; 5(1): 3950. https://doi.org/10.1038/ncomms4950 PMID: 24862402

84. Zaborska A, Carroll J, Papucci C, Torricelli L, Carroll ML, Walkusz-Miotk J, et al. Recent sediment accumulation rates for the Western margin of the Barents Sea. Deep Res II. 2008; 55(20–11): 2352–2360. https://doi.org/10.1016/j.dsr2.2008.05.026

85. Wu G, Berger WH. Planktonic foraminifera: Differential dissolution and the Quaternary stable isotope Record in the west equatorial Pacific. Paleoceanography. 1989; 4(2): 181–198. https://doi.org/10.1029/PA004i002p00181

86. Nürnberg D. Magnesium in tests of Neogloboquadrina pachyderma sinistral from high northern and southern latitudes. J Foraminifer Res. 1995; 25(4): 350–368. https://doi.org/10.2113/gsjfr.25.4.350

87. Petro SM, Pivel MAG, Coimbra JC. Foraminiferal solubility rankings: A contribution to the search for consensus. J Foraminifer Res. 2018; 48(4): 301–313. https://doi.org/10.2113/gsjfr.48.4.301

88. Malmgren BA. Ranking of dissolution susceptibility of planktonic foraminifera at high latitudes of the South Atlantic Ocean. Mar Micropaleontol. 1983; 8(3): 183–191. https://doi.org/10.1016/0377-8398(83)90023-3

89. Spindler M. On the salinity tolerance of the planktonic foraminifera Neogloboquadrina pachyderma from Antarctic sea ice. Proc NIPR Symp Polar Biol. 1996; 9: 85–91.

90. Kimoto K. Planktic Foraminifera. In: Ohtsuka S, Suzaki T, Horiguchi T, Suzuki N, Not F, editors. Marine protists: diversity and dynamics. Tokyo: Springer Japan; 2015. pp. 129–178. https://doi.org/10.1007/978-4-431-55130-0

91. Iwasaki S, Kimoto K, Sasaki O, Kano H, Honda MC, Okazaki Y. Observation of the dissolution process of Globigerina bulloides tests (planktic foraminifera) by X-ray microcomputed tomography. Paleoceanography. 2015; 30(4): 317–331. https://doi.org/10.1002/2014PA002639

92. Johnstone HJH, Schulz M, Barker S, Elderfield H. Inside story: An X-ray computed tomography method for assessing dissolution in the tests of planktonic foraminifera. Mar Micropaleontol. 2010; 77(1–2): 58–70. https://doi.org/10.1016/j.marmicro.2010.07.004

93. Kroon D, Wouters P, Moodley L, Ganssen G, Troelstra SR. Phenotypic variation of Turborotalita quinqueloba (Natland) tests in living populations and in the Pleistocene of an eastern Mediterranean piston core. In: Brummer GJA, Kroon D, editors. Planktonic Foraminifers as Tracers of Ocean-Climate History. Amsterdam: Free Univ. Press; 1988. pp. 131–143.

94. Falk-Petersen S, Leu E, Berge J, Kwasniewski S, Røstad A, Keskinen E, et al. Vertical migration in high Arctic waters during autumn 2004. Deep Res II. 2008; 55: 2275–2284. https://doi.org/10.1016/j.dsr2.2008.05.010

95. Kobayashi HA. Growth Cycle and Related Vertical Distribution of the Thecosomatous Pteropod Spiratella (" Limacina ") helicina in the Central Arctic Ocean. Mar Biol. 1974; 26: 295–301. https://doi.org/10.1007/BF00391513

96. Lampert W. The Adaptive Significance of Diel Vertical Migration of Zooplankton. Funct Ecol. 1989; 3(1): 21–27. https://doi.org/10.2307/2389671

97. Bednaršek N, Ohman MD. Changes in pteropod distributions and shell dissolution across a frontal system in the California Current System. Mar Ecol Prog Ser. 2015; 523: 93–103. https://doi.org/10.3354/meps11199

98. Mekkes L, Renema W, Bednaršek N, Alin SR, Feely RA, Huisman J, et al. Pteropods make thinner shells in the upwelling region of the California Current Ecosystem. Sci Rep. 2021; 11(1): 1–11. https://doi.org/10.1038/s41598-020-79139-8 PMID: 33414495

99. Peck VL, Oakes RL, Harper EM, Manno C, Tarling GA. Pteropods counter mechanical damage and dissolution through extensive shell repair. Nat Commun. 2018; 9(1): 264. https://doi.org/10.1038/s41467-017-02692-w PMID: 29343708

94

100. Peck VL, Tarling GA, Manno C, Harper EM, Tynan E. Outer organic layer and internal repair mechanism protects pteropod Limacina helicina from ocean acidification. Deep Res Part II Top Stud Oceanogr. 2016; 127: 41–52. https://doi.org/10.1016/j.dsr2.2015.12.005

101. León P, Bednaršek N, Walsham P, Cook K, Hartman SE, Wall-Palmer D, et al. Relationship between shell integrity of pelagic gastropods and carbonate chemistry parameters at a Scottish Coastal Observatory monitoring site. ICES J Mar Sci. 2020; 77(1): 436–450. https://doi.org/10.1093/icesjms/fsz178

102. Bednaršek N, Feely RA, Tolimieri N, Hermann AJ, Siedlecki SA, Waldbusser GG, et al. Exposure history determines pteropod vulnerability to ocean acidification along the US West Coast article. Sci Rep. 2017; 7(1): 1–12. https://doi.org/10.1038/s41598-016-0028-x PMID: 28127051

103. McDonald MR, McClintock JB, Amsler CD, Rittschof D, Angus RA, Orihuela B, et al. Effects of ocean acidification over the life history of the barnacle Amphibalanus amphitrite. Mar Ecol Prog Ser. 2009; 385: 179–187. https://doi.org/10.3354/meps08099

104. Smith HEK, Tyrrell T, Charalampopoulou A, Dumousseaud C, Legge OJ. Predominance of heavily calcified coccolithophores at low CaCO3 saturation during winter in the Bay of Biscay. Proc Natl Acad Sci. 2012; 109(23): 8845–8849. https://doi.org/10.1073/pnas.1117508109 PMID: 22615387

105. Rigual-Hernán AS, Trull TW, Flores JA, No SD, Eriksen R. Full annual monitoring of Subantarctic Emiliania huxleyi populations reveals highly calcified conditions. Sci Rep. 2020; 10: 2594. https://doi.org/10.1038/s41598-020-59375-8 PMID: 32054880

106. IPCC. Climate Change 2013: The Physical Science Basis. Contribution of Working Group I to the Fifth Assessment Report of the Intergovernmental Panel on Climate Change. Stocker TF, Qin D, Plattner G-K, Tignor M, Allen SK, Boschung J, et al., editors. Cambridge University Press. Cambridge, United Kingdom and New York, NY, USA: Cambridge University Press; 2013. https://doi.org/10.1017/CBO9781107415324

107. Lischka S, Riebesell U. Synergistic effects of ocean acidification and warming on overwintering pteropods in the Arctic. Glob Chang Biol. 2012; 18(12): 3517–3528. https://doi.org/10.1111/gcb.12020

108. Lischka S, Büdenbender J, Boxhammer T, Riebesell U. Impact of ocean acidification and elevated temperatures on early juveniles of the polar shelled pteropod Limacina helicina: Mortality, shell degradation, and shell growth. Biogeosciences. 2011; 8(4): 919–932. https://doi.org/10.5194/bg-8-919-2011

95